STUDIES IN EQUATORIAL AERONOMY

"LANGMUIR PROBE STUDIES OF THE LOWER EQUATORIAL IONOSPHERE AT THUMBA"

Thesis presented by

B. H. SUBBARAYA

to the

Poona University

for the Ph.D degree.

July 1968

PHYSICAL RESEARCH LABORATORY

AHMEDABAD.

S T A T E M E N T

This thesis is the results of Langmuir probe experiments conducted from the Equatorial Rocket Launching Station at Thumba (TERLS). Working at the Physical Research Laboratory under the guidance of Profs. V.A. Sarabhai and Satya Prakash, the author was responsible for the design and development of the Langmuir probe system, the construction and testing of the Langmuir Probe instrumentation used in these experiments, and took part in the prelaunch checks for the Langmuir probe instrumentation on the various rocket flights conducted from Thumba. The author was also responsible for the data analysis and the interpretation of the experimental results.

There have been very few direct experimental studies over the geomagnetic equator so far and the results reported here represent valuable new material. Attempts are made in the thesis to understand the experimental results in terms of processes taking place in the equatorial ionosphere. These attempts reveal interesting new possibilities.

B. H. Subbaraya 29/7/68

(VIKRAM A. SARABHAI)
Professor and Director
Physical Research Laboratory

(B.H. SUBBARAYA)

ACKNOWLEDGEMENT

The author wishes to acknowledge with gratitude his indebtedness to Prof. Satya Prakash who guided and supervised the authors' work in all its facets, and to Prof. V.A. Sarabhai for his guidance, supervision, encouragement and advice. The author is also grateful to Profs. K.R. Ramanathan and P.R. Pisharoty who gave valuable suggestions and advice on many occassions.

Acknowledgements are also due to Mr. H.G.S.Murthy, Director, TERLS and his colleagues, Messrs A.P.J. Abdul Kalam, R. Arvamudan, D. Easwardas, P.P. Kale and B. Ramakrishna Rao to mention only a few, whose enthusiastic cooperation was responsible for the success of the rocket launchings involved in the present study. Flight time ionograms were supplied by Drs. R.G. Rastogi and J.C. Bhattacharya for the stations Thumba and Kodaikanal respectively. Dr. Bhattacharya also provided facilities to study the Kodaikanal ionograms during the authors' visit to the Astrophysical Observatory, Kodaikanal. These are gratefully acknowledged.

Prof. P.R. Pisharoty read through the manuscript of the thesis and gave many valuable suggestions for improvement. His interest and effort are most gratefully acknowledged.

It is a pleasure to thank the authors' colleagues Messrs S.P. Gupta and R.I. Patel for their help in the instrumentation and data analysis respedtively.

B. H. Subbaraya

(B.H. Subbaraya)

TABLE OF CONTENTS

CHAPTER - I

INTRODUCTION

1. Equatorial Aeronomy deals with the studies of the atmosphere of the earth in the vicinity of the earth's equator. The properties of the earth's atmosphere are greatly influenced by the sun through its electromagnetic radiations in the infrared, ultraviolet and the X-ray bands, as well as by particle radiations. The sun together with the moon also affects the earth's atmosphere through gravitational forces and produces tides. At heights above 200 km charged particles dominate the dynamics of the atmosphere. Even at heights as low as 90 km, the charged particles have a considerable effect on the dynamics of the atmosphere, through their interactions with the neutral constituents. Since charged particles are constrained to move along the magnetic field lines, the earth's magnetic field also has an important role to play in determining the properties of the atmosphere above 90 km. At the magnetic equator the earth's magnetic field is horizontal. This gives rise to many interesting magnetic and ionospheric phenomena of great interest. The special features of equatorial aeronomy have been studied for quite some time now. The studies have been greatly intensified since the IGY. The following are the special features of equatorial aeronomy.

2.1 Equatorial D region:

The incidence of a nearly uniform flux of solar radiation throughout the year gives rise to a fairly stable neutral atmosphere in the equatorial regions. At the equator the cosmic ray flux is minimum and phenomena like particle precipitation are absent. Consequently the D region ionisation there is more directly dependent on solar radiations and the local photochemistry than elsewhere.

The experimental results of the equatorial D region would be valuable in understanding the various photochemical reactions that take place in this complex region of the ionosphere (Aikin, 1965).

2.2 The equatorial electrojet:

In the lower E region, in a narrow belt around the magnetic equator, there exists a strong horizontal electric current called the 'equatorial electrojet'. It is a consequence of the earth's magnetic field being horizontal at the magnetic equator. In the presence of the purely north-south magnetic field of the earth, an east-west (horizontal) electrostatic field produces, vertical currents which are inhibited by a vertical polarization field. This polarization field, coupled with the north-south magnetic field produces a significant east-west Hall current which augments a Pederson current, (due to the original east-west electric field) flowing in the same direction as the electric field. On either side of the magnetic equator, the vertical component of the earth's magnetic field increases and with it the thickness of the polarised layer inhibiting the vertical currents also increases. The enhancement of the Pederson current is thereby reduced, confining the electrojet to a narrow belt (Baker and Martyn, 1953). This current sheet, whose existence was first deduced from ground-based magnetic measurements, was directly detected through rocketborne magnetometers by Cahill, first in the Pacific in 1959 (Cahill, 1959) and later at Thumba in 1964 (Maynard et al, 1965). From the ground based magnetic measurements it has been possible to study extensively several parameters of the equatorial electrojet, such as the peak current intensity, width of the current sheet, position and movement

of the jet axis etc. A recent study by Rosemary Hutton (1967) contains a summary of the properties of the electrojet.

2.3 Equatorial sporadic E:

Another feature of the equatorial E region of considerable interest is the equatorial sporadic E, also called the 'q type E_s'. It occurs regularly on almost all days during the daylight hours at stations near the magnetic equator. It is seen on the ionogram as a diffuse trace with a vertical extent which often extends to 20 km or more. The echo seldom blankets F region reflections. It has been studied both with the help of the ionosonde as well as the high frequency radar. It is now known that the echo is not due to reflection from a genuine layer of ionisation where the plasma frequency equals the observed critical frequency F_o E_s, but that it is due to ionisation irregularities embedded in the electrojet (Cohen et al, 1962). Matsushita (1962) and Cohen & Bowles (1963) have established a close correlation between the 'q type E_s' and the equatorial electrojet. In order to explain their observations, with high frequency radar, Bowles et al (1963) suggested that these irregularities are caused by plane quasi acoustic waves which propagate through the medium and perturb the medium as they progress. Farley (1963) has shown that these waves are due to a plasma instability akin to the "two-stream" instability, associated with the electrojet. The plasma becomes unstable when there are two or more interpenetrating streams of charged particles with a relative velocity comparable to the velocity of the particles in one stream. In a collisionless plasma with no magnetic field and equal electron and ion temperatures, the waves develop instability and grow in amplitude only when the relative electron drift speed is comparable to the mean

thermal velocity of the electrons. For smaller drift velocities the waves are damped by the Landau mechanism. In the presence of a magnetic field this damping is greatly diminished since the electrons are restricted to move along the magnetic field lines. Bernstein (1958) has shown that in a collisionless plasma, Landau damping disappears in the limit of $\cos \alpha = 0$ where α is the angle between the external magnetic field and the wavenormal. Hence for $\cos \alpha = 0$ even small values of the relative drift velocity can give rise to instabilities and produce waves in specified directions. Farley's work includes the effect of magnetic field and collisions in a realistic manner and shows that the instability can occur in the equatorial electrojet.

2.4 Other irregularities in the equatorial E region:

Apart from the 'q type E_s' which is a manifestation of the equatorial electrojet, other irregularities have been observed in the equatorial E region. Bandyopadhyay and Montes (1963) have found that the flat type E_s ('f type E_s') is a common occurrence in the equatorial E region during night time. Similar day time occurrences, classified as 'l type E_s' have also been seen on occassions. There are also large scale irregularities in the E region whose drifts have been measured by the ground-based technique employing spaced-receivers. Near the equator these irregularities have been found to be elongated along the magnetic field lines. Skinner et al (1958) find an axial ratio of 5 : 1 (assuming the irregularities to be elliptical in shape) for Ibadan (magnetic dip 6^{o}S). For Thumba which is on the magnetic equator (magnetic dip 0^{o} 47'S) the ratio is found to be slightly less (Deshpande, Ph.D thesis). Near the equator these irregularities

show an average westward drift. The average speeds are found to be 100 meters/sec at Ibadan (Skinner et al, loc cit) and 132 meters/sec at Thumba (Deshpande and Rastogi, 1966).

2.5 F region anomalies at the equator:

The equatorial F region presents several interesting anomalies. Of these the 'Appleton anomaly' or simply called the 'equatorial anomaly' well known. The noon time electron density at a given height in the F region shows a pronounced minimum at the equator with maxima on either side of it at about 30^{o} dip latitude. This feature, first noticed for the E_2 peak, although reported by Maeda and his coworkers in 1942, is known after Appleton who observed it in 1946 (1946). Since then it had been studied by several workers and the dependence of the anomaly on the dip latitude rather than the geomagnetic or geographic latitude has been clearly established (Rastogi, 1959). The anomaly has been found to extend to a considerable height on both sides of the F_2 peak (Croom et al, 1959; Thomas et al, 1966). Attempts have been made to explain the anomaly either in terms of diffusion along the magnetic field lines or in terms of diffusion and electrodynamic drift (Duncan, 1960; 1964; Goldberg and Schmerling, 1962, 1963; Lyon 1962, 1963; Baxter, 1964; Bramley and Peart, 1965; Hanson and Moffet, 1966).

A prominent feature which the equatorial F region shares with other latitudes is the daily variation of the ionisation at any given height. The daily maximum is reached not at noon but several hours earlier. Norton and Van Zandt (1964) have been able to compute, based on certain assumptions, theoretical electron density distributions which explain this feature.

2.6 Equatorial F region irregularities:

The equatorial F region is also known for certain special irregularities. Radio star scintillations (Koster, 1958) and transequatorial VHF scatter propagation (Cohen and Bowles, 1961) have been found to be correlated with certain spread F configurations which are seen frequently on night time equatorial ionograms. Two different types of irregularities which give rise to equatorial spread F have been recognised. The first type consists of thin irregularities which are field aligned, with dimensions of the order of a kilometre along the field lines and of 10 meters or less across these lines. These are situated at the base of the F layer (Cohen and Bowles, loc cit). The other type called the thick irregularities are embedded in the F region. They are 10 to 50 kms thick and extend upto 300 kms east-west. They drift eastwards with velocities of the order of 100 meters/sec (Calvert and Cohen, 1961). The equatorial spread F is distinct from the temperate latitude type spread F in that the former supports scatter propagation while the latter does not; the equatorial spread F shows a negative correlation with geomagnetic activity (Lyon et al, 1958).

3.1 The problems:

Most of the features described above have not yet been completely understood. In the D region, while there has been in recent years a certain amount of understanding with regard to the ionising radiations, the relative importance of the various radiations concerned has not yet been established. The photochemical process that occur have also not been understood completely. The various estimates, from ionospheric experiments,

of the effective recombination coefficient in the D region, have yielded widely different results and these results are very often inconsistent with laboratory measurements of the rate coefficients of the various reactions that are believed to be going on there. While simple theory expects the predominant positive ions in the D region to be O_2^+ and NO^+, rocket experiments (Narcissi and Bailey, 1965) have shown that certain heavy ions which are probably of metallic origin are important and ions of water vapour and its higher hydrates constitute a majority of the D region positive ions. Aikin (1966), has proposed certain reactions which can explain the presence of these ions. But a major revision of the processes in the D region may be necessary before the experimental results are completely understood. The dominant negative ion in the night time D region is also not known with certainity. Results of certain PCA studies have been found to be incompatible with the earlier belief that O_2^- is the major negative ion. It has also been found that the negative ion may be different on different occassions. A knowledge of the dominant negative ion at night is of importance in determining the initial development of the D region at sunrise.

As mentioned earlier measurements at the equator would be more helpful in understanding the D region processes than elsewhere. However there have been very few direct or indirect measurements of the equatorial D region. Radiowave absorption measurements are available for Ibadan (magnetic dip 6^oS) for over a solar cycle (Skinner and Wright, 1956; 1964) and more recently for Colombo (magnetic dip 5^oS), (Gnanalingam and

Ratnasiri, 1966). But there have been no direct measurement of the D region near the magnetic equator.

The equatorial E region phenomena are also not completely understood. While the general principles underlying the formation of the electrojet are known the details of the processes involved are not yet clear. It is still an open question whether the electrojet is a mere enhancement of the worldwide S_q current system in a narrow belt near the equator as envisaged by Baker and Martyn or a separate current system (Osborne, 1963; Ogebuehi et al, 1967). If it is a separate current system, the location of the return current and its effects on ionospheric and magnetic phenomena need to be studied in detail. The study of night time VHF radar echoes has led Balsley (1967) to consider the presence of a westward flowing current during night as a possibility. Such a current system has not yet been detected by direct measurements.

The understanding of the nature of the irregularities in the equatorial E_s, and their motion is incomplete. While the work of Cohen and Bowles has given experimental support to Farley's theory, it is not clear that these are the only irregularities which are present in the electrojet. Farley's mechanism can explain only those irregularities which travel with acoustic velocities and which have a pronounced east-west component. Occassionally irregularities which travel with velocities very much different from acoustic velocities are seen. Knox (1964) has shown that conditions in the electrojet are such that even statistical fluctuations can get amplified if they are field aligned, for wave numbers less than about 10^{-2}/cm (λ = 6 meters). This

theory allows for a wide range of wave velocities, upto about 1.5 km/sec. Obviously there are different types of irregularities, it is important to classify them and identify the types associated with the electrojet.

It has not also been possible to explain the F region irregularities, and the cause of equatorial spread F. Irregularities in the ionosphere are generally explained in terms of turbulence, gradients in the background ionisation and plasma instabilities. Turbulence is not expected at F region heights and gradients in electron density are not large enough to give rise to irregularities. The presence of plasma instabilities can not also be conceived in the F region. Processes which involve mass vertical movement of ionisation in irregular formations such as the ones suggested by Martyn (1959) and Calvert (1963) are not favoured by Dougherty (1959).

Thus there are many phenomena in the field of equatorial aeronomy, which are understood only partially. Detailed measurements of the parameters involved, such as solar radiations in specified spectral regions, densities of the neutral as well as the ionised constituents, electron and ion temperatures, electric fields, winds in the neutral atmosphere, etc., will be required before any precise theoreis can be worked out. While there has been an intensive study of the atmosphere over the middle and higher latitudes, similar studies over the equator are relatively scarce. The need for intensive experimental studies of the various aspects of equatorial aeronomy can not be over emphasised.

This thesis reports experimental studies on

(a) the relative importance of Lyman α and solar X-rays as sources of D region ionisation,

(b) the effect of electrojet currents on the electron temperature in the lower equatorial ionosphere,

(c) the E_2 layers in the equatorial regions, and

(d) the night-time E region.

CHAPTER - II

EXPERIMENTAL TECHNIQUES

Ionospheric studies have been carried out using a variety of techniques. These techniques can be broadly classified into two types : (i) ground based techniques (ii) rocket and satellite techniques. While the ground based techniques have been in use for a long time, rocket and satellites have come into use only in the last decade or two. But in this small period they have made substantial contribution to our knowledge of the ionosphere. The advantages of ground based techniques in making continuous observations from a single station over an extended period of time compensates for the capabilities of an earth satellite in probing a good part of the globe within a relatively short time and those of a high flying rocket in obtaining a vertical profile of the ionospheric parameters over a given station within a few minutes.

1.1 Ground based techniques:

Most of the ground based techniques involve the propagation of electromagnetic waves in the medium under study. The most popular technique has been vertical sounding using swept frequency recorders in which the time delay of the echo of a vertically transmitted electromagnetic wave is used to estimate the height of reflection. When the frequency of the wave is swept over a certain range the resulting echo pattern, called the ionogram can be used to investigate the E and the F regions of the ionosphere. The D region has been mostly studied through measurements of radio wave absorption, partial reflection and cross modulation.

Ground based studies have also been carried out utilising certain naturally occuring transmissions. Cosmic radio noise studies, studies using whistlers and VLF emissions come under this category. Cosmic radio noise studies have been used as a solar flare patrol and to detect precipitation events. More recently they have also been used to obtain some information about F region electron temperatures. Whistler studies have been used to obtain vertical electron density profiles at exospheric heights in the equatorial plane of the earth.

The incoherent backscatter technique, used at several places, is the only ground based technique which is capable of giving vertical profiles of the ionospheric parameters concerned. In this technique a high power VHF signal is transmitted into the ionsosphere and the backscattered echoes are studied to obtain information about the electron densities, electron and ion temperatures etc. The technique has been found to be capable of measuring these parameters from heights of 100 km to 1000 km in the ionosphere. Coherent backscattered echoes have been analysed to determine movements of ionospheric irregularities and their scale sizes. Movements of large size irregularities in the E and F regions have also been studied by the spaced receiver technique.

2.1 Rocket and satellite based studies:

Rocket studies of the upper atmosphere began in 1945 with the use of V2 rockets for scientific investigations by the Michigan university. With the launching of the Soviet sputnik in 1957, satellites also began to be used for atmospheric research.

While ground based studies were mostly limited to indirect experiments involving radio wave propagation the advent of rockets and satellites has made direct probing possible. Many types of studies which were not possible before are now being carried out and our knowledge of the upper atmosphere has grown beyond expections.

Rocket and satellite borne techniques have been used to study the various parameters and processes in the ionised as well as neutral constituents of the upper atmosphere. The techniques that are used to study electron densities and electron temperatures are of two types. The first type include the propagation type experiments involving measurement of Doppler shifts (Seddon, 1953; Jackson and Seddon 1958), Faraday rotation and differential absorption (Seddon 1958, Bauer and Jackson, 1962; Knoebel and Skaperdas 1966) on one or more radiowaves propagating between the rocket or satellite and a suitable ground station. These determinations involve problems of ray tracing, problems connected with the particular magnetoionic mode of propagation etc. Another disadvantage with propagation type studies is that transitory phenomena occuring in the intervening medium can give rise to spurious results. The second type of experiments for determining electron densities and temperatures involve the use of 'in situ' probes. Elecftrostatic probes such as the Langmuir probe, various types of impedance probes, the resonance probe and ion traps have been used. Probe techniques on rockets and satellites have problems of their own, such as, limitation of the volume sampled outgassing from metal surfaces on the vehilce, development of ion

sheaths around the vehicle, and effect of magnetic field on particle collection. These problems are treated in detail in the next chapter.

In addition to the probes for measurement of charged particle densities and temperatures there are other in situ measurements that are possible on rockets and satellites. Instruments like mass spectrometers for finding the neutral and ion composition of the atmosphere, magnetometers for the measurement of magnetic field and electric currents, photon counters and ionisation chambers for measuring the flux of solar radiations in specified bands and their absorption in the atmosphere, have been extensively used.

The satellite drag technique has been used to determine neutral atmosphere densities and their variations. Pressure gauges, grenades etc. have been used on rocket to determine neutral atmosphere temperatures. Parameters concerning neutral atmosphere motion such as winds, wind shears and turbulence have been studied by the release of fluorescent and photochemically reacting vapours into the atmosphere from rockets. Release of certain readily ionisable vapours such as barium has also enabled the measurement of electric fields in the ionosphere. There have also been attempts at a direct measurement of electric fields in the ionosphere.

3.1 Probe techniques:

The various probes that have been used for electron density and electron temperature measurements in the ionosphere can be divided into two basic types. The electrostatic or the

Langmuir type probes and the radio frequency probes. The theory and practice of Langmuir probes are described in the next chapter. The radiofrequency probes can again be classified into two types. The first type involves the more or less direct measurement of the impedence of a probe immersed in the plasma at one or more radiofrequencies. When the frequency employed is much above the gyrofrequency in the medium and the plasma frequency, the measured impedance can be interpreted in terms of the electron density and the collision frequency in the medium. To this category belongs: (a) NASA impedance probe (Jackson and Kane, 1959) in which the impedance of an antenna is measured by sweeping a variable capacitor and noting the value of the capacitor which brings the antenna into resonance: (b) the capacitance probe of Sayers (1963) and its modifications due to Heikkila (1965), in which the probe forms one element of a tuned circuit whose resonance frequency is determined; and (c) the standing wave impedance probe of AFCRL in which the standing wave ratio on the transmission line feeding the antenna is measured, wherefrom, the impedance of the antenna is deduced (Pfister et al, 1961).

The second type of radiofrequency probes may be called the resonance probes. In this type the frequency of the probe is swept through a wide range of frequencies and the impedance of the probe determined over the range. The resonance frequency is determined by the sharp changes the impedance undergoes, at this frequency. The various swept frequency admittance probes and the resonance relaxation probe (Calvert et al, 1965) fall under this category. In the Japanese resonance probe (Miyazaki et al, 1960) an applied rf voltage causes a rectified current to be

collexted by the probe. When the frequency is swept this current goes through a maximum which was believed to occur at the plasma frequency, but is now known to occur at a frequency slightly below the plasma frequency.

All of the above mentioned probes have been extensively used for ionospheric studies individually as well as in combination Each type has its own advantages and disadvantages. Recently a comparative study of the various probes in the ionosphere has been made by Heikkila et al (1967). It is found that most of the probes are best used in the E region of the ionosphere. The swept frequency admittance probes and the resonance relaxation type of probes are found to be best suited for absolute measurement of electron density. The rf impedance probes, while more convenient in practice for the study of fine structure in the medium, do not give correct electron densities. The effective size of the sheath around the rocket and satellite borne probes, which effect the measurements cannot be determined experimentally. A correction factor (which is not accurately known) has to be applied for all such probe measurements. The electrostatic type of probes are ideal for studying the fine structure in the medium. Electron temperature measurements made by the classical Langmuir type probe do not have any apparent problems and seem to be accurate. Electron density measurements from such probes suffer from effects due to the earth's magnetic field, electron depletion in the probe surroundings due to charge collection by the probe etc, which are not understood. Hence these measurements need an independent calibration. Therefore, inspite of its limitations, the Langmuir

type probe seems to be the most convenient probe; it is reliable when independent and frequent calibrations at different heights in the ionosphere are possible. The effects of depletion are minimum for cylindrical Langmuir probes and the mesh type probes used by the Japanese workers (Ichimiya et al, 1960). These probes Therefore yield the best results. A simple modification of the Langmuir's technique has enabled Boyd and Willmore (1963) to study the energy distribution of the electrons and thereby arrive at more accurate estimates of electron temperature.

CHAPTER - III

LANGMUIR PROBE - THEORETICAL CONSIDERATIONS

1. Langmuir probe:

The technique first used by Irwing Langmuir consists of exposing a small metallic probe to the medium under study and measuring the current collected by it as the probe voltage is slowly varies from a convenient negative value through zero to a convenient positive value. The resulting current-voltage characteristics are analysed to obtain information about various plasma parameters.

The above technique was employed for ionospheric studies, for the first time, in 1946 by Spencer and his colleagues (1953). Since then the technique has been improved. The dumbbell probes of the Michigan University group (Spencer et al, 1962), the tip probes of NASA (Smith, 1964), the satellite borne cylindrical probes of Brace and others (1964), and the mesh probes of the Japanese workers (Ichimiya et al, 1960) are some of the examples of the Langmuir type probes now in use. The author has used a modified version of the Smith type Langmuir probe. The two frequency probe of Boyd and Willmore (1963) makes use of a refinement in the basic theory; it has enabled a more accurate determination of the energy distribution in the ionosphere. The Gerdien condenser (Bourdeau et al, 1959; Pederson 1965) and the parachute borne blunt probe of Hale (1967) are techniques similar to Langmuir's technique, but they are applicable only in the high collision regions where Langmuir's theory is not directly applicable.

2. Langmuir probe theory

2.1 Classical concepts: According to the classical concepts a probe immersed in a plasma and left to itself acquires a negative potential with respect to the plasma called the 'floating potential' or the 'wall potential'. This arises out of the excess of the random electron flux in the medium due to the average electron velocity being larger than the average positive ion velocity in the medium.

When a voltage is applied to the probe charges of one sign are attracted to it while charges of the opposite sign are repelled and the probe is soon surrounded by a space charge sheath which shields the surrounding plasma from the probe-field. The thickness of the sheath depends on the probe voltage, the size of the probe as well as the electron density and the electron temperature in the medium. A rough idea of the sheath dimensions can be obtained from the Debye shielding distance in the medium. The latter is a function of only the electron density and the electron temperature in the medium; it is therefore a characteristic parameter of the plasma. The shielding distance is given by

$$\lambda_D = \sqrt{\frac{\epsilon_0 k T_e}{n_e e^2}} = 6.9 \sqrt{\frac{T_e}{n_e}} \quad \text{cms} \qquad (1)$$

where λ_D is the dielectric permitivity in the medium,

k is the Boltzmann's constant,

e is the electronic charge,

T_e is the electron temperature and

n_e is the number of electrons per cc in the medium.

In the classical Langmuir's theory the probe is surrounded by a space charge sheath into which charged particles diffuse from the surrounding plasma from large distances. Once a charged particle enters the sheath it does not suffer any collisions until it is collected by the probe. Loss of charges due to charge collection by the probe is replenished from the surrounding plasma and there is assumed to be no depletion in the immediate neighbourhood of the probe. It will be shown later that this simple picture does not hold for a practical probe in a plasma, especially in the ionospheric plasma; the earth's magnetic field introduces additional complications. However, this theory, with some modifications has been used extensively to obtain useful information about the ionosphere. Obviously, the application of this theory is valid only when charge depletion and effects due to the magnetic field are negligible.

2.2 Probe at plasma potential: When a probe is at the same potential as the ambient plasma the current collected by the probe is entirely due to the thermal motion of the charged particles in the medium. Since the average electron velocity is much larger than the average positive ion velocity, the probe current can be considered to be entirely due to electrons. According to kinetic theory the average number of particles colliding against a unit area of surface exposed to a gas in unit time is $\frac{n\bar{v}}{4}$. Therefore the probe current is given by

$$J_o = Aj_o = A \frac{n_e \cdot e \cdot \bar{v}_e}{4} \qquad (2)$$

Where A is the surface area of the probe, j_o is the current

density and $\bar{v}_e$ is the average electron velocity in the medium, given by

$$\bar{v}_e = \sqrt{\frac{8kT_e}{\pi m_e}} = 6.21 \times 10^5 \sqrt{T_e} \text{ cm/sec.} \qquad (3)$$

2.3 Slightly negative probe: Retarding potential analysis:

For small negative voltages of the probe the probe current consists of two parts (i) A positive ion current limited by the space charge and (ii) a current due to the electrons which overcome the repelling voltage of the probe. When the distribution is Maxwellian the retarded electron current to a negative probe is given by

$$j_e = j_o \exp\left(\frac{eV}{kT_e}\right) \qquad (4)$$

where j_o is as before the random electron current density and V is the probe voltage. This property is generally used to determine the electron temperature in the medium.

2.4 A positive probe: attracting potentials:

In this case positive ions are repelled and electrons are attracted towards the probe. Even a small positive voltage is sufficient to make the positive ion component of the probe current negligible compared to the electron component. Determination of the electron current to a positive probe is complicated by considerations of both the size and shape of the probe. The size of the probe, in comparison with the Debye length plays an important role in determining the current collected by it. In general, the procedure involves writing down the Poisson's

equation and solving it. A detailed knowledge of the probe and the sheath geometry will be needed. Langmuir and Mott Smith (1926) have obtained the following expressions for spherical, plan and cylindrical geometries.

(i) A small sphere, radius smaller than the Debya length. The current is given by

$$j_e = j_0 \left(1 + \frac{eV}{kT_e} \right) \tag{5}$$

where j_0 is the random electron current and V is the probe voltage.

Any complex shaped body can be approximated to a sphere as long as its size is small. This is a good approximation since the distant field is coulombian regardless of the shape of the body.

(ii) A large plane, large when compared to the thickness of the plane and the sheath:

$$j_e = j_0 \tag{6}$$

Here the probe current is determined by the surface area of the probe and the plasma parameters and not on the potential difference across the sheath. The probe current is independent of the probe voltage.

(iii) A long thin cylinder: In this case the original expressions of Langmuir and Mott Smith reduce to

$$j_e = j_0 \left\{ \frac{2}{\sqrt{\pi}} \left(\frac{eV}{kT_e} \right)^{1/2} + \exp\left(\frac{eV}{kT_e} \right) P \left(\frac{eV}{kT_e} \right)^{1/2} \right\} \tag{7}$$

where P is the error function defined by

$$P(x) = \frac{2}{\sqrt{\pi}} \int_0^x e^{-y^2} dy \tag{8}$$

Fig.1 compares the electron collection in the various cases considered above. The abscissa represent the normalised probe voltage $\frac{eV}{kT_e}$ and the ordinates represent j_e/j_{e_0} the electron current to the probe normalised to the random electron current.

Positive ion collection by a strongly negative probe is given by equations similar to (5), (6) and (7). But the actual positive ion currents would be much smaller than the corresponding electron currents due to the large ion mass.

3. Recent work on probe theory:

Recently there has been a considerable amount of interest in extending the classical Langmuir theory. A series of studies by Bohm (1949), Bohm et al, (1949) and Schulz and Brown (1955) have shown that in the case of a strongly negative probe, the positive ion sheath does not perfectly shield the probe field. A stable sheath is possible only when the ions reach it with a kinetic energy which is at least half the mean kinetic energy of the electrons in the plasma i.e $kT_e/2$. Therefore the potential at the edge of the sheath is about $kT_e/2$. A consequence of this field penetration is that the positive ion current to a negative probe is determined by the electron temperature in the medium and not by the positive ion temperature. This explained the experimental results of Boyd (1950) in which the positive ion currents were found to be much larger than expected by Langmuir's theory and also pointed out the impossibility of measuring the ion temperature from the experimental data. Extending the work of Bohm, Allen et al (1957) computed the potential distribution and the positive ion current-voltage

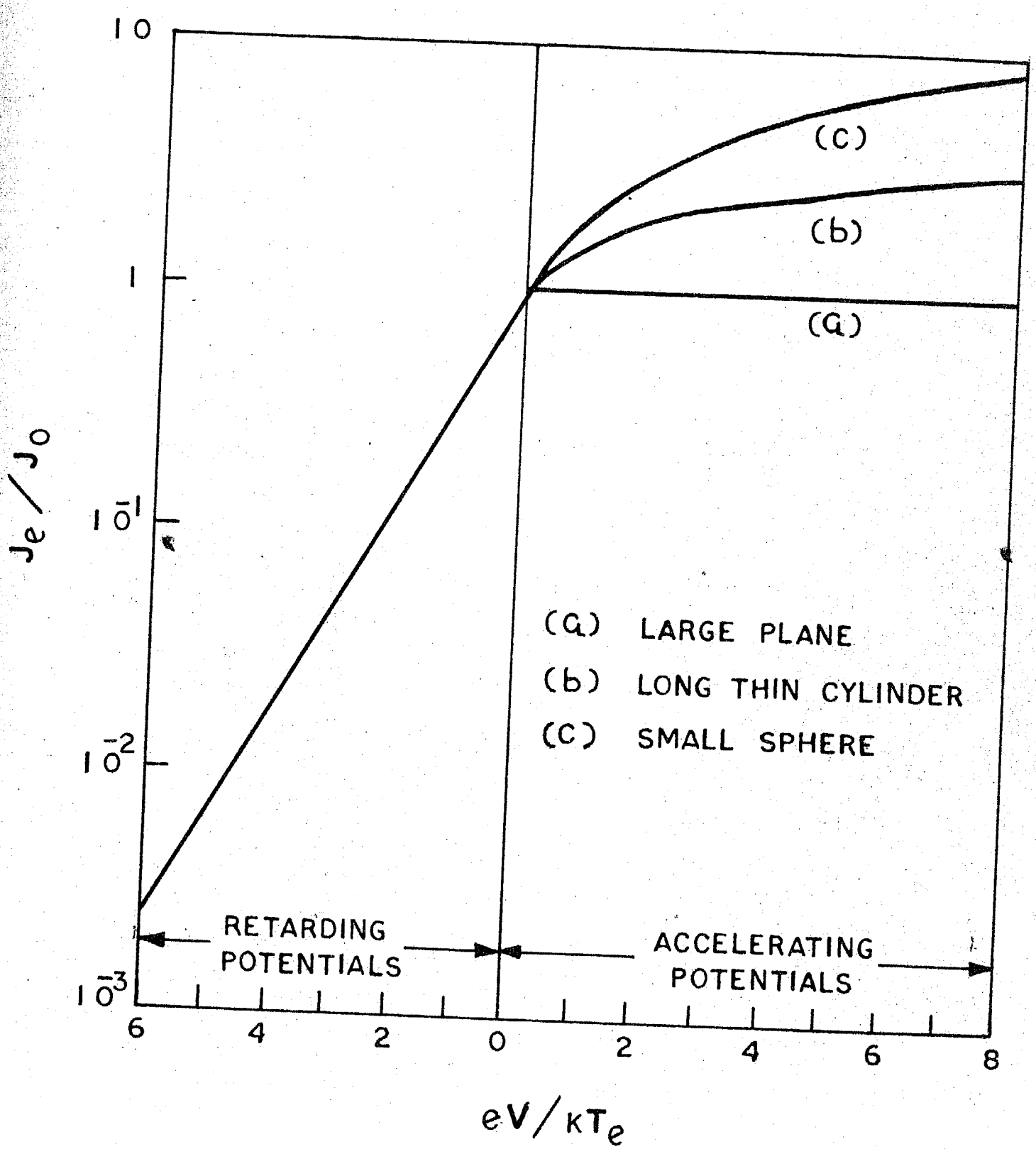

Fig 1. Comparison of electron collection by probes of different geometries (Schematic)

characteristics of a cylindrical and a spherical probe. Their relations could be used to interpret experimental data in terms of $n_+ \frac{T_e}{M_+}$. n_+ and M_+ are the positive ion density and positive ion mass respectively. More recently, Bernstein and Robinowitch (1959) have shown, that for a given probe radius, there exists a critical probe voltage beyond which ions can get trapped in troughs of the effective potential energy near the probe. Consequently the positive ion current to a negative probe is not quite independent of the positive ion temperature even though the ion temperature can not be determined from the probe characteristics.

Attempts have been made to determine the current-voltage characteristics for a probe in some specific cases. Considering a dense but slightly ionised gas in which the frequency of collisions is high enough to justify the treatment of the gas as a continuum, Su and Lam (1963) wrote down the differential equations for the potential distribution and the charge distribution in the region surrounding a large probe (radius >> Debye length). The equations turned out to be highly nonlinear. They were able to obtain some approximate analytical solutions under certain simplyfying assumptions. Su and Lam's equations were solved numerically by Cicerone and Bowhill (1967) without any approximations. Current voltage characteristics could not be drawn over a wide range of probe potentials because of the instability of the numerical procedure used. However the behaviour of the solutions could be studied. The charge distribution in the neighbourhood of the probe obtained by them illustrates the importance of the sheath for positive ion collection. The positive ion density is found to

have a nearly constant value equal to 0.4 N_∞ over a large distance beyond the immediate neighbourhood of the probe before it increases gradually to the free space value .

A kinetic theory approach has also been attempted for a large probe in a collision-dominated gas by I. M. Cohen (1963) and more recently by Wasserstrom et al (1965). Their studies show that the current voltage characteristic never really saturates, even for large probe biases, although there is a tendency for saturation with increasing values of the ratio of the probe-radius to the Debye length. The reason for this is found to be the penetration of the probe-field beyond the sheath. The probe-created electric field penetrates far beyond the space charge sheath and the charged particles are collected from larger and larger distances. The Debye shielding in the sheath is incomplete since the potential decays only inversely with the first power of the distance for large distances from the probe. When no current is collected by the probe one can expect better shielding. Boyd (1965) has pointed out that the electron current across a Debye sphere is 10^{-7} amps. Hence for probe sizes so small that the saturation electron current is less than 10^{-7} amps penetration of probe field beyond the sheath may not be of importance.

Wasserstrom et al (loc cit) found that when the probe is at space potential there is an inward electron density gradient accompanying the steady flux of electrons to the probe, but no potential gradient in the neighbourhood of the probe. This is necessary to satisfy the continuity condition. According to them

$$\frac{n_p}{N} = \frac{1}{2(1 + r_p/L)} \qquad (9)$$

where n_p = electron density at the probe surface

N = ambient electron density

r_p = probe radius

L = mean free path for electrons

It is seen that the ratio $\frac{n_p}{N}$ is maximum for $r_p << L$ ie. for small probe radii. Even under these conditions the density at the probe surface is only one half the density at infinity.

4. Langmuir probe in the ionosphere:

4.1 Region of applicability: In order that the equations of section 2 may be applicable it is necessary that the Debye length is less than the mean free path, so that a charged particle entering the sheath does not suffer collisions before it is captured at the probe surface. Optimum conditions for applicability of the theory are

$$r_p < \lambda_D < L$$

where r_p = probe radius, λ_D = Debye length and L = mean free path. The mean free path for the collisions between electrons and neutral particles is about 1 cm at 85 km, decreasing rapidly with decreasing height. Negative ions which are not considered in Langmuir's theory become important below 85 km. The ratio of the negative ion density to the electron density varies from 0.1 at 85 km to about 20 at 60 km during day time (Sagalyn and Smiddy, 1964). Therefore 85 kms is the lower limit for the applicability of Langmuir probe theory.

The upper limit for the region of applicibility is set by considerations of photoelectric effect. The photoelectric yield of a metal surface such as tungsten, when exposed to

unattenuated solar radiation is, according to Hinteregger et al (1959), about 4×10^{-9} amp/cm^2. A similar value seems to have been estimated by Bourdeau et al (1961) from Explorer VIII data. Hence the photoemission effect would be equal to the random current density at higher altitudes than about 1000 kms under normal conditions.

Hence the altitude region 100 - 1000 kms seems to be amenable for exploration by Langmuir probes, and this has been done extensively. Different geometries have been used, the main considerations being those of mechanical simplicity as well as minimising of the errors due to motion of the vehicle. Spherical and cylindrical geometries have been more popular because of their easier methematical treatment. Spherical electrodes and meshed spheres, either projected at the front or from the sides, at the end of large booms in order to keep them sufficiently away from the vehicle, long thin wires, conical and ogive electrodes situated at the nose tip of rockets, have all been used for ionospheric investigations. Some of the more important problems of a rocket or a satellite borne probe are discussed below.

4.2 Effect of the earth's magnetic field: In the presence of a magnetic field the charged particles spiral around the magnetic field lines and diffuse along them. Diffusion across the lines of force is inhibited. The effective free path for the particles becomes the Larmor radius $\rho = \frac{m v_\perp}{eB}$. In the lower ionosphere the Larmor radius is about 1 cm for electrons and is of the order of a metre for positive ions. Therefore any probe

of practical dimensions will be larger than the effective free path of electrons. When the probe size is larger than the mean free path it collects more particles than can be made up by diffusion from distant regions resulting in a depletion in its immediate neighbourhood. This decreases the efficiency of the probe for particle collection. Since motion along the field lines is uninhibited while motion across is inhibited the final result is a compromise in which the probe collects electrons from regions distant along the field lines but not far away across these lines. Electron collection is dependent in a complicated manner on the probe radius, the electron temperature, the electron density and the magnetic field. Positive ion collection is however not affected by the magnetic field.

Whipple (1965) has shown that for a spherical probe, when the probe radius is larger than the average gyro-radius of the electrons the effect of the magnetic field can be to reduce the electron current to it, by a factor of about two. However, it is generally believed that the magnetic field does not affect the retarding potential analysis and electron temperatures can be determined even in the presence of a magnetic field. In the retarding potential analysis one is concerned only with the high energy electrons which can overcome the probe field and since the magnetic field effect is less for the high energy electrons (due to the smaller Larmor radii of these electrons) the retarding-potential analysis is not considerably affected by magnetic fields.

4.3 Reference electrode: In a rocket or a satellite borne probe the sweep voltage is applied between two electrodes both of

which are floating in the ambient medium. Such a system was first treated theoretically by Johnson and Malter (1950). In the dumbbell probes of Spencer et al (loc cit) the two electrodes are of equal area and the variations in potential are included in the interpretation of the experimental data. But in most of the probe systems it is customary to make one of the electrodes much smaller than the other; use the smaller electrode as the probe and the larger electrode as the reference electrode. Due to its large size the potential of the latter is assumed not to vary as the probe voltage is varied and the probe collects current from the medium. When the probe collects charges of one sign, it should be possible for an equal and opposite current to flow into the reference electrode. This condition is easily satisfied when the probe collects positive ions. On the other hand when the probe is collecting electrons an equal number of positive ions can flow into the reference electrode only if it is larger than the probe by a factor equal to or greater than the ratio of the velocity of the electrons to that of the positive ions.

Smith (loc cit) has shown that a practical Langmuir probe system can be treated as a single probe if the area ratio of the two electrodes is at least ten time j_e/j_+. The ratio j_e/j_+ is about 170 in most of the regions of interest in the ionosphere. On an average, in a two stage rocket such as the Nike Apache, the area available for the reference electrode is between 2×10^4 and 3×10^4 cm^2. Therefore surface area of the probe should not exceed 10 to 15 cm^2 if the system is to be treated as a single probe system.

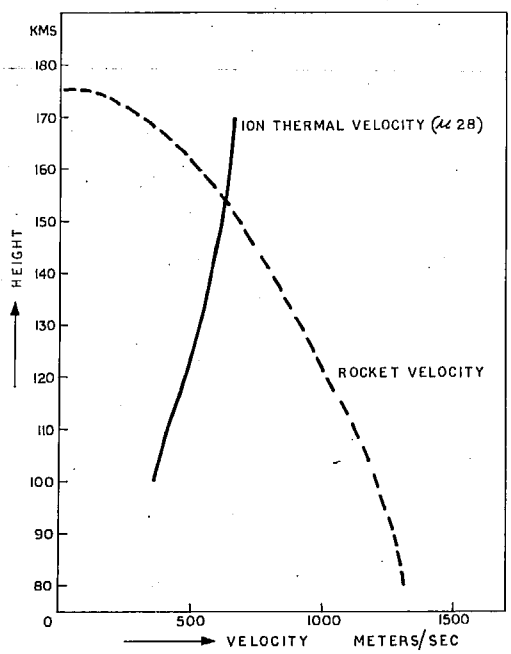

Fig.2: Vertical velocity of a Nike Apache rocket in a typical trajectory compared with the ion thermal velocity in the medium.

4.4 Vehicle velocity: Fig.2 shows the vertical velocity of an average two stage rocket during a typical flight. These velocities are much smaller than the average electron velocity in the medium which is about 100 km/sec and therefore electron collection is not affected by the vehicle velocity. However, the average ion velocity (shown in Fig.2) is seen to be comparable to the rocket velocity. The positive ion collection is therefore, affected by the vehicle velocity.

Dote et al (1962, 1963) have shown that the ion current to a spherical probe moving in a plasma can be written

$$J_+ = 4\pi r_0^2 \, j_{0+} \, Q_0(\eta_0) \qquad (10)$$

where j_{0+} = random ion current in the medium

r_0 = radius of sheath in a direct at α to the motion

and $Q_0(\eta_0)$ is a function of the velocity parameter η_0.

$$\eta_0 = \frac{M_+ u_0^2}{2kT_+}$$

where M_+ = mass of ion

u_0 = vel of the probe in the medium.

The form of $Q_0(\eta_0)$ was obtained both experimentally and theoretically by the above authors and the results were found to agree with one another. (An illustrative value is $Q_0(\eta_0) = 4$ when $\eta_0 = 10$). Using these results observed positive ion currents can be corrected for vehicle motion. The retarding potential analysis for electron temperatures is, however, not affected by the motion of the vehicle .

4.5 Aspect of the vehicle:

Effect of spin and precession: Unless despin mechanisms and attitude controls are used the rocket spins around its longitudinal axis and performs precessional motion during its flight. (Typical periods for an average two stage Nike-Apache rocket are: spin rate = 6 to 10 cycles/sec, precessional rate = once in 30 to 40 secs). The aspect of the probe changes during the spin and precession. In the presence of the earth's magnetic field this changing aspect gives rise to a modulation of the probe current. When a symmetrical sensor such as the ogive is used on the nose tip of a rocket the effect of spin will be a small ripple on the probe current profile if there are no marked small scale inhomogenieties in the ambient medium. Outgassing from the nose cone and similar effects can give rise to spurious modulations. Fig.3 shows

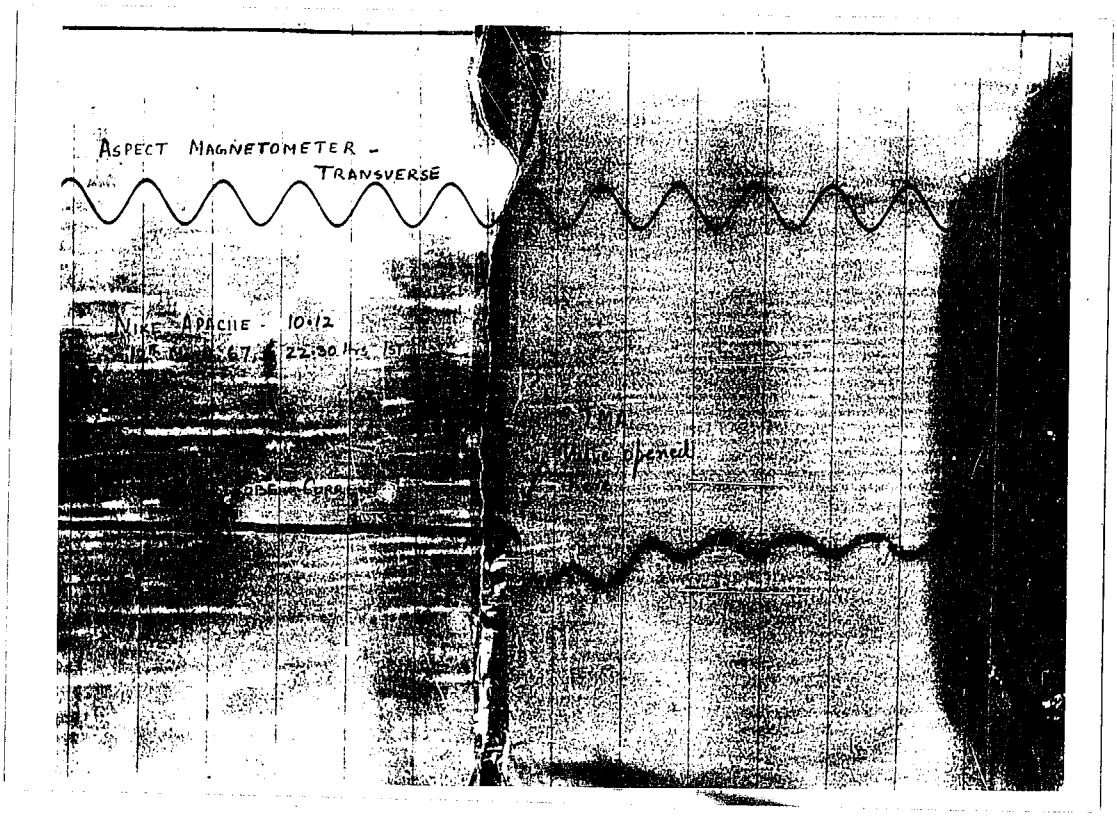

Fig.3. Spin modulation on the probe current observed on flight 10.12, due to the release of TMA from the rocket.

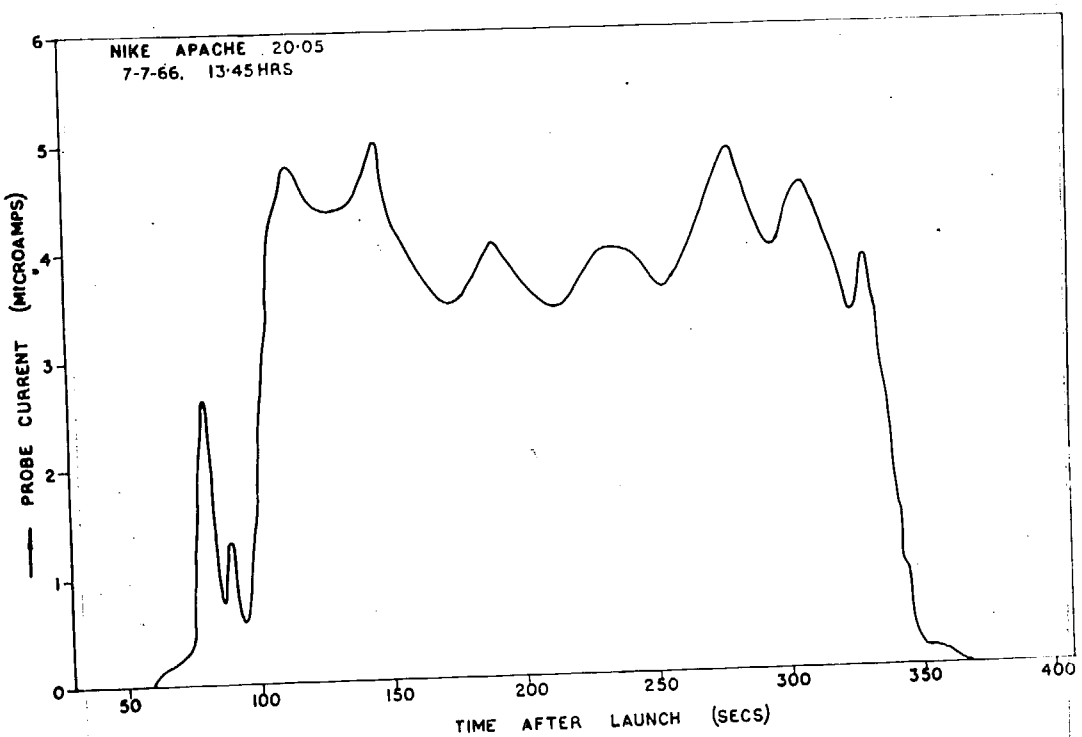

Fig.4: The probe current at + 2.4 V, measured on flight 20.05, plotted against time, illustrating the effect of rocket precession on probe current.

the spin modulation on the current to an ogive nose tip obtained from flight 10.12 during the part of the flight when TMA was being released from a port on the side of the nose cone. The effect of rocket precession can sometimes give rise to a more marked modulation on the probe current. Fig.4 shows the probe current to an ogive nose tip obtained on flight 20.05. The profile shows a clear modulation of 1 cycle in about 40 secs which is the expected precession frequency of the rocket. These effects are found to differ from flight to flight. Therefore experience from one flight can not always be used to interpret unambiguously the data from other flights. A proper evaluation of probe data needs complete information of the rocket aspect obtained from aspect sensors.

The spin and precession effects would be even more pronounced on cylinders or planes used at the side of the rocket unless they are close to the tip.

4.6 Effect of the wake of the vehicle: When a rocket or a satellite is travelling with a velocity greater than the mean ion velocity in the medium, positive ions cannot penetrate into the rear of the vehicle, although electrons of a sufficiently large velocity can. Hence the absence of a neutralising space charge of positive ions creates a negative potential in the wake of the vehicle. This produces a rarefaction in the electron density distribution. The shape of the wake and the ion and electron potential distributions in it have been described by Alpert, Gurevich and Pitaevasky (1963)

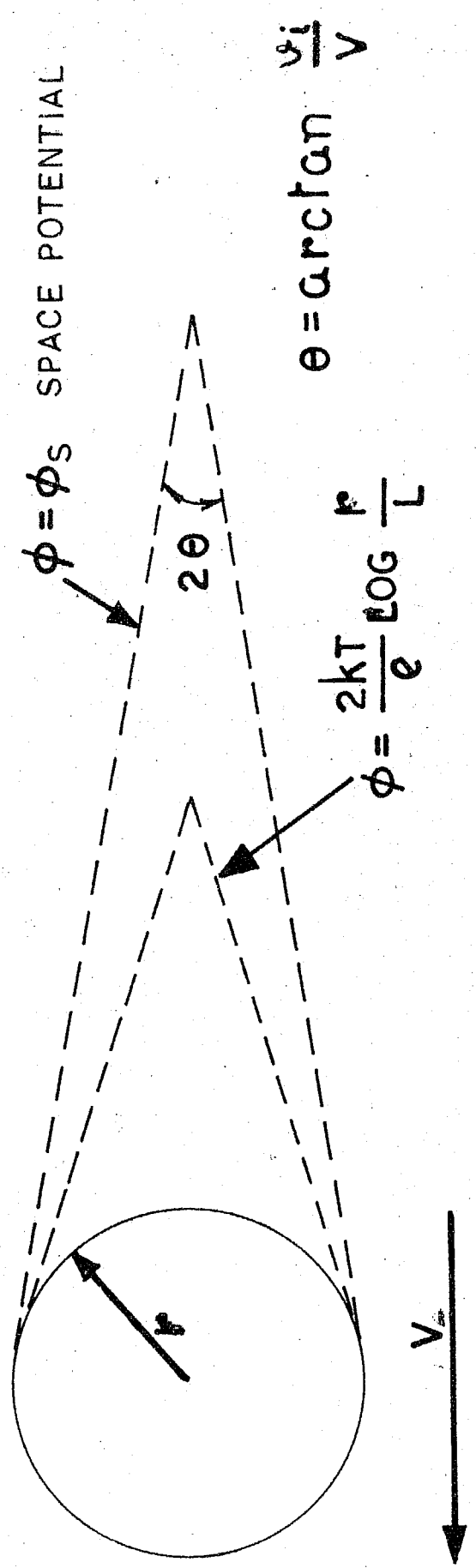

Fig 5 POTENTIAL IN THE WAKE OF THE VEHICLE

and Alpert (1965) who show that the potential in the wake can reach velues of the order of

$$\varphi = -\frac{2kT}{e} \log \frac{r}{L} \qquad (11)$$

(fig.5).

Hence a probe should avoid the wake of the vehicle. This is done best by locating it at the nose tip of the rocket or by projecting it far into the medium using booms. A probe at the nose tip may enter into the wake during the descent if the rocket comes down with its nose up, depending upon the elevation at launch. The effect of the probe entering into the wake would obviously be a reduction in the electron current to it. Such an effect was seen on a test flight where a wire release mechanism for projecting a long thin wire was tested. The wire was used as a Langmuir probe. Its performance was satisfactory in the initial stages. Afterwards a large shift in rocket potential was observed and this was accompanied by increased positive ion currents, and an increased aspect sensitiveness of the electron current. These are considered to be due to the low elevation taken by the rocket at that time.

4.7 Vehicle potential: A body exposed to a plasma will acquire an equilibrium potential called the floating potential at which the sum of the electron and positive-ion fluxes to it is zero. For a body at rest, assuming it to be perfect collector of charges, this potential, is given by

$$j_+ = j_0 = j_0 \exp\left(-\frac{eV_f}{kT_e}\right)$$

$$\therefore V_f = -\frac{kT_e}{e} \log \frac{j_0}{j_+} \qquad (12)$$

j_0 = random electron current, j_+ = random positive ion current

For typical ionospheric conditions this reduces to

$$V_f = -5.1 \frac{kT_e}{e} \tag{13}$$

and ranges from -0.2 to -1.0V. But in practice there are spurious effects due to the motion of the body, solar radiation, the presence of fields on the moving vehicle, the earth's magnetic field and contact potentials due to dissimilar work functions of different parts of the vehicle.

The effect of vehicle velocity changes eq (12) to

$$V_f = -\frac{kT_e}{e} \log \frac{v_e}{v_R} \tag{14}$$

where v_e = random electron velocity, v_R = vehicle velocity (Bourdeau and Donley, 1964). This does not change the results radically. Solar radiation falling on the surface of the body gives rise to photo-emission which tends to make the vehicle acquire a positive voltage at large heights. It also tends to enhance the positive ion current to the probe. Rectification of antenna voltages also tends to make the vehicle more negative. Aono et al (1961) show that the effect is negligible when the frequency is much greater than the plasma frequency in the medium. The effect of magnetic field is to give rise to an aspect sensitiveness in the vehicle potential since electron diffusion currents are affected differentially. The contact potential is an unknown quantity and often is different for different parts of the vehicle.

Experimental results on the potential of a body in space have been of a varied nature. Krassovsky (1959) reports

negative voltages as high as 6V on Sputnik III. Bourdeau and Donley (1964) find that the night time potentials of Explorer VIII are between -0.5V and -0.75V, in better agreement with theory. Experience on rockets has also been equally inconclusive. Serbu (1963) using a tungsten plate flush with the rocket skin and L.G. Smith (loc cit) using tip probes found that the net probe current becomes zero only when the probe voltage is clearly positive and not for negative voltages. The implied rocket to ionosphere potentials of more than + 1 volt were explained by Smith by taking into consideration both resonance rectification by antenna voltages and contact potentials. Contact potentials were believed to be responsible for the observed effects. Results from the Langmuir probe flights from Thumba also show similar features. The net probe current goes to zero only for positive voltages both with ogive electrodes at the nose tip and with cylindrical probes.

Fig. 6 shows the voltage at which net probe current is zero for the sweeps of flight 20.05, a daytime flight. It is possible to discern a modulation at 1 cycle per 40 secs which is due to rocket precession. Apart from this effect the voltages are everywhere more than +1 Volt. The results of flight 10.11 and 10.14 which carried identical probes, slightly different from the one on flight 20.05, are shown in Fig. 7. These flights were conducted during evening and morning twilights respectively. From these figures it is seen that the potentials can be very much different on different occassions.

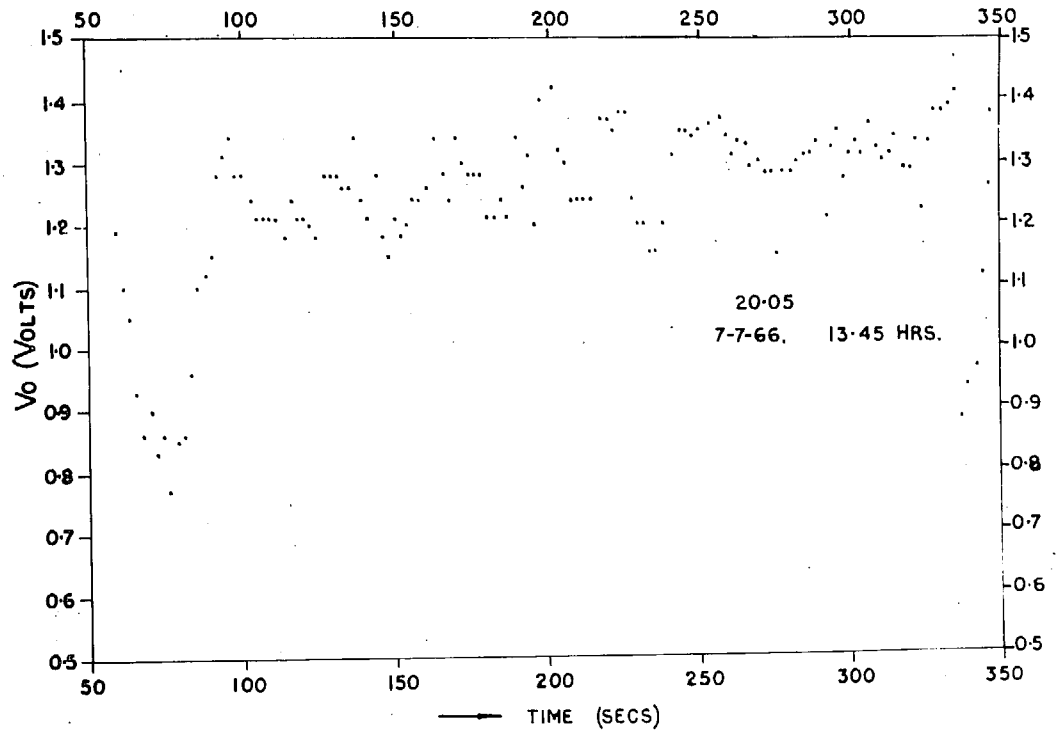

Fig. 6: Potential at which the net probe current becomes zero during a sweep cycle, measured for the different sweeps of flight 20.05.

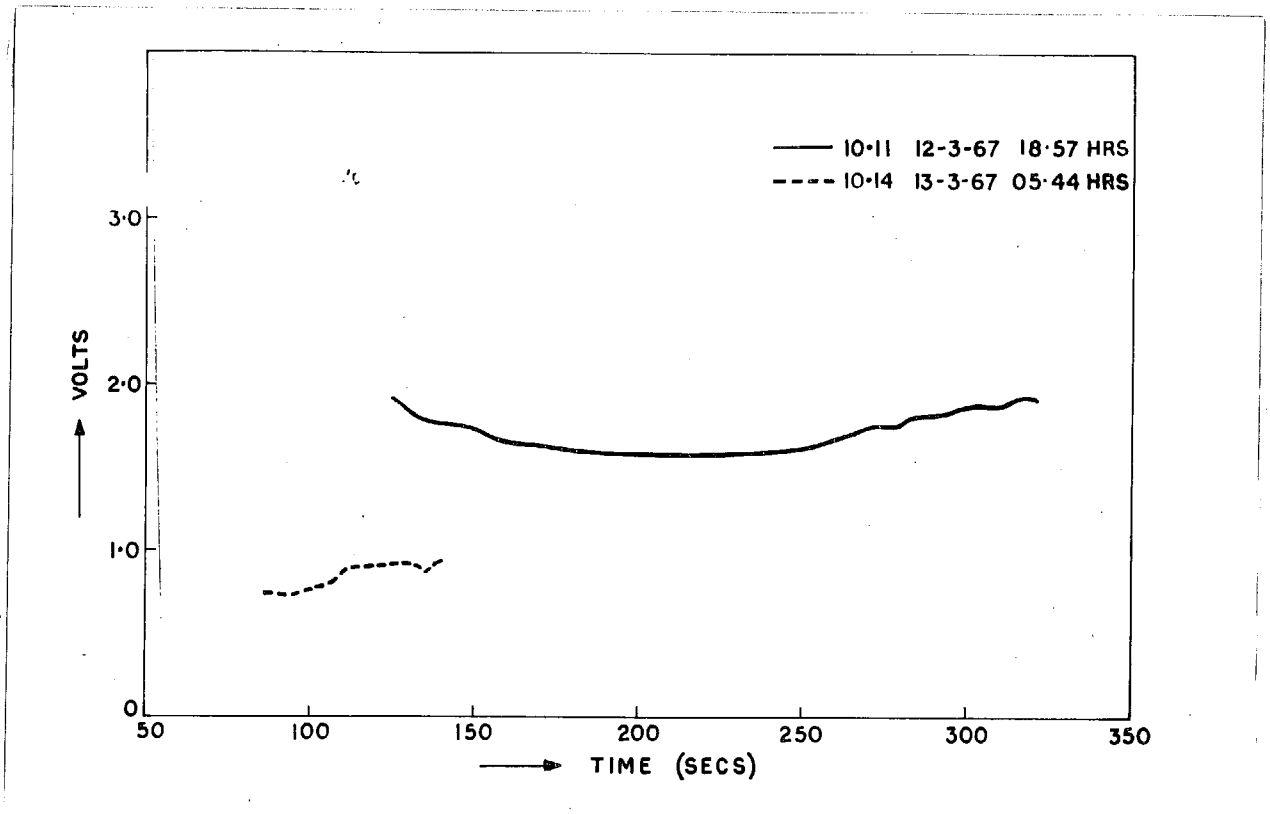

Fig.7: Potential at which the net probe current becomes zero during a sweep cycle, measured for the different sweeps of flight 10.11 and 10.14.

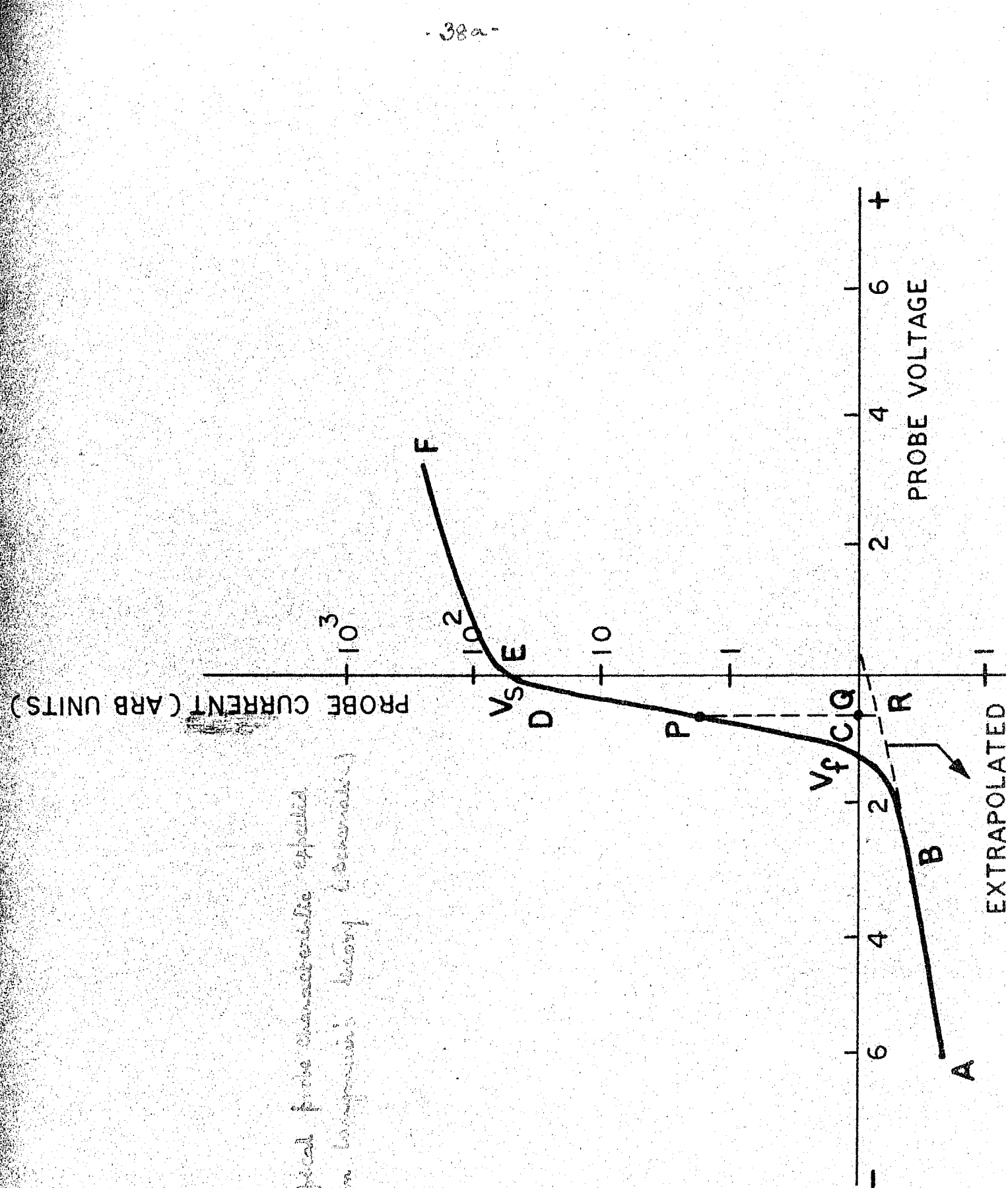

Fig. Typical Langmuir probe characteristic (schematic)

5. Determination of electron temperature and electron density:

Fig.8 shows a typical current-voltage characteristic one would expect from considerations of section 2. At the negative end of the sweep the probe current is predominantly due to positive ions and decreases with decreasing numerical value of the negative probe voltage. This portion of the characteristic is represented by AB in figure. As the value of the probe voltage numerically decreases further the probe current diminishes much faster since the positive ion current to it decreases and the electron current due to those electrons which can overcome the repelling probe voltage increases. The net probe current becomes zero at the floating potential V_f, when the positive ion current equals the electron current. With a further numerical decrease in the probe voltage, ie as the voltage approaches zero, the electron current to it increases rapidly as shown by the section CD of the characteristic curve. This portion of the characteristic can be used for the determination of the electron temperature in the medium. In this portion, the probe current is given by

$$J_{obs} = J_e - J_+$$

The positive ion current at any point P on the characteristic can be determined by extrapolating the portion AB of the curve, as shown in the figure, and the electron current to the probe estimated. A semi log plot of this electron current against the probe voltage gives a straight line and the slope of this line is equal to $\frac{e}{kT_e}$, where T_e is the electron temperature.

When the probe is at plasma potential (V_s), the probe current is almost wholly due to electrons as given by eq.2. For positive voltages of the probe the electron current increases with probe voltage and even though it does not really saturate, the rate of increase is very small after a small positive voltage. This situation is represented by Ef in fig. 8. In principle it should be possible to find the electron density in the medium from the probe current at plasma potential using eq.2, since the electron temperature is known from the section CD of the characteristic. But in practice it is difficult to locate the point S since the change of slope at S is not sufficiently sharp. Apart from this practical difficulty, all attempts to determine the electron density in the ionosphere from the electron current to a probe at space potential have yielded values smaller by nearly an order of magnitude (L.G. Smith, loc cit). This has been attributed to the effect of the earth's magnetic field. From the discussions on page 28 it is seen that the earth's magnetic field can reduce the probe current and thereby give rise to lower values of electron density. The observed low values may also be partly due to the electron density gradient in the neighbourhood of the probe, when the probe is at plasma potential (cf page 25).

Fig.9 is a reproduction of an actual experimental current-voltage characteristic. It is interesting to compare this with Fig.8. The nonlinearity in the current axis is due to the experimental technique involved. The d.c shift in the characteristic curve along the voltage axis illustrates the

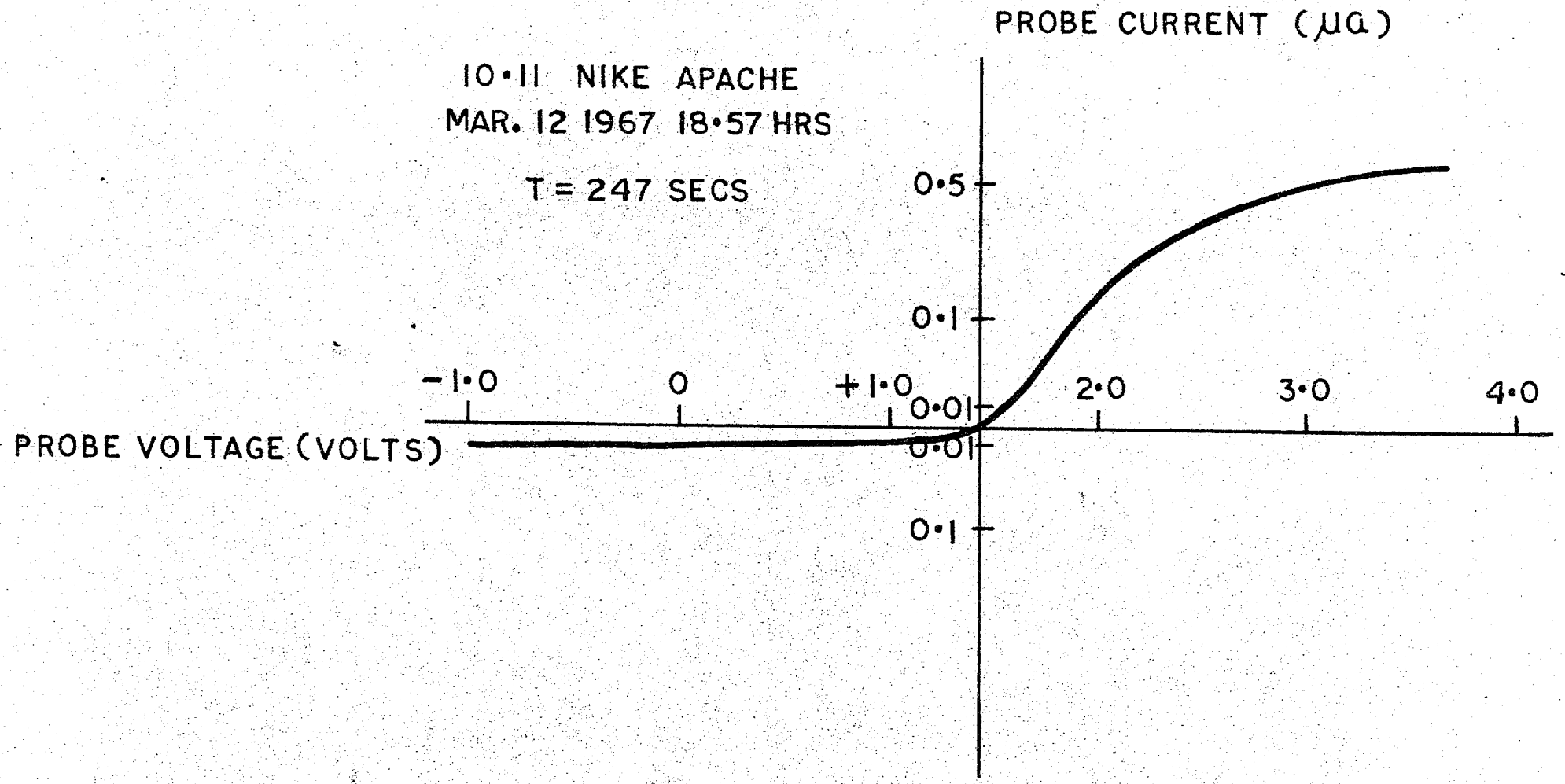

Fig 9: Typical experimental current - voltage plot

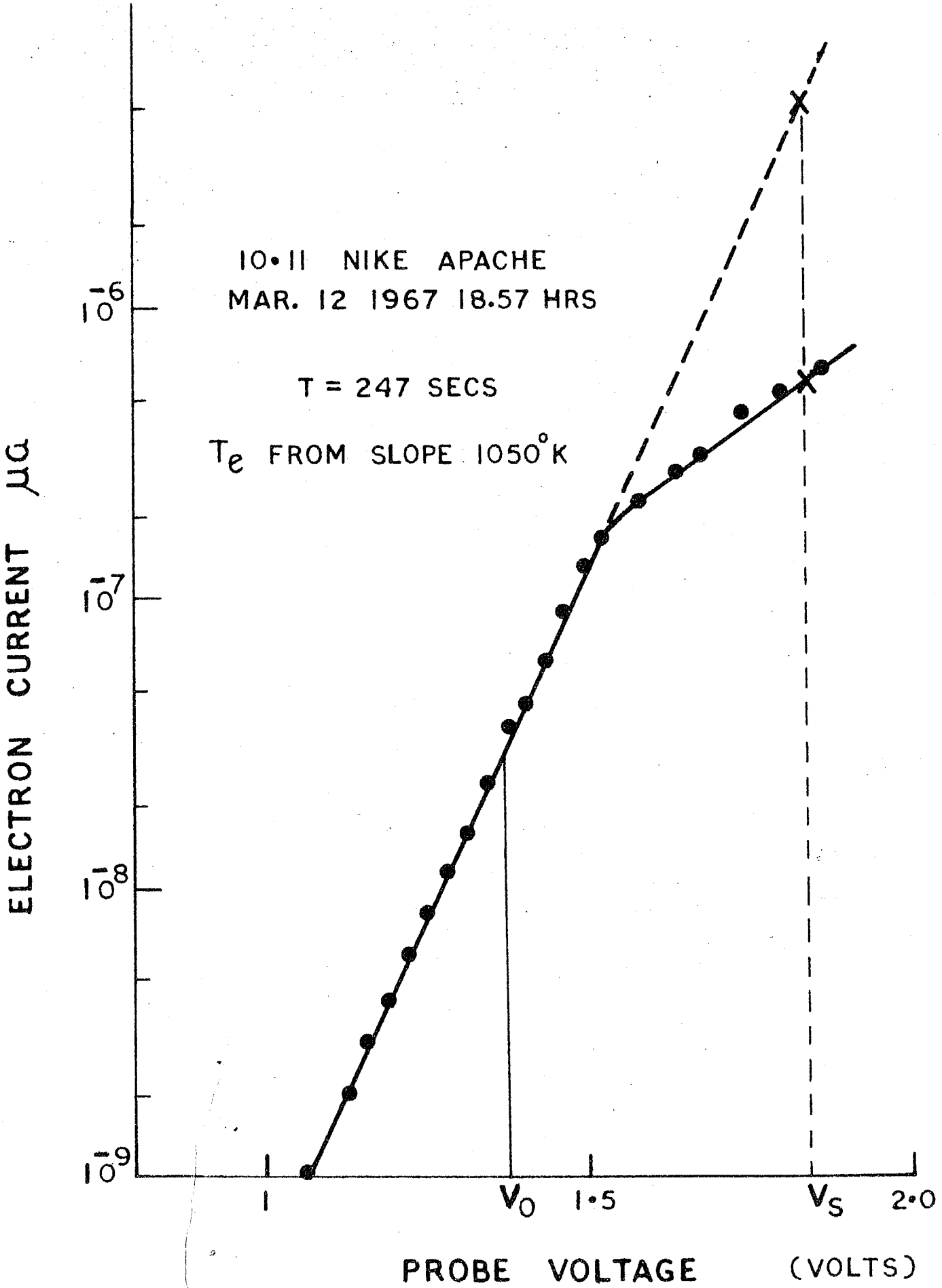

fig 10. Semi log plot of probe current Vs probe voltage for the characteristic of fig 9

discussions of section 4.7. A semilog plot of the electron current against probe voltage for this curve is shown in Fig.10 V_o is the point where the net probe current was observed to be zero. From the slope of the straight portion AB the electron temperature was calculated to be 1050°K. This gives a floating potential of -0.46 V. Therefore the space potential can be put at +0.46 V ahead of the point V_o ie at V_s. Now Langmuir's theory expects the semilog plot to be linear upto this point. The experimental curve is seen to depart from linearity much below the space potential. The inability of the probe to collect sufficient number of electrons to give correct values of electron density from probe current measurement at space potential is clearly illustrated in this figure. The increasing departure from linearity as the probe potential approaches the plasma potential shows that the probe is inefficient for collection of the lower energy electrons. By extrapolating the straight portion upto the space potential it is seen that the ratio of the expected current to the observed current is about 10. This figure cannot be explained by the magnetic field effect alone. It is likely to be due to the combined effect of magnetic field, presence of electron-density gradients in the neighbourhood of the probe and charge depletion due to electron collection by the probe.

Even though there are practical difficulties in determining the electron density from the probe current at space potential it is seen from eq. 5 that the probe current to a small sphere (or any geometry that can be approximated to a sphere) kept at a positive voltage large enough to make

is proportional to the electron density in the medium. If electron temperature variations are neglected, the probe current is directly proportional to the electron density in the medium. This property is used in a mixed mode of operation in which the probe potential alternates between a sweep and a fixed voltage mode. The probe current profile at the fixed voltage has been used to study the electron density variations in the ionosphere. Absolute values of electron density can be obtained by calibrating the Langmuir probe current with the help of an accompanying propagation type of experiment or a resonance relaxation type of experiment. When such an accompanying experiment is not possible it is customary to use flight time ionograms from the nearest ionospheric station for calibration purposes. Whenever possible the ionograms are subjected to a true height analysis and several calibration points are obtained at various heights in the ionosphere.

CHAPTER - IV

LANGMUIR PROBE INSTRUMENTATION

1. The Langmuir probe system

1.1 The normal Langmuir probe system: A rocket borne Langmuir probe system consists of a probing electrode, generally referred to as the 'sensor', well insulated from a reference electrode which in most cases may be the body of the vehicle itself. An insulated portion of the rocket body can be used as a reference electrode. A third, guard electrode is sometimes used to give a definite geometry to the electric field of the sensor and thereby improve its performance. In a typical Langmuir probe experiment a sweep voltage, varying from a convenient negative value to a positive voltage of 2 to 5 volts is generated with respect to the reference electrode and applied to the sensor. The current collected by the sensor from the surrounding plasma is converted into a voltage suitable for telemetry by an electrometer amplifier and telemetered to the ground. At the ground the current voltage characteristics of the probe are analysed to obtain the required information about the ionospheric parameters.

Fig.11a illustrates the working of a typical rocket borne Langmuir probe system. The sweep voltage is generated and applied to the sensor with respect to a reference voltage which is tied to the input of the electrometer amplifier, the ground of the amplifier being connected to the rocket body. Since the electrometer amplifier is a current measuring instru-

ment its input impedance is kept very low and there is only a small voltage drop between the amplifier-input and the amplifier-ground. In practice this drop is of the order of 10 mV or less. Hence the sweep applied to the sensor is with respect to the rocket body. The current collected by the sensor from the surrounding plasma passes through the sweep generator and into the electrometer amplifier where it is converted into a suitable voltage.

While this system looks straightforward, in practice it is quite complicated involving many precautions and a sophisticated handling of the system, if meaningful data are to be collected from it. The sweep generating system must be run on floating batteries while the rest of the electronics needs a battery with one terminal common with the rocket body. Hence the system needs at least two independent batteries feeding power to it. This necessitates a complicated procedure since in a rocket payload every battery system that feeds power to the payload needs an associated relay system and an external battery system for pre launch checks. Also the entire sweep generating system must be floating, with only the two points G and G' having connections with the rest of the system. Hence the entire portions enclosed in dashes in Fig.11a must be well shielded to avoid current leakages between this part of the system and the rest of it. Internal leakage currents must be much less than the sensor current of 10^{-10} amp or less. The distributed capacity of the network at the input of the electrometer amplifier must be small so that the frequency response of the system does not become very low.

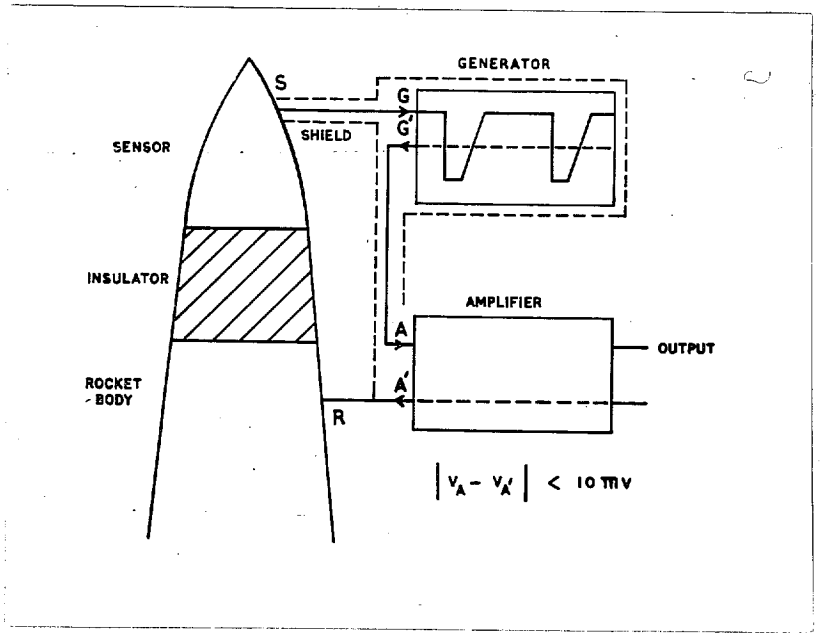

Fig.11 (a)

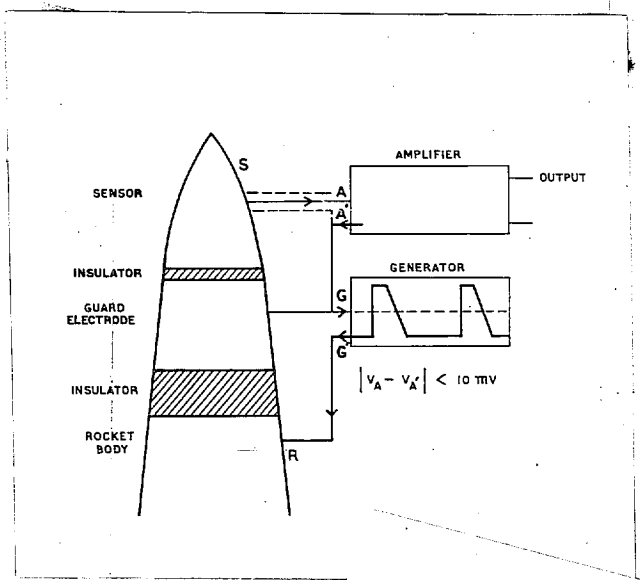

Fig.11

Fig.11: Comparison of the new Langmuir probe system with a co
Langmuir probe system. 11(a) illustrates the workin
conventional Langmuir probe system. 11(b) illustrate
of the new Langmuir probe system.

tem

- 44 -

ding
lators
to

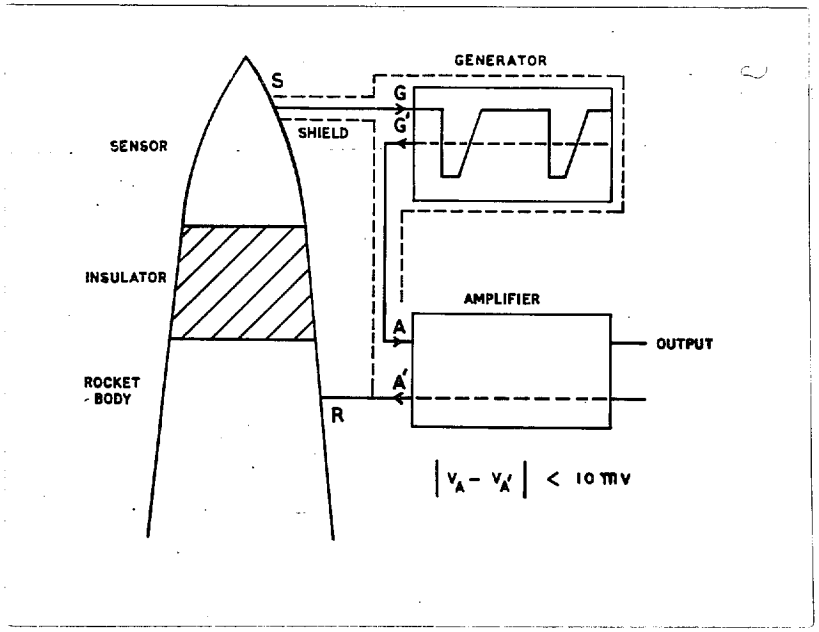

Fig.11 (a)

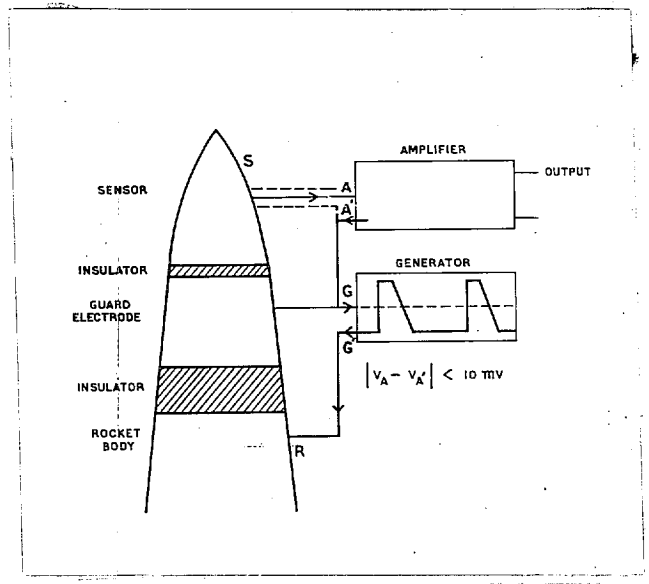

Fig.11 (b)

Fig.11: Comparison of the new Langmuir probe system with a conventional Langmuir probe system. 11(a) illustrates the working of a conventional Langmuir probe system. 11(b) illustrates the working of the new Langmuir probe system.

1.2 New Langmuir probe System: A new Langmuir probe system which works on a single floating battery was designed and developed at the Physical Research Laboratory, Ahmedabad (Satya Prakash and Subbaraya, 1967). It reduces the leakage currents to a very small value, permits a more through pre-launch checkouts and has many other advantages over the conventional system currently in use. The system was sucessfully flight tested on several rockets flown from Thumba and the results have been good.

Fig.11b illustrates the working of the new system. An electrode when immersed in a plasma and left to itself acquires a voltage called the 'floating potential' (page 19). This potential is negative with respect to the plasma potential and is a function of the plasma parameters. Neglecting the effects due to different work functions and other disturbances the sensing electrode and the reference electrode (the rocket body) are expected to acquire the same floating potential when exposed to the plasma (However there can be a constant potential difference due to effects such as contact potential etc. as discussed on page 37. But this does not affect the present discussion). A voltage V_G' which varies with respect to a fixed voltage V_G in a manner reverse to the sweep that is to be applied to the sensor is generated and connected to the rocket body as shown in Fig.11b. The voltage V_G is connected to the amplifier reference A' so that $V_G = V_G'$ and the sensor is directly connected to the amplifier input A as shown. Due to the small input impedance of the amplifier the voltage drop between A and A' is small (about mV) and the sensor develops the

same voltages as the reference part of the amplifier. Hence the sensor voltage varies with respect to the rocket body in the desired manner.

1.3 Advantages of the new system: Some of the advantages and special features of the new Langmuir probe system are:

(1) Since it operates on a single battery and since the sensor is directly connected to the input of the amplifier internal leakage currents are reduced to the irreducible minimum.

(2) A special feature of this system is the availability of the reference point $V_G = V_A'$ which follows closely the sensor potential. When a guard electrode is to be used it can be directly connected to this point (fig.11 b) and no additional electronics will be needed to maintain the guard electrode at the same potential as the sensor.

The use of a guard electrode greatly improve the performance of the sensor by rendering the electric field near the sensor normal to its surface (and thereby giving it a definite geometry) and by enhancing the function of the insulator which separates the sensor from the rest of the system. Since the guard is nearly at the same potential as the sensor direct current leakage between the two is very much reduced. The reduction is by a factor

$$\frac{V_S - V_R}{V_G - V_R} \leq \frac{4}{0.01}$$

V_S = Sensor potential
V_R = Rocket potential
V_G = Potential of the guard

which is a factor of about 400. Any surface leakage between the guard and the reference electrode does not affect the measurements.

(3) Since the internal leakages and capacitance leakages are reduced the system has additional advantages of practical value. The frequency response of the system is limited by the frequency response of the electrometer amplifier if the sensor is directly to be connected to the amplifier. Electrometer amplifiers with a frequency response of 0-10 khz can be made. Hence the present system can be used to detect audio frequency fluctuations in the ambient ionised medium. Useful studies of such fluctuations have been made using this system (Satya Prakash et al 1968).

With this system the probe electronics can be located anywhere within the nosecone of the rocket and a cable used to connect the sensor to the amplifier. When the sensor is connected through a cable the effective distributed capacity in the cable is reduced to $\frac{C}{g}$ where C = cable capacity and g is the gain of the amplifier.

(4) A thorough check up of the probe electronics just before launch is necessary if the data are to be meaningfully interpreted. All the test points are brought out of the rocket through a main connector called the umbilical connector. Any lead connected to the sensor can not be brought to the connector since it will not only produce leakages but also act as an additional sensor during the flight and affect the sensor current in a complicated manner. Therefore in any ordinary Langmuir probe system no test point is brought out from the sweep generator an

It is not possible to ensure a completely satisfactory performance of the electronics before launching. In the present system the reference point which follows the sensor potential can be brought out and hence the performance of the sweep electronics chekced prior to launching.

1.4 Description of the system: Fig.12 is a block diagram of the Langmuir probe system. A voltage function which varies in a manner reverse to the sweep to be applied to the sensor is generated at G' and connected to the reference electrode (rocket body). The electrometer amplifier works on voltages V_A' + 18 V, V_A' and V_A' and V_A' - 9V with $V_A' = V_G$ as the reference voltage of the amplifier. The rest of the system works on the 27 volts supply obtained from V_A' + 18 V and V_A' - 9 V. The amplifier output is an analog voltage which is a known function of the input current (the current collected by the sensor). This output is fed to auitable voltage controlled oscillator which converts it into a frequency which can be modulate the rf carrier on an IRIG subcarrier channel. Since in practice a large dynamic range of probe current is encountered two subcarrier channels are used to obtain optimum information efficiency. One channel is used for lower probe currents and the amplifier output is directly fed through a limiter network to the voltage conctrolle d oscillator. The other channel which is used for larger probe

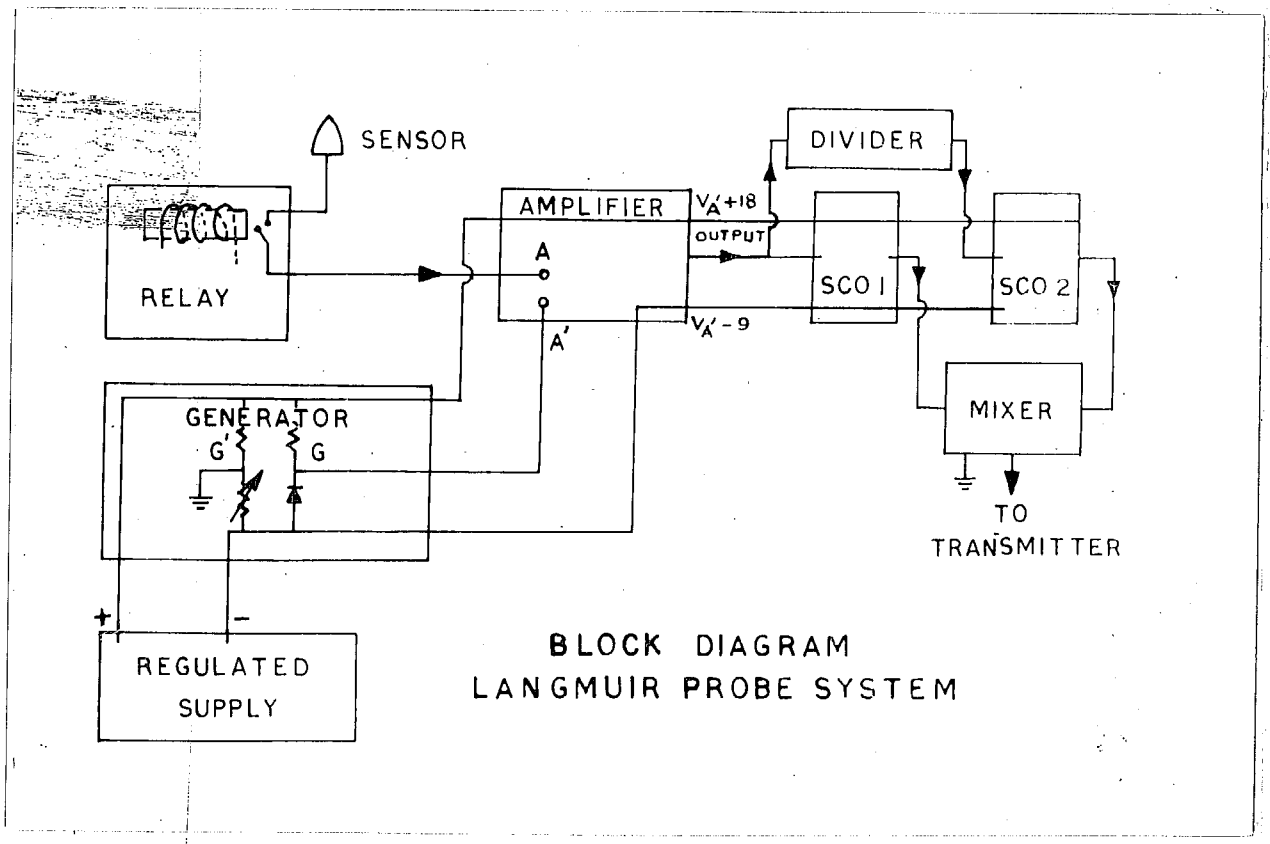

Fig.12: Block diagram of the new Langmuir probe system working on a single floating battery.

currents is fed by the amplifier output through a dividing network. The outputs of the two voltage controlled oscillators are mixed using a passive mixer and the mixed output allowed to modulate the rf carrier from a suitable transmitter.

To facilitate data reduction and to check for amplifier drifts a calibration mark is obtained for zero input current to the amplifier for about 50 milliseconds at the end of every operational cycle of the Langmuir probe. A small signal of a few mV at 500 hz can be superimposed on the sweep that is applied to the sensor. If the a.c component of the amplifier output is amplified and detected it will be a measure of the instantaneous slope of the probe current-voltage characteristic. Since this measurement is not affected by fluctuations in rocket potential it can be more useful in determining the electron temperature than the actual current voltage characteristic.

2. The probe assembly

Fig.13 illustrates the probe assembly used on most of the experiments. The sensor is a stainless steel ogive with a base diameter of abou 1" separated from the guard by the insulator. The teflon piece which insulates the probe assembly from the rocket body is shaped to mate with the nose cone of the rocket. Electrical connections to the sensor and the guard can be made by means of the long bolt which is screwed in at the centre and the guard leads. A connector can be used at the end with its shield connected to the guard leads through a metal ring and the central conductor connected to the holt by means of a pin.

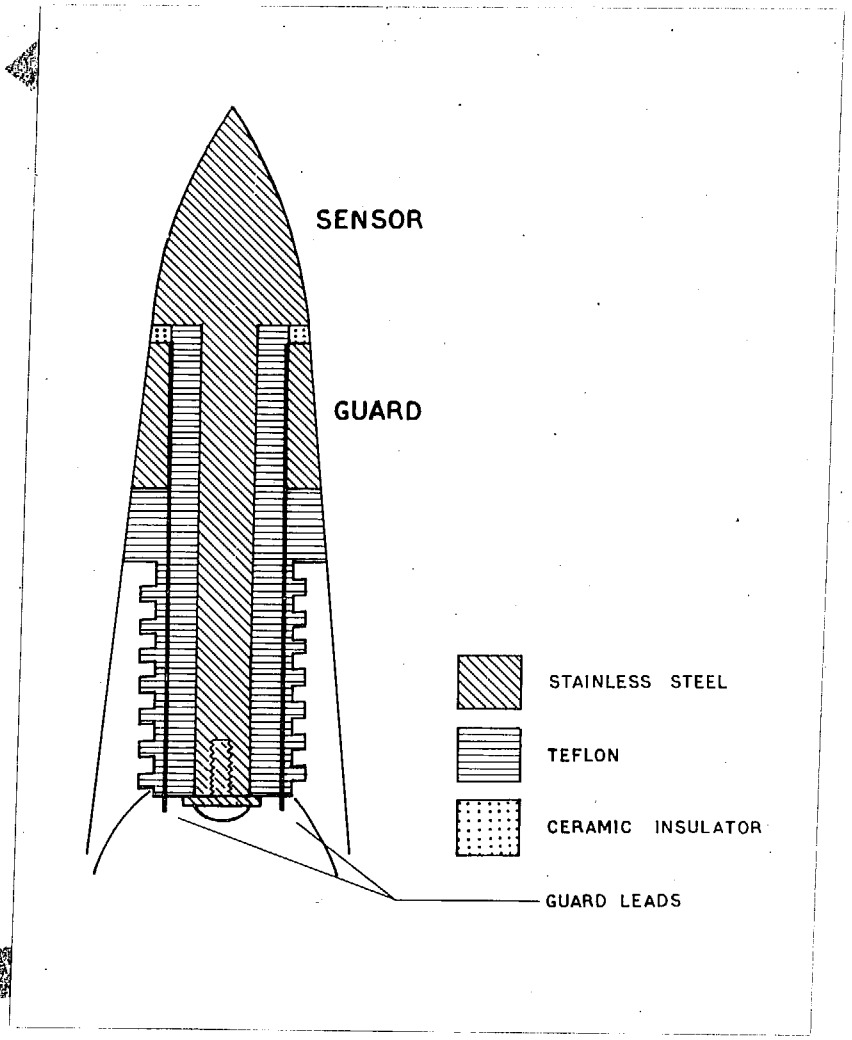

Fig. 13: The Langmuir probe assembly

An insulator with height 1" was used in the early flights. Later it was felt that charge build up in the neighbourhood of the insulator can affect electron temperature measurements. The ideal size of the insulator would be such that while it electrically insulates the sensor from the rest of the system it is not physically seen by the charges in the ambient medium. Therefore an insulator with smaller height was preferred and the height reduced from 1" to 1/8".

Aerodynamic friction causes considerable heating at the nose tip during the rocket flight and the materials used for the electrodes and the insulators must be able to withstand the resulting high temperatures. Stainless steel was considered adequate for the electrodes. In the case of the insulator, in addition to its ability to withstand high temperatures the material should have high insulation properties as well as mechanical strength. There is a rather limited choice of materials. Ceramic insulators (99% Alumina) have been sucessfully used. The 1" insulators used in the early experiments were made of ceramic and were obtained from the Ceramic grinding Co.of Massachusetts U.S.A. But insulators of height 1/8" could not be made to order. Boron nitride which has the required insulating properties and which can be easily machined was experimented with. But it was found to be hygroscopic and create leakage problems. In later experiments teflon has been used. Teflon can be easily machined and shaped. It has the added advantage that it is impervious to moisture and other contaminants such as grease and dirt. Attempts are being made to use mechinable ceramic and bake the insulator at a high temperature.

The probe system was fitted to the rocket nose cone in the final stages of rocket assembly. Connections to the sensor and the guard were made and the probe assembly screwed into the nose cone. While the shape and the size of the sensor are not quite ideal from the theoretical point of view, it has many practical advantages. It makes the system mechanically simple and no special release mechanisms or opening devices

are required. Since the sensor is at the nose tip its performance is not affected by the flow of gas around the vehicle, except when it goes into the wake. The surface area of the sensor is large enough to collect measurable currents.

3. Probe electronics:

The probe electronics consists of a regulated power supply a sweep generator, an electrometer amplifier and the subsystems needed for telemetry. The latter include voltage controlled oscillators with associated filters, the mixer and the telemetry transmitter with its power supply and the antenna assembly. Since the present Langmuir probe system works on a floating power supply the reference level of the amplifier does not remain fixed with respect to the rocket body during a sweep and the amplifier output can not be directly fed to voltage controlled oscillators working on a different power supply. Hence the voltage controlled oscillators and the filters form part of the Langmuir probe system. The a.c signals from the filters or the composite a.c from the mixer is brought out of the system and allowed to modulate the radiofrequency from a transmitter.

The transmitters used on most of the experiments were standard commercial transmitters delivering 2 watt power at a frequency in the neighbourhood of 240 Mhz.

3.1 The regulated power supply: The transistorised regulated power supply shown in Fig.14 is used to obtain voltages V_A' + 18 volts, V_A' and V_A' - 9 volts needed for the probe electronics from a floating battery.

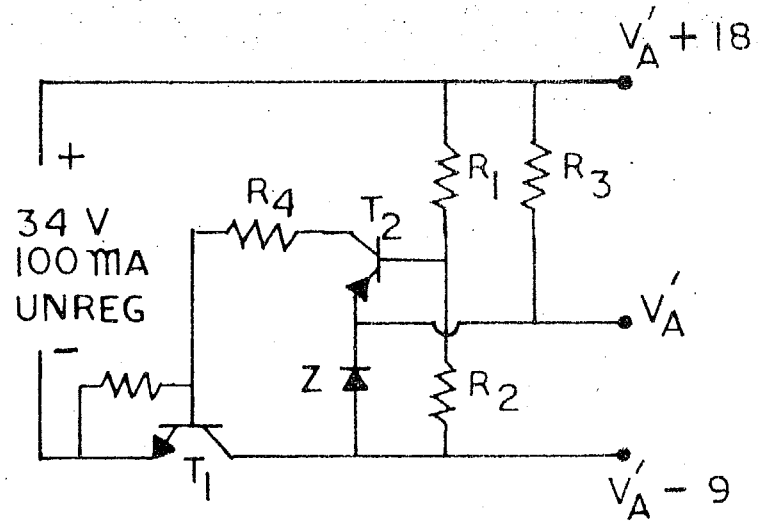

FIG. 14 TRANSISTORISED POWER SUPPLY 1

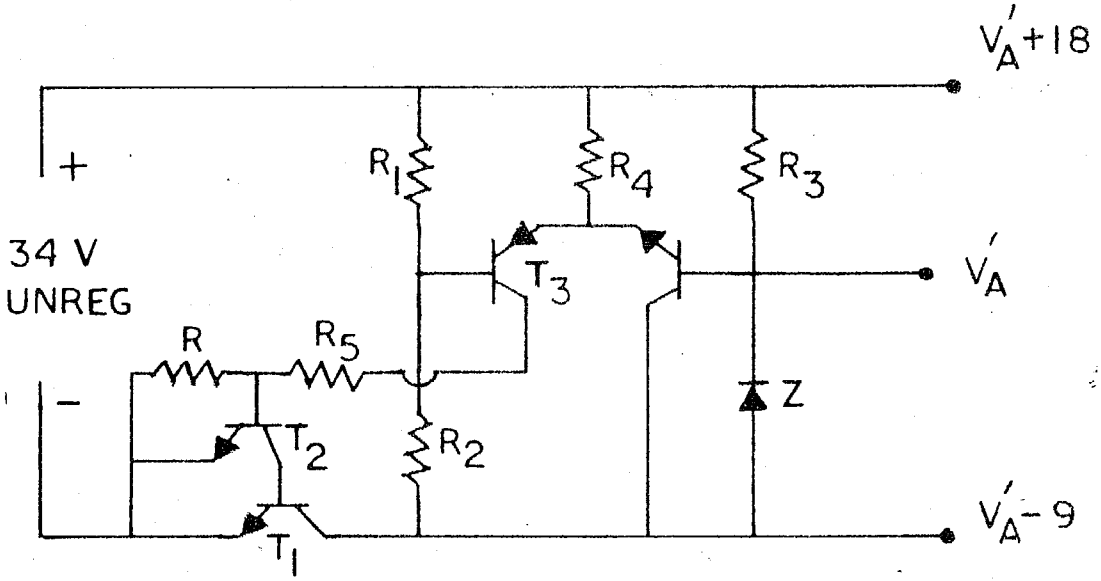

FIG. 15 TRANSISTORISED POWER SUPPLY 2

Using a divider R_1 and R_2, 1/3rd of the total supply voltage is compared with a 9 volts reference voltage. The reference voltage is obtained by using a temperature compensated reference diode IN 935, which required 7.5 ma of current for operation in the plateau region. This is supplied through the resistance R_3. The transistor T_2 amplifies the difference between the reference voltage 1/3rd of the supply. Any decrease in the voltage makes T_2 more conducting which in turn makes the series transistor T_1 more conducting and decreases the voltage at B. This keeps the supply voltage across AB well stabilised. Table shows the degree of stabilisation that can be obtained from this simple circuit.

Table: Regulation characteristics of the power supply shown in Fig.14.

V_{IN}	V_{out} No Load	V_{out} at Load	
39V	27V	26.9V	40 ma
34V	26.95V	26.9V	35 ma
29V	26.9V	26.85V	30 ma

In this table V_{IN} represents the unregulated input voltage. V_{out} is the regulated output. The table gives the regulation characteristics both for variations in input voltage as well as for loaded conditions.

The above power supply was used in some of the early experiments where the current requirements were small (30 ma). In later payloads with the addition of new subsystems the current

requirements of the payload increased and the power supply had to be modified to the one shown in Fig.15. In this powersupply the one transistor amplifier T_2 of Fig.14 is replaced by a two transistor difference amplifier T_3 and T_4 and the base current of the series transistor T_1 is fed through T_2. This circuit was capable of giving regulation upto 100 ma.

3.2 The sweep generator: Fig.16 shows the sweep voltage that is to be applied to the sensor. Such a voltage function can be obtained either by generating the linear sweep AB and the constant voltage BC separately and programming the

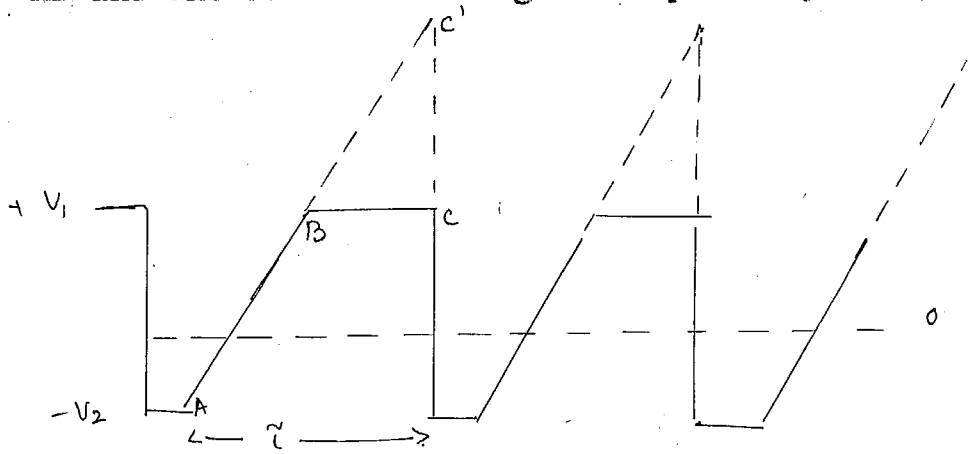

Fig.16: Programming of the probe voltage

probe voltage between the two as required or by generating a sweep ABC' for the total time interval secs and clipping it at the level of BC. The present sweep circuit adopts a procedure similar to the latter.

A linear wave form was obtained by charging a condenser through a resistor across which a constant potential difference was maintained, by suitable feedback networks. Fig.17 shows the actual circuit used to obtain the required

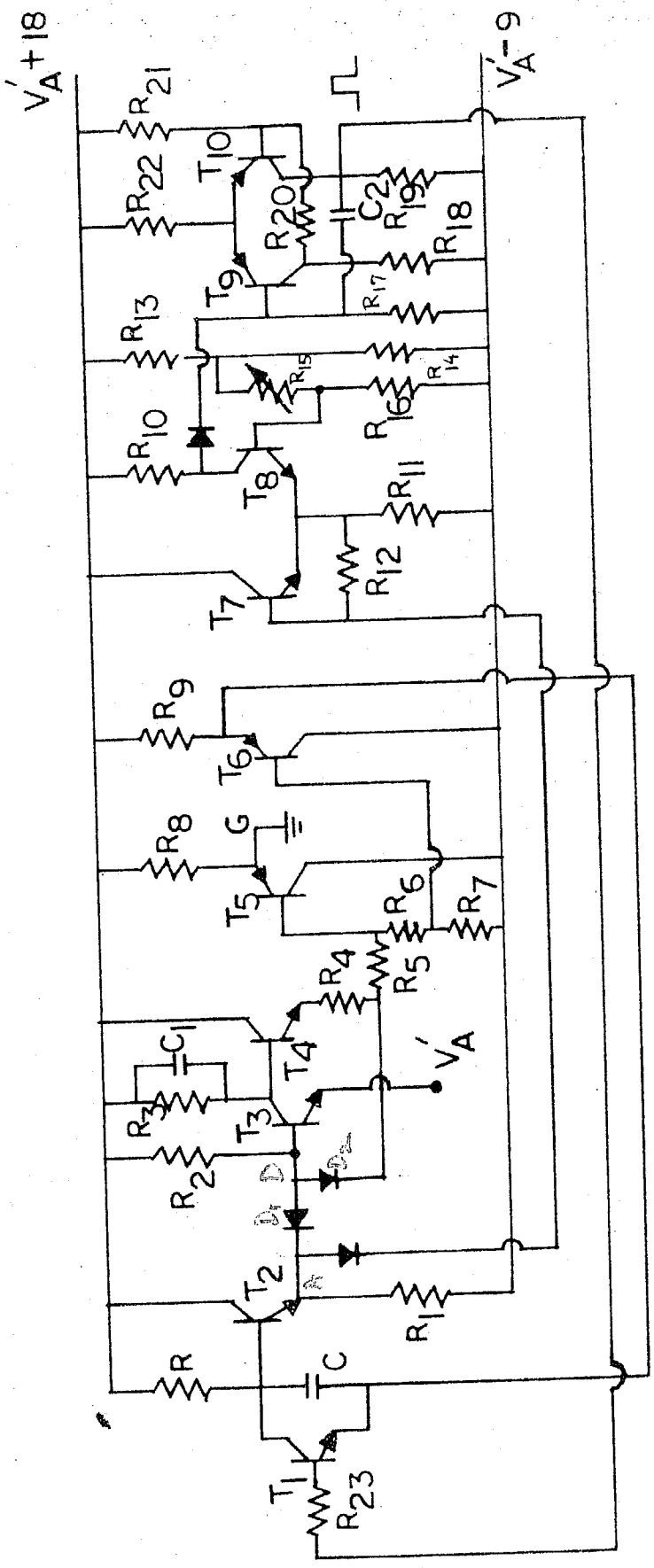

FIG. 17 SWEEP GENERATOR

sweep voltage. R and C form a charging network with a fairly large time constant. T_2 is an emitter follower and the diode network D_1 D_2 selects the smaller of the voltages at A and B. The selected voltage at D is fed to the base of T_3 whose emitter is connected to the reference voltage V_A'. When the voltage at D is larger than V_A' the difference is amplified and a fraction of the output controls the potential V_2 to which the condenser C is returned, through the emitter followers T_4 and T_6. As the potential at D rises due to the charging of C, that at B falls until V_D and V_B become equal. Till this stage is reached the potential V_2 decreases as V_1 tries to increase thereby maintaining a constant current through the resistance R. Hence both V_1 and V_2 vary linearly with respect to V_A'. When V_D becomes equal to V_B V_2 no longer varies and the waveform at V_1 is exponential. This is not seen at the output of T_3 and hence at G. The net wave form between V_A' and G is as required in Fig.16.

Termination of the sweep and restart of the sweep cycle is generally obtained by discharging the condenser through a suitable low resistance path after the lapse of the required time or when the condenser voltage reaches a predetermined value. The discharge network can be a unijunction transistor or an ordinary transistor suitably biased or even a small resistance. The choice of the particular network depends upon the leakages allowed, the sharpness of fall etc. Also in an all electronic circuit it is more straightforward to sense a voltage than a time interval. The present sweep circuit

utilises a difference amplifier and a monstable multivibrator and the termination of the sweep is effedted by a low leakage transistor.

The difference amplifier T_7 - T_8 triggers the monostable multivibrator T_9 - T_{10} when the voltage at A exceeds a value determined by the bleeder network R_{13}, R_{14}, R_{15} and R_{16}. The pulse from T_{10} makes the transistor T_1 offer a low resistence path to the condenser voltage V_1. The pulse from T_{10} lasts for 50 milli secs, a time large enough to ensure complete discharge of the condenser before the start of the next cycle.

3.3 Electrometer amplifier: Typical currents expected during a Langmuir probe experiment vary from 10^{-10} amp to several tens of microamps. Such small currents can not directly operate a telemetry system. The required current amplification is generally obtained by using an electrometer amplifier. In an electrometer amplifier the current to be measured is passed through a suitable resistance and the voltage across the resistance measured by means of a suitable amplifier (Fig.18). The voltage drop in the amplifier set up is negligible and the instrument becomes essentially a current meter. The value of the resistance used should be such that the low currents to be measured produce appreciable voltage drops. Hence the input stage of the amplifier should have a high imput impedance. Hence an all transistor amplifier generally does not serve the purpose. Vacuum tubes have to be used at the input stage. For very low current measurement

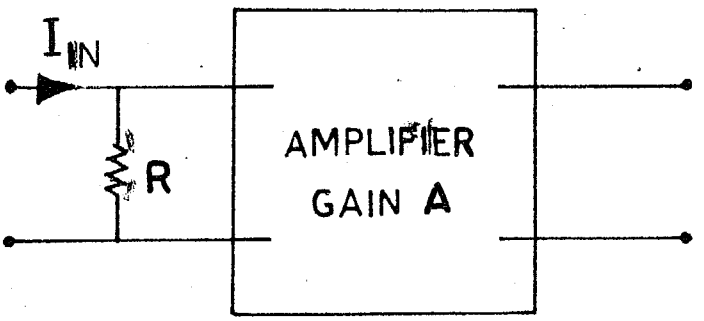

$R_{IN} \simeq R$

Fig 18 : Measurement of small currents by a simple voltmeter

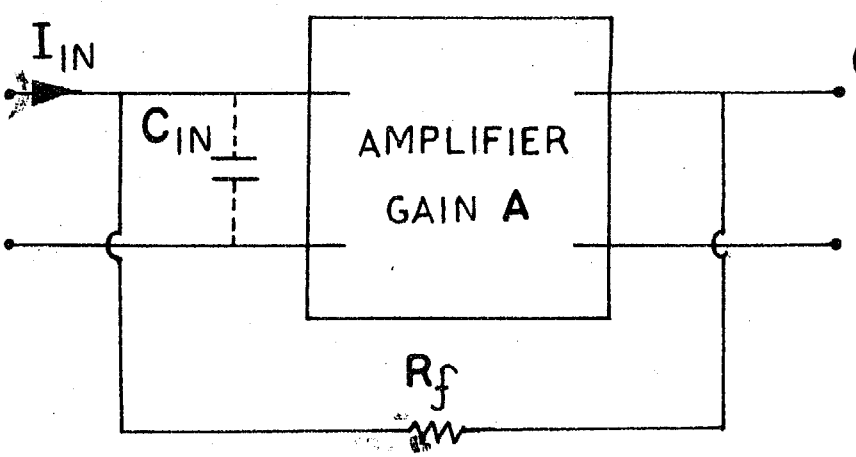

$$R_{IN} = \frac{R_f}{A+1}$$

Fig 19 : A 100% negative feedback bypass for high current measurements

special electrometer tubes with grid currents less than 10^{-12} amp are available. Typical electrometer tubes are Raytheon CK 5886, CK 5889, Philips 4067 etc.

More recently a special type of transistor known as the field effect transistor is becoming commercially available. Different types of field effect transistors depending upon the process of manufacture are available (Cullis 1965). They are all voltage controlled devices and are therefore more nearly equivalent to vacuum tubes than the more common bipolar transistors which are current controlled devices. The input impedance of a field effect transistor is that of the reverse biased gate diode and is therefore high. Typical gate currents are of the order of 10^{-9} amp. (A recent type of field effect transistor known as the MOSFET is reported to have typical gate currents of the order of 10^{-14} amp) So field effect transistors can effectively replace electrometer tubes. The smaller size and the low power consumption of the field effect transistor makes it a much more convenient component than the electrometer tube. Moreover when used in a d.c amplifier it eliminates drifts due to filament voltage variations, even though there exists a drift term associated with the leakage current of the reverse biased gate diode.

The basic considerations in the design of an electrometer amplifier are stability, frequency response and signal to noise ratio. Use of negative feed back reduces zero drifts considerably even though it does not give large voltage gains (ex. Bode: 1945). The frequency response problem can be illust-

treated by taking a typical example. If an amplifier is designed to measure currents of the order of 10^{-10} amp the input impedances will be of the order of 10^{+10} ohms. Even in the absence of external capacitances and stray capacitive effects (which can never be completely eliminated) there is always the input capacitance of the electrometer tube or the field effect transistor which is of the order of a few picofarads. Assuming a typical value of 5 pf at the input of the amplifier one has an RC combination with a time constant of 50 millisecs. Hence the amplifier is insensitive to frequencies more than 20 cycles per second. Such a system would not be useful in many applications. In the present case it would not be suitable for retarding potential analysis of probe current, study of fine structure in probe current profile, etc. Here again the use of negative feedback very much improves the situation. Refering to Fig.19 the effective input impedance of an amplifier which utilises 100% negative feeback is given by

$$R_{IN} = \frac{e_{IN}}{i_{IN}} = \frac{R_f}{A+1} \qquad (15)$$

Since the input impedance is effectively reduced by a factor (A + 1) the frequency response of the system goes up by the same factor. Hence a high frequency response can be obtained by having large loop gains. Since gains of the order of 10^4 are not uncommon the use of negative feedback solves the problem of frequency response. (In the above illustrated example even a loop gain of 100 would give a frequency response up to 2 khz which is adequate for the present investigation. For large

loop gains the sensitiveness of the system is equal to that of a voltmeter with a shunt resistance R_f and as long as the circuit is used with a current source the drift is the same as that of the voltmeter of Fig.18 (Praglin and Nicholas, 1960).

With large loop gains there will be a tendency for oscillations. Stabilising networks have to be used to prevent them. Internal as well as external networks are used. Internal networks consisting of feedback capacitors give stabilisation to each stage while external networks give overall stability.

Signal to noise ratio: In an electrometer amplifier of the type under consideration the only important source of noise is due to internal noise generators in the electrometer tube or the field effect transistor at the input stage. This source is generally unaffected by the circuit capacitances, the noise source remains constant over a wide band of frequencies and is amplified from stage to stage as the forward gain increases. Therefore it can be bothersome beyond a certain frequency. Praglin and Nicholas (loc cit) have shown that if 'S' is the tolerable signal to noise ratio the amplifier gain (A) should not be increased beyond a value given by

$$A = \frac{i_{IN} R_f}{S e_n} \qquad (16)$$

where e_n = noise source amplitude, considered as a voltage generator. Typical values for e_n are a fraction of a μv for electrometer tubes and a few μv, up to a maximum of about 10 for field effect transistors.

At $i_{IN} = 10^{-8}$ amp with $R_f \simeq 5 \times 10^7 \Omega$ $i_{IN} R_f \simeq 0.5$ V

If $e_n = 1\mu V$ from eq 16 the max allowed gain is

$$A = \frac{0.5}{5 \times 10^{-6}} = \frac{5 \times 10^5}{S}$$

with S = 500 this gives an upper limit of A = 1000.

Electrometer tubes have much smaller noise figures than field effect transistors even though low noise field effect transistors are available recently.

Fig.20 shows an electrometer amplifier employing field effect transistors which was used in some payloads. The input stage is a difference amplifier (T_1, T_2) using field effect transistors Crystalonics 2N 3084 which is an N channel epitaxial device with a rated maximum grid current of 10^{-10} amp. (For the Crystalonics series of field effect transistors the manufactuers use the terms anode, cathode and grid to represent the three terminals of the transistor). It is therefore suitable for measuring currents down to at least 10^{-9} amp. The characteristics of different pieces of the same type of field effect transistor from a given sample, were found to differ considerably from one another and from the manufacturers published data. Hence characteristics were determined for individual transistors and pairs with nearly identical characteristics were selected for use in the difference amplifier. From the pair, the transistor with lower grid current was selected for the input transistor T_1. Quiescent conditions for the amplifier were determined from the experimentally drawn characteristics of the pair. For a N channel device, looking from outside the

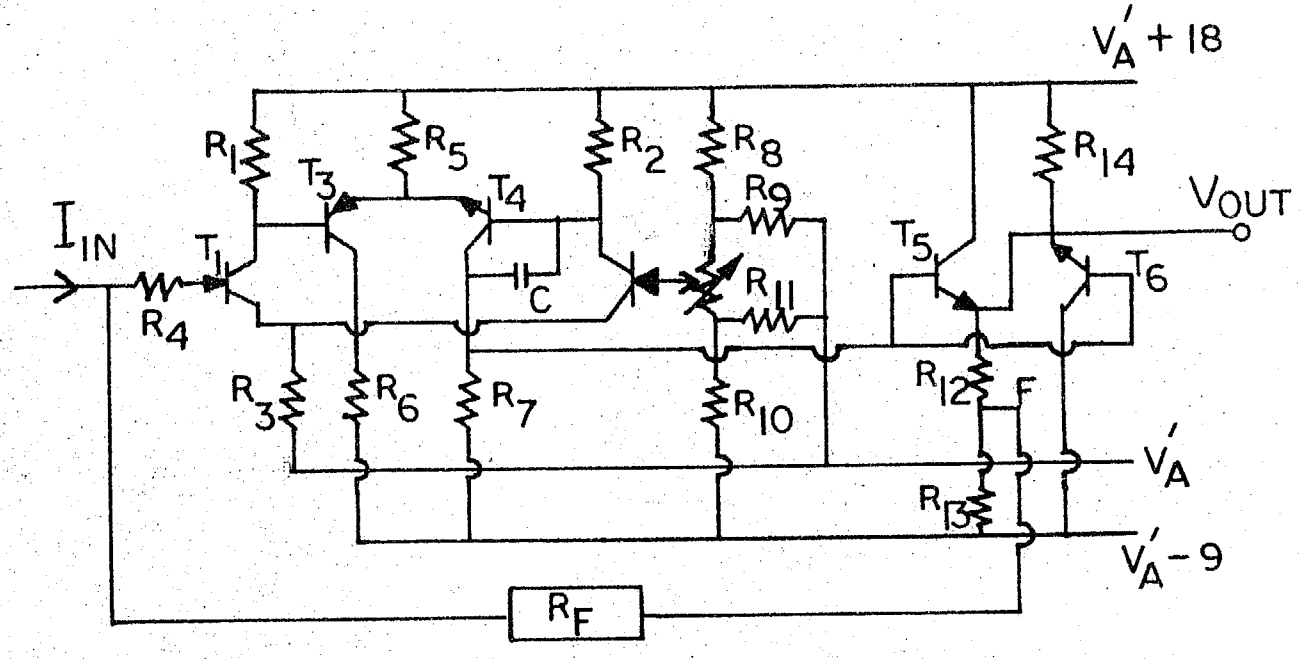

FIG. 20 ELECTROMETER AMPLIFIER USING FIELD EFFECT TRANSISTORS

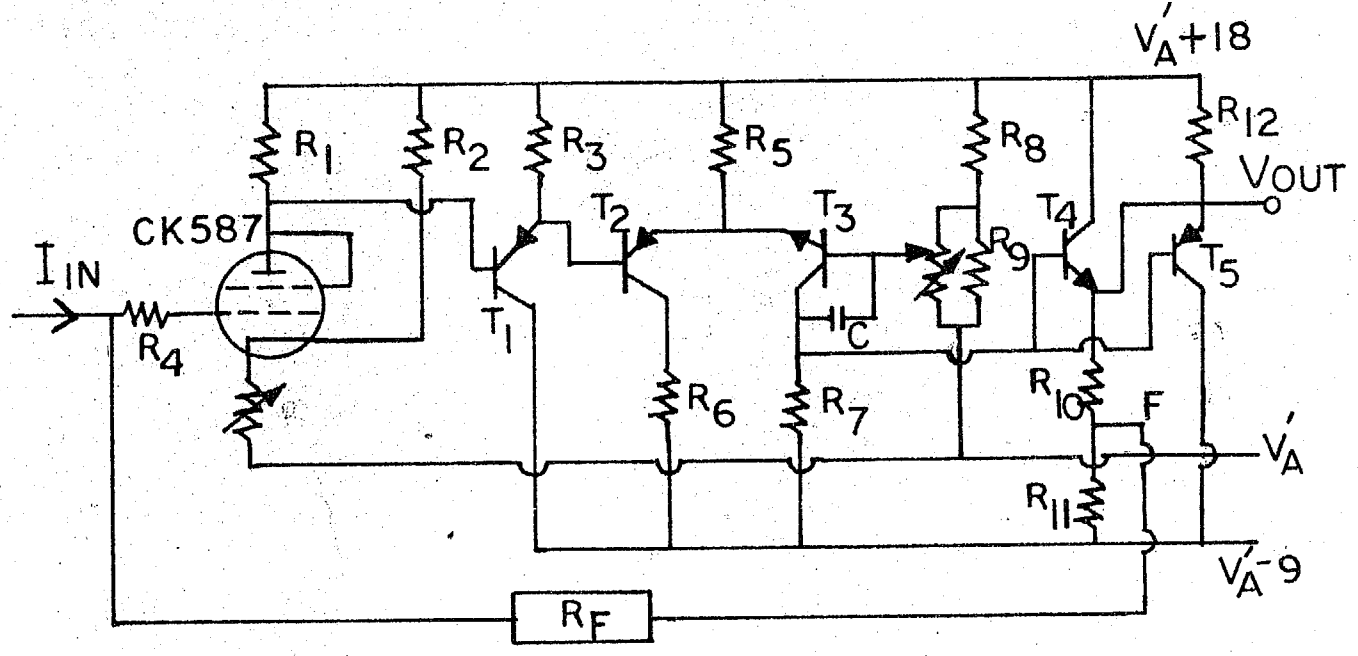

FIG. 21 SINGLE ENDED ELECTROMETER AMPLIFIER USING ELECTROMETER TUBE

transistor the grid current is a positive current flowing out of its grid. Its value increases with increasing negative bias. Hence steps were taken to avoid a large negative bias of T_1. The operating point of T_1 is determined such that it is in the linear range of operation and the grid current of T_1 is small and the values of the resistance R_1, R_2 and R_3 in Fig.20 calculated.

The transistor difference amplifier (T_3, T_4) gives most of the loop gain of the amplifier. When the anode currents of (T_1, T_2) are small interstage emitter followers employing low leakage transistors are used. The voltage drop across the common emitter resistor R_5 is decided by the previous stage. For a given R_5 maximum gain can be obtained by directly connecting the collector of T_3 to the negative supply and using a large value of R_7, the collector resistance of T_4. But a small resistance R_6 is used at the collector of T_3 to protect it from large current changes. The values of R_5 and R_7 are calculated from considerations of the total voltage swing expected at the output (and hence at the collector of T_4) and the loop gain needed. The feedback condenser between the collector and base of T_4 reduces the tendency towards oscillations.

(T_5, T_6) is an emitter follower stage using a NPN, PNP pair of transistors. It gives a very low output impedance. Nearly 100% feed back is given from a suitable point on the emitter resistor of T_5. The actual feedback point and therefore

the percentage feedback is determined by an constraints on the value of the amplifier output for zero input current.

Fig.21 shows a single ended electrometer amplifier employing an electrometer tube, Raytheon CK 587 with a rated grid current of less than 10^{-14} amp which was used in some of the experiments. It has better signal to noise ratio and can be used to measure smaller input currents depending upon the feedback element used. But a difference amplifier stage at the input as in Fig.20 would give better stability.

The feedback element: The amplifier is required to cover a wide range of input currents. But the output of the amplifier is limited by supply voltages and considerations of telemetry requirements. In such cases it is customary to use an amplifier which has a non linear input - output relationship or employ a range switching device in which the sensitiveness of the amplifier is sequentially increased or decreased as the input current decreases or increases.

In order to obtain a nonlinear relationship between input current and the output voltage a nonlinear feedback element is used. A logarithmic device such as a thermionic diode operated in the space charge region or a sillicon junction diode operated over a narrow portion of the forward biased region is common in some applications. It gives a relationship of the form

$$V_{out} = A \log I_{IN} + B \qquad (17)$$

where A and B are constants.

While such an element covers a wide range of input currents (about 5 to 6 orders of magnitude) the compression produced is too large for the present purpose.

The present requirements are :-

(i) Currents from 10^{-9} amp to several tens of micro amperes must be measured. (ii) The output voltage should be measurable at the lowest current 10^{-9} amp, a value of 0.05V or more would be convenient. (iii) The output voltage should attain nearly the maximum available value (5 to 10V depending upon the amplifier design) for a current of about 10 a.

Smith has used thyrites in a similar experiment (1964). A thyrite or a varistor is a non linear resistance material such as silicon carbide in which the current varies as a power of the voltage across it.

$$I = KV^n \qquad (18)$$

The exponent n depends upon various factors in the manufacturing process (in addition to the composition of the material). It has a minimum value lying between 1 and 2, and increases with voltage. In special cases n may be as high as 6. (The higher the value of n the more nonlinear is the device). The constant K depends upon the dimensions of the thyrite. It is proportional to the area available for flow of current and varies inversely as the thickness. It is possible to choose a proper thyrite to suit the required purpose.

Some of the general Electric thyrites such as 65D5010, 67D5010 and 68D5010 can generally handle currents in the range

10^{-9} to 10^{-5} amp. Depending on the experimental circumstances different types and some times different combinations of these were used to get optimum results. Fig.22 shows the characteristics of one such set used in one of the flights. Even thyrites of the same type were found to differ markedly from one another in characteristics. The potential - current curves were drawn separately for individual pieces and suitable ones were selected. Thyrites which showed a polarity effect (voltage across it depending on the current direction) were rejected.

A disadvantage of thyrite is the fairly high dielectric constant (30-100) of its material. Hence the use of a thyrite would introduce considerable capacitance along the feedback and affect the frequency response of the amplifier. (The thyrites used were found to be unsuitable for frequencies greater than 3 khz). Also in general the use of any non linear element affects the frequency response of the amplifier since adequate compensation will not be possible for its distributed capacitances.

Amplifier zero: An inflight calibration of the amplifier output corresponding to zero input current will make data reduction easy and also give a useful check for amplifier drifts and leakages in the system. Such a calibration can be made either (i) by introducing a relay at the input of the amplifier which cuts off the input to it by disconnecting the sensor from it for a given interval of time (τ = 50 millisecs) at the end of every operational cycle or

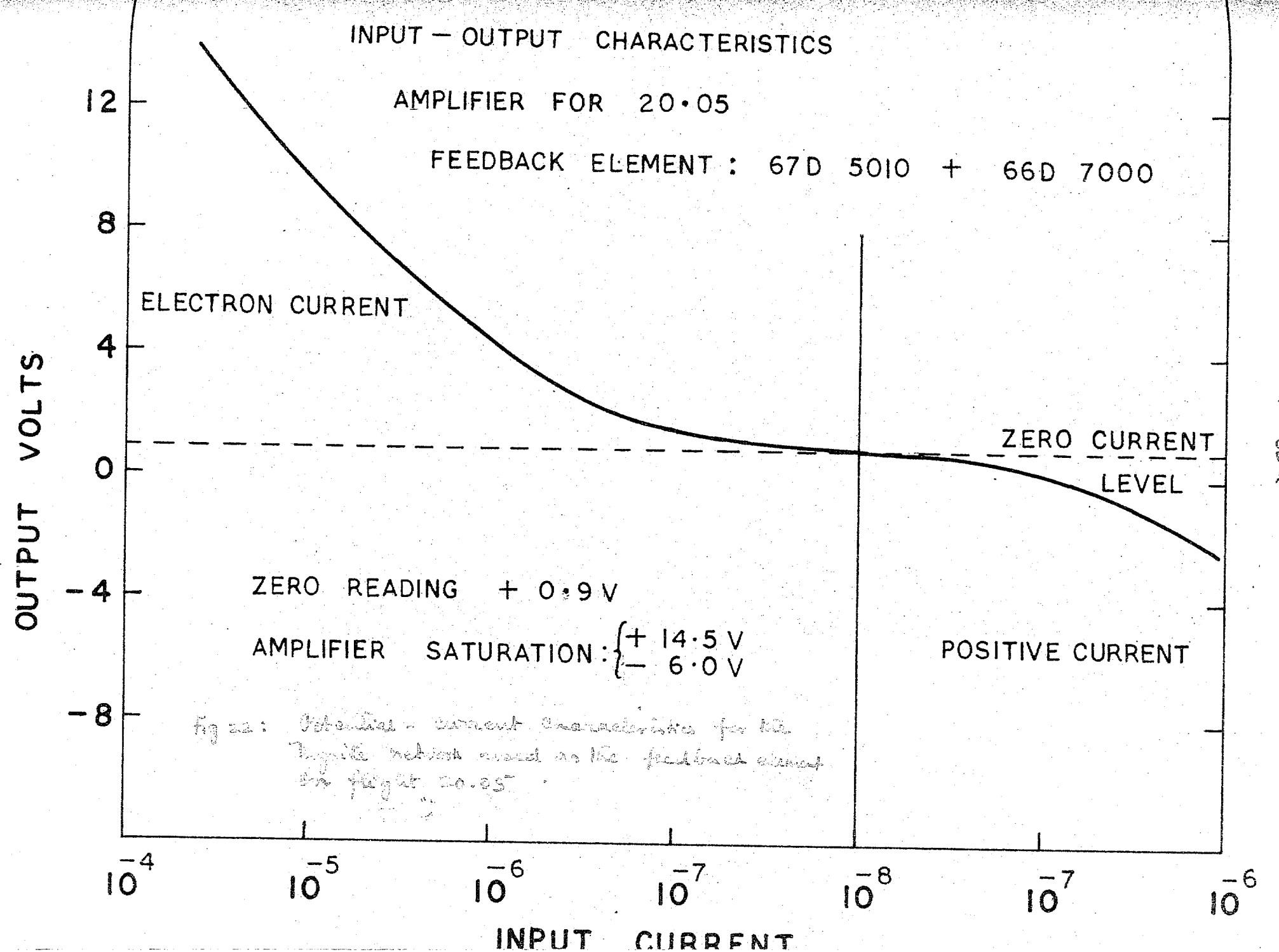

fig 22 : Potential - current characteristics for the Triplite network around the feedback element for flight no.05.

(ii) by using the relay to short the feedback element for the required time.

Fig.23 shows the circuitry used to obtain the calibration mark. The pulse from the monostable multivibrator (T_1, T_2) with a time constant of about 50 mili - secs, drives the relay through the current amplifier T_3 at the end of every Langmuir probe cycle. The relay was obtained by winding a coil around a G.E. reed switch (DR - 100); it required a current of about 10 ma at 6V.

3.4 Output channels: The amplifier has linear response in the output range of -6V to +12V. In order to get optimum information efficiency the entire range of output voltages was utilised to cover a current range of about 1 a for positive current and 10 a for electron current. (A large margin is given to accommodate larger positive currents to the probe which may arise due to photoemission, degassing etc.) The output was telemetered on two channels:- one with high sensitiveness which would give good resolution even at low input currents and the other with lower sensitiveness which would be useful for large probe currents. The amplifier output is directly fed to the higher sensitive channel after passing it through a suitable limiting network. Most of the voltage controlled oscillators used could cover a range of -0.3V to + 1.2V. So the limiting network limited the voltage fed to the VCO within these limits. The lower sensitive channel was fed by the amplifier output after passing it throgh a dividing network where the output was reduced by a factor of

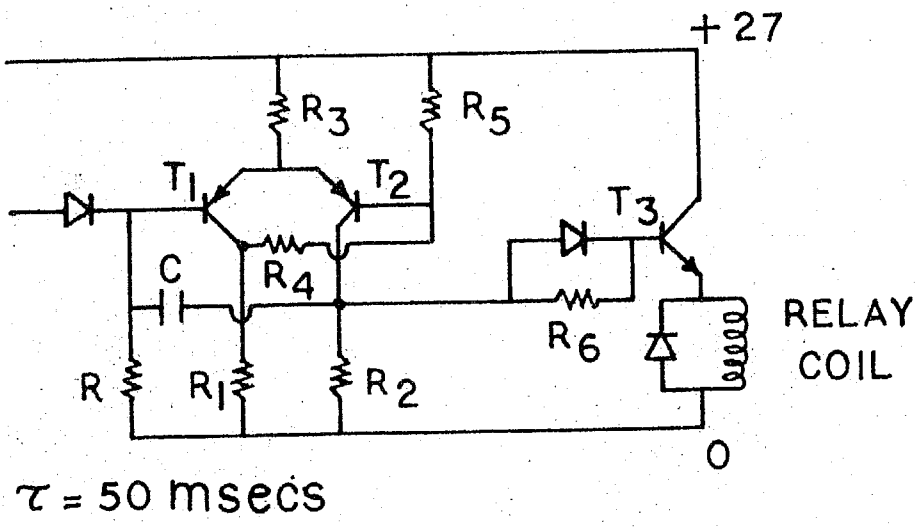

Fig 23. Circuitry used to obtain the calibration mark

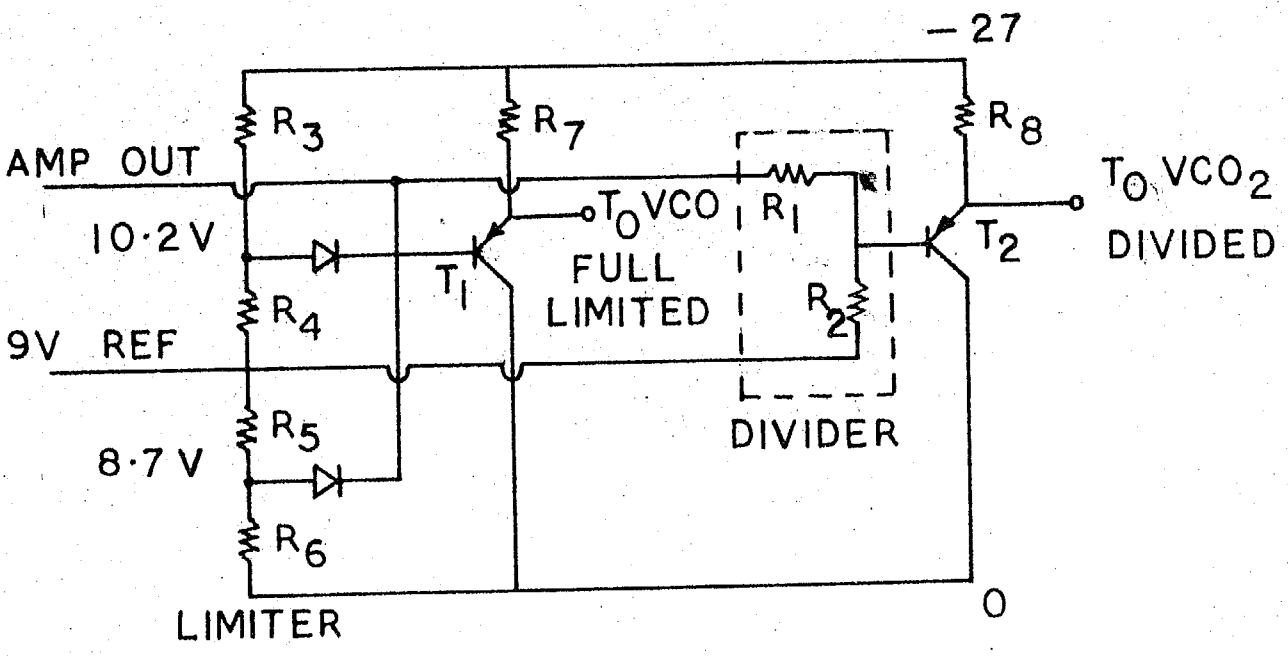

Fig 24: Divider and limiter networks.

about 10. This channel gives useful information even after the higher sensitive channel saturates. Fig. 24 shows the arrangement used.

When the number of channels available is limited and two channels are not available for telemetring Langmuir probe data the sensitiveness for the system can be switched between high and low every alternate cycle by using a relay as shown in Fig. 25. The same can be effected without disturbing the amplifier by using a system shown in Fig.26. In this system R_1 and R_2 form a dividing network when T_1 and T_2 are both conducting (every alternate Langmuir probe cycle) and the sensitiveness of the channel will be low. When T_1 and T_2 are both not conducting (which happens for every other alternate cycle) the full signal with a little attenuation determined only by the leakage current in T_3) is fed, and the sensitiveness of the channel is high. Complete circuitry for both these systems was developed and tested.

3.5 Subcarrier oscillators: The amplifier output is converted into a suitable frequency which can be telemetred on one of the IRIG subcarrier channels using voltage controlled oscillators. Selection of the particular subcarrier channel depends upon the intelligence frequency needed. The intelligence frequency is generally 20% of the band width on the subcarrier channel, which in most cases is generally $\pm$ 7.5% and in some cases $\pm$15% of central frequency. The minimum intelligence frequency needed for a Langmuir probe experiment is decided by the slope in the retarding potential region of

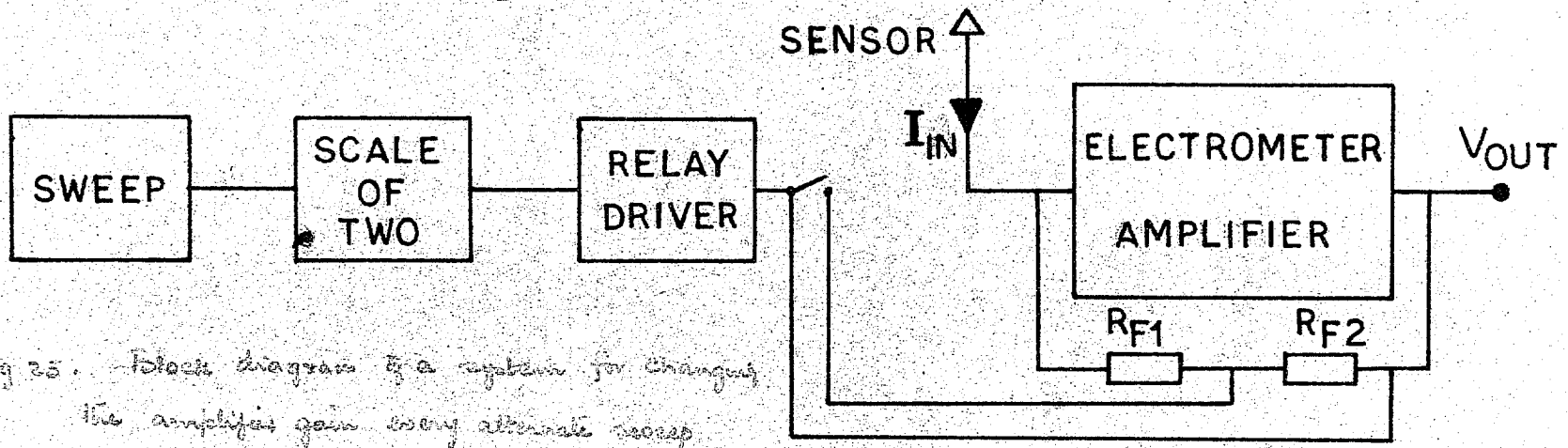

fig 25. Block diagram of a system for changing the amplifier gain every alternate sweep cycle

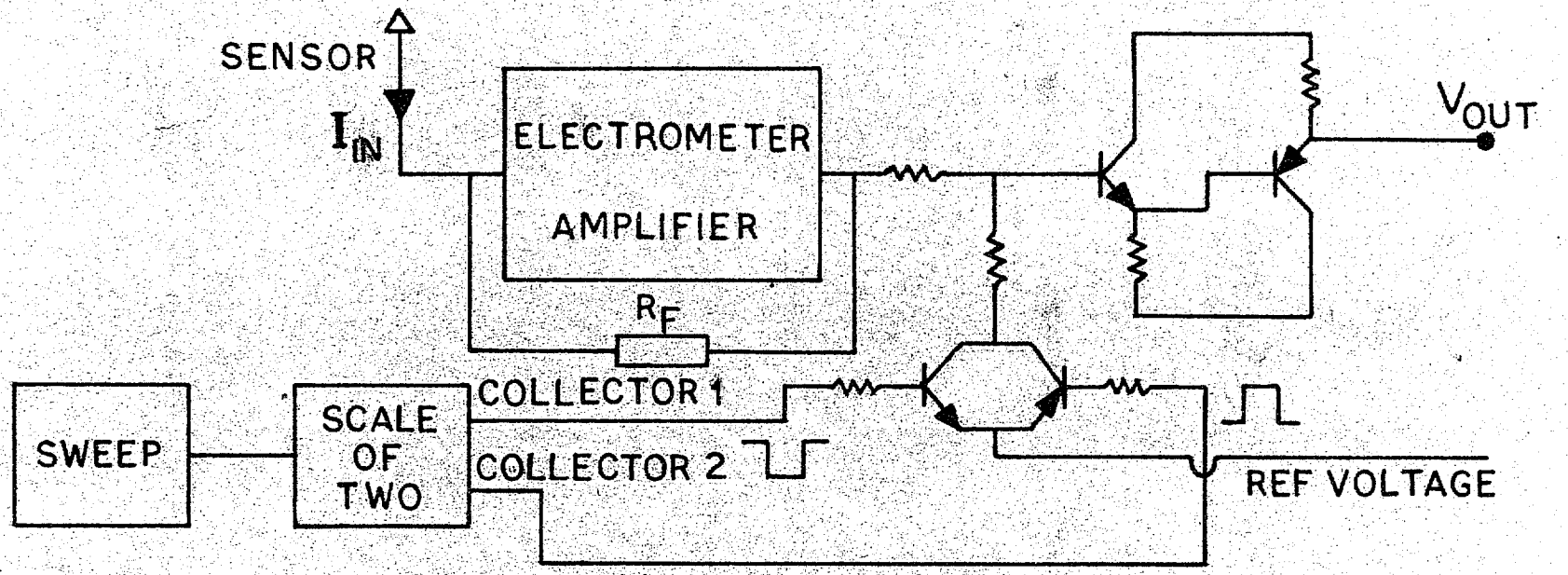

fig 26. Block diagram of a system in which the gain is changed every alternate sweep cycle without disturbing the amplifier

the probe characteristic. An electron temperature of 200°K corresponds to a mean electron energy of 0.023V. If this is to be faithfully recorded in a sweep of 10V an intelligence frequency of about 450 Hz is needed. This needs a central frequency of about 30 khz or more for a maximum deviation of ± 7.5%.

Multivibrator type of voltage controlled oscillators* where used because of their stability and reliability. In fig.27 T_2, T_3 form a multivibrator whose frequency varies when the voltage input to the base resistors R_4 and R_5 is varied. The frequency Vs input voltage relationship is linear within a certain range of input voltages. Limiting the collector voltage swings to a convenient value using diodes gives a good waveform at each collector and also frequency stability. The transistor T_4 and the network, (R_9, C_3), functions as a low pass filter which decreases the harmonic content.

Adjustments and precauation for the voltage controlled oscillators: The maximum value of the feeding resistor (R_4, R_5) which will give good square waves at the two collectors over the required range of input voltages is determined. A suitable value below this maximum is used The coupling condensers C_1 and C_2 and if necessary the values

---

* The voltage controlled oscillators used on most of the flights were developed by the author's colleague Mr. S.P. Gupta.

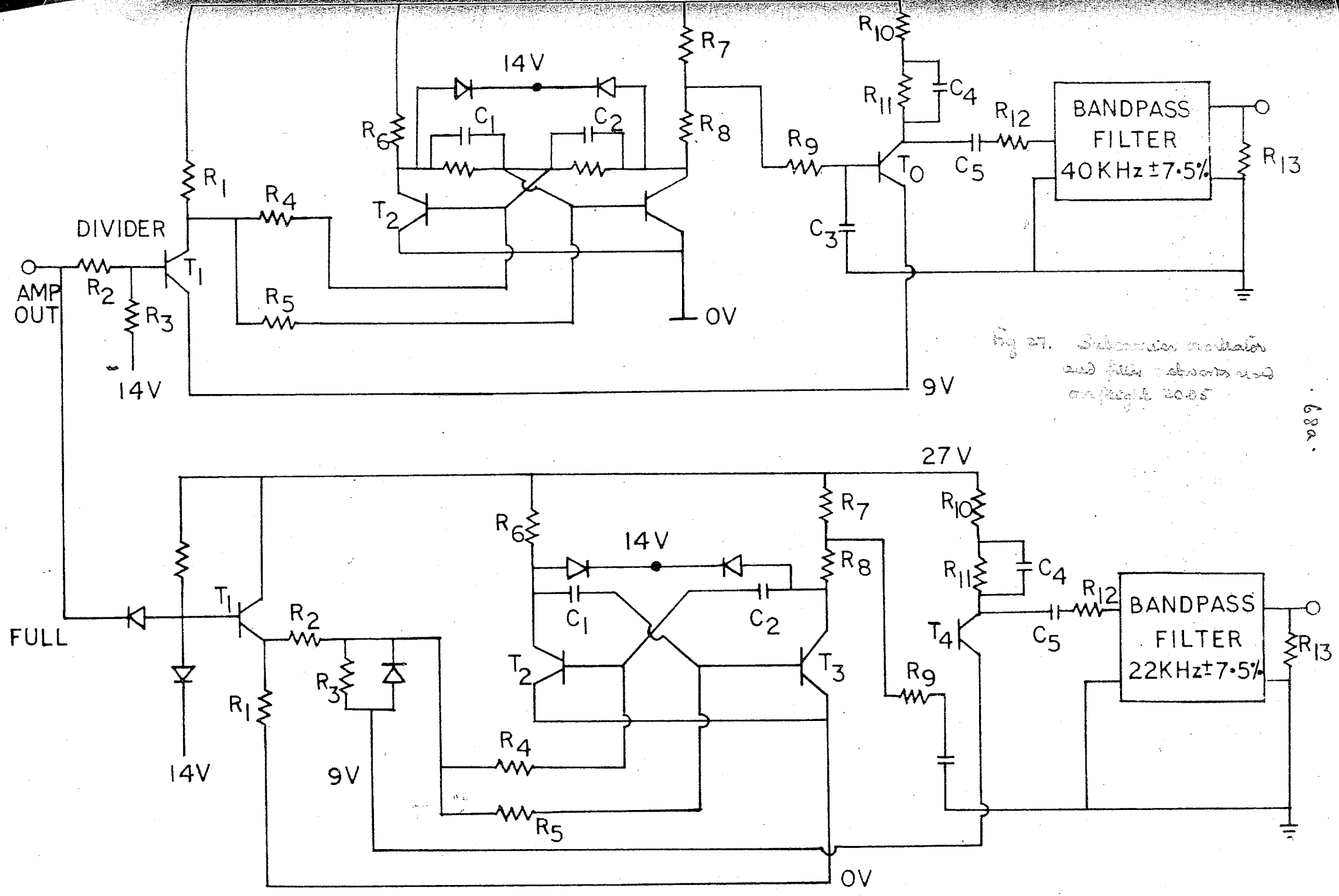

Fig 27. Subcarrier modulator and filter boards and output 20.05

688.

of the resistors R_{14} and R_{15} are adjusted to give the required frequency and bandwidth. Once the central frequency and bandwidth are adjusted the oscillator is tested for linearity by feeding different voltages at the input and measuring the frequency on a frequency counter. Figs.28 and 29 show the performance of a set of voltage controlled oscillators used on one of the experiments (flight 20.05). The voltage controlled oscillators were also tested for stability against temperature variations by enclosing the circuitry in an oven at 150°F for about half an hour. Its performance such as centre frequency, bandwidth and linearity are tested when the circuitry was within the oven.

3.6 Subcarrier filters: In order to prevent any possible inter-channel interference the output of the voltage controlled oscillator was passed through a band pass filter with a pass band of ± 7.5% about the centre frequency. In the early experiments filters employing frequency selective amplifiers with twin T networks (which give a broad null in the pass band) as feedback elements were used. Even though their performance was satisfactory the advantages of using a passive filter were obvious. On some experiments commerical telemetry bandpass filters (U.T.C. and Thordarson & Co) were used. More recently band pass filters using molybdenum permalloy toroidal cores were developed and found satisfactory. These were used on the later experiments.

3.7 The Mixer: When more than one subcarrier channel is being used the signals from the various sub carrier oscillators (after passing through the filters) are mixed in proper propor-

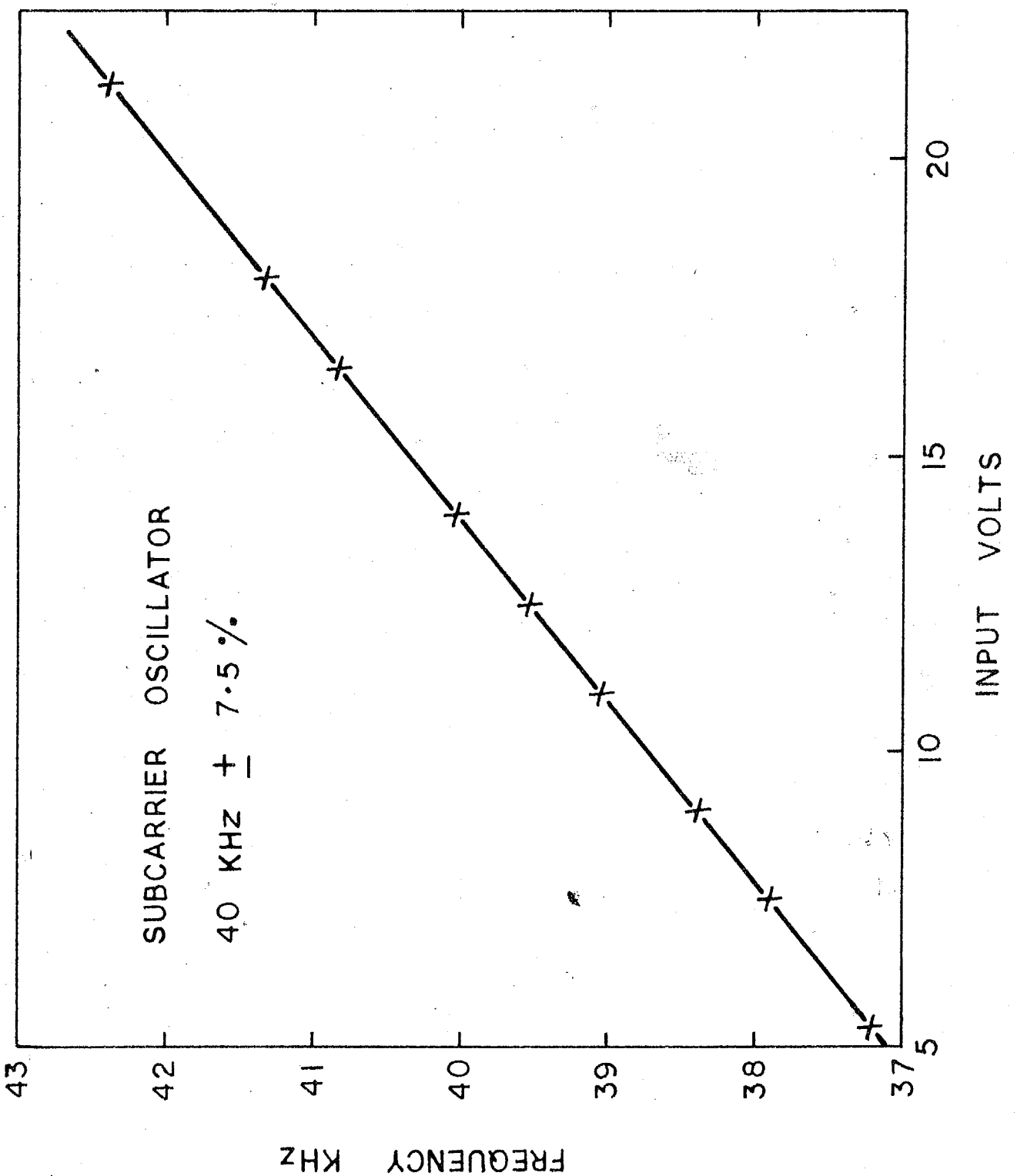

Fig 28. Frequency to input voltage for the 40 kHz subcarrier oscillator used on freight cars

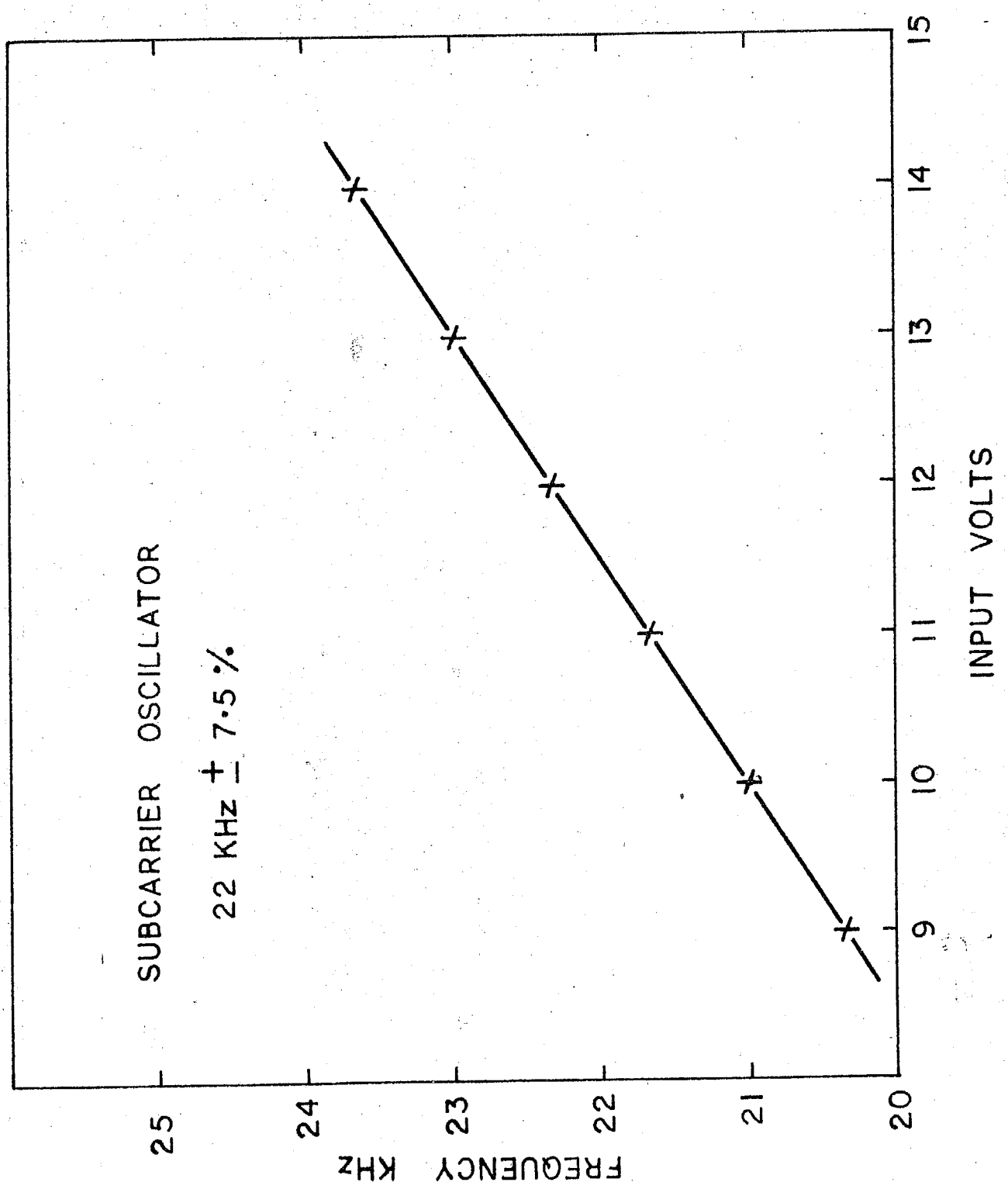

Fig 2.9. Frequency vs Input voltage for the 22 kHz subcarrier oscillator used on flight 20.05

tions before the modulation stage. Both passive and active networks can be used for mixing. When only a small number of channels are used a passive mixer using resistance networks is convenient. The amplitudes of the individual subcarrier frequencies is determined on the following considerations.

The major consideration is the signal to noise ratio. It becomes important if the rf carrier level is low or is expected to become low during the flight. In a FM/FM system the subcarrier signal amplitude to noise ratios will become equal for all channels at the receiver input, if the carrier deviations are proportional to 3/2 power of the central frequency (Leroy Foster 1962). However in practical systems there are other important factors. Unless the carrier deviation due to a given sub carrier channel is above a certain value noise modulation of the transmitter becomes dominant. Generally a minimum deviation of 3 khz is recommended.

So one method of determining the subcarrier amplitudes is to normalise the deviations in the ratio of 3/2 power of the subcarrier frequency subject to a lower limit of 3 khz. The total carrier deviation is determined by the characteristics of the transmitter. For most commercial transmitters in the 215-260 Mhz band the available carrier deviation is 125 khz. So the actual values are adjusted such that the total deviation is 125 khz.

However in many cases the 3/2 power law does not prove to be satisfactory. It gives high subcarrier amplitude ratios between the high and the low frequency channels. For

Example the ratio between the amplitudes of the 10.5 khz and the 70 khz channel will be about 20. Such large ratios in addition to being inconvenient in practice can produce intermodulation. Cross products produced by the high frequency subcarriers have an amplitude proportional to the large amplitudes of the frequencies producing them while the bands with which they interfere are likely to be at low frequencies and hence have low amplitudes. Thus percentage wise the cross product amplitudes may be magnified several times. Therefore compromise systems involving linear taper, or sometimes even a half power taper, have been suggested.

The best method in practice was found to be actual experimental determination of the optimum amplitudes which do not give any intermodulation effects and which give sufficient signal to noise ratio at the receiver input when the transmitter is operated at low power. This method was adopted in the experiments.

3.8 The transmitting system: The telemetry transmitter used on most of the experiments was a commercial transmitter (Bendix or equivalent) which could deliver a power of 2 Watts at a frequency in the neighbourhood of 240 Mhz. The transmitter needed a 130-200V plate supply and a 6V filament supply which were obtained from DC-DC converters fed from Yardney silver cells. The telemetring antennas consisted of four turnstile antennas located in quadrature.

The transmitted signals were received at a ground receiving station. The details of receiving equipment are given on the pages 43-53 of the TERLS hand book (1967).

4. Payload tests:

During flight a rocket payload is likely to be subjected to vibrations and shocks and considerable heating. In order to ensure that the payload performs satisfactorily under such adverse conditions the various subsystems of the probe electronics were individually and collectively subjected to a certain environmental tests. Individual electronic cards, such as the sweep generator, the amplifier, VCO's etc. were tested for proper performance upto temperatures of 150°F. For this purpose the card under test was kept in a constant temperature oven at 150°F for about half an hour to ensure that all the components have attained that temperature. The performance of the circuit was tested at this temperature (with the card still in the oven). When the individual circuit cards are found satisfactory they are potted in Eccofoam (Emerson & Cuming Inc), so that the components are protected from vibration and shocks.

After the individual cards were tested for proper performance the payload was completely assembled and the assembled payload was subjected to vibration tests, by using the shake table facility available at the Thumba rocket range. The payload was generally tested for proper performance up to 200 cycles and 10 g - the limits of the facility at TERLS.

5. Pre launch checks:

The payloads are checked for proper performance after assembly in the rocket and when the rocket is on the launch pad before launch, The prelaunch checks are done using an external battery source and the payload is switched on to the internal batteries only a few minutes before launch to conserve internal battery power. The switching is done using relays situated inside the rocket, but operated from outside. Electrical connections for operating the relay and the various test points from the payload must be brought out of the rocket to the control station. Generally all such connections are taken out of the rocket through a main connector which is called the umbilical connector. The male connector is fitted to the rocket skin and the female connector removed from it just before launch but after all the control operations.

Since all the electrical connections and the test points brought to the umbilical connector remain with the rocket skin and are exposed to the ambient medium during the rocket flight it is necessary to ensure that none of these points remain live during the flight. Any power point coming to the umbilical is disconnected from it using relays before launch and before the female connector is removed from it.

Fig.30 illustrates a typical set up used for payload control before launch. Hermetically sealed latching relays (Potter and Brumfield type SLG11DB 24V) were used for switching the payload from external to internal batteries.

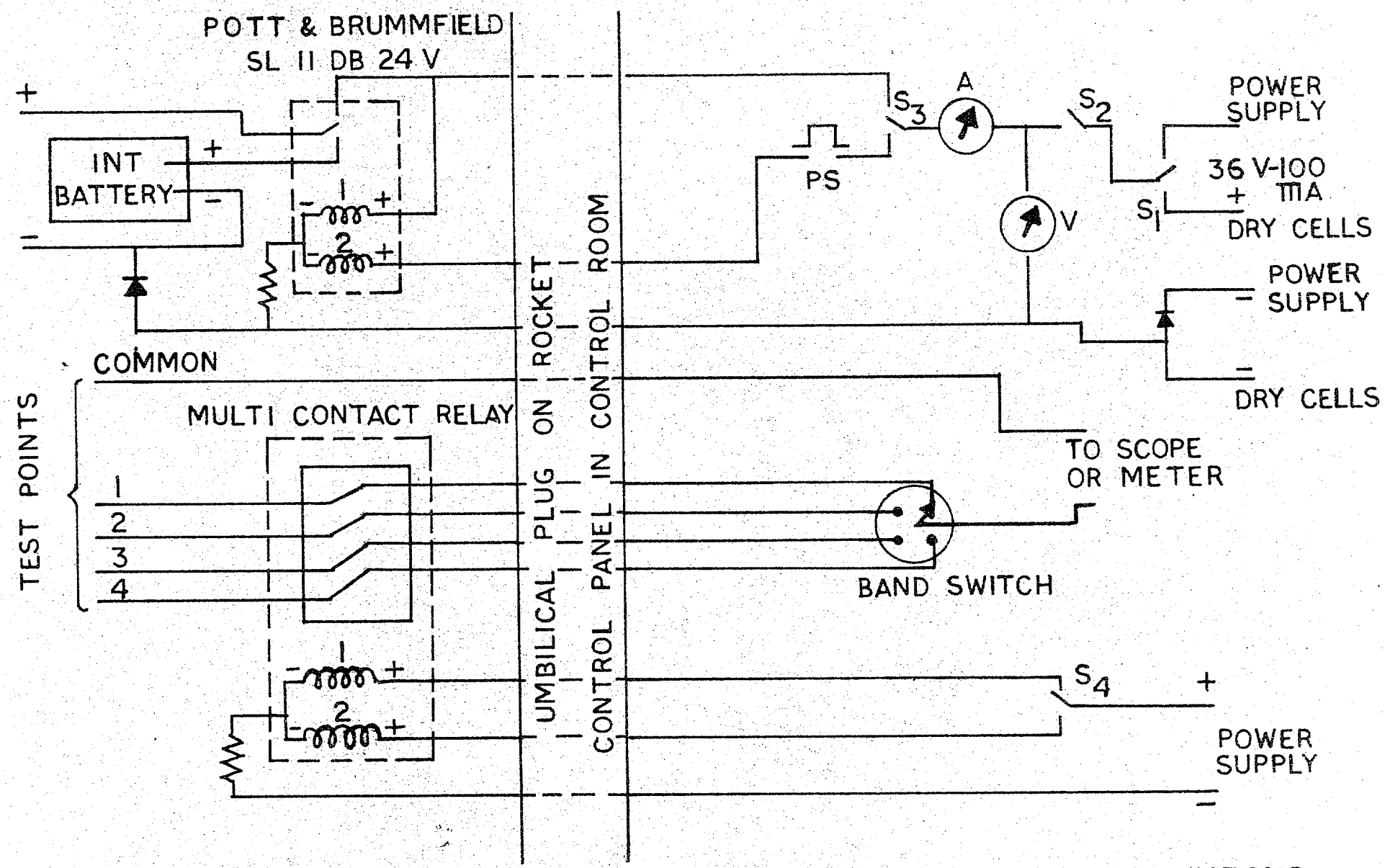

Fig 30 TYPICAL SET UP FOR PAYLOAD CONTROL AND PRELAUNCH CHECKS

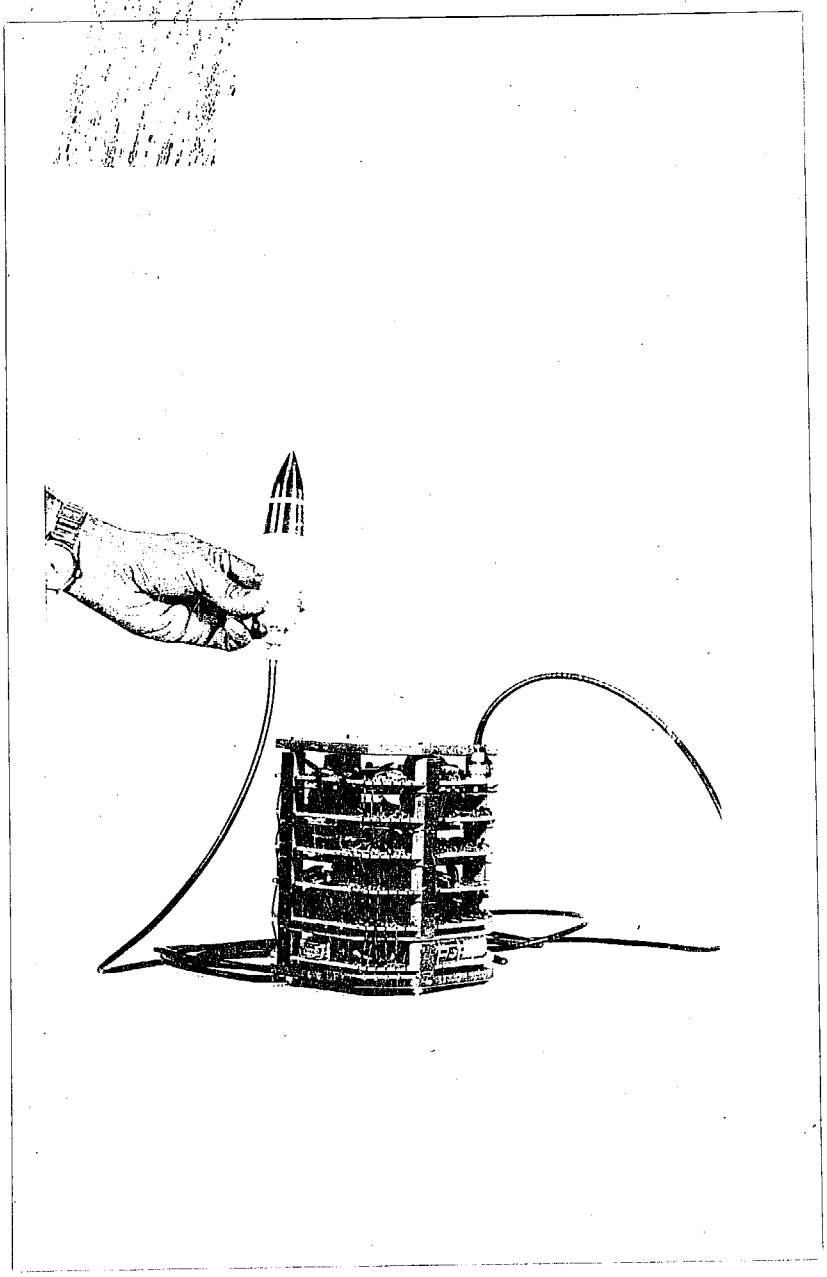

Fig. 31: Langmuir probe electronics with sensor assembly.

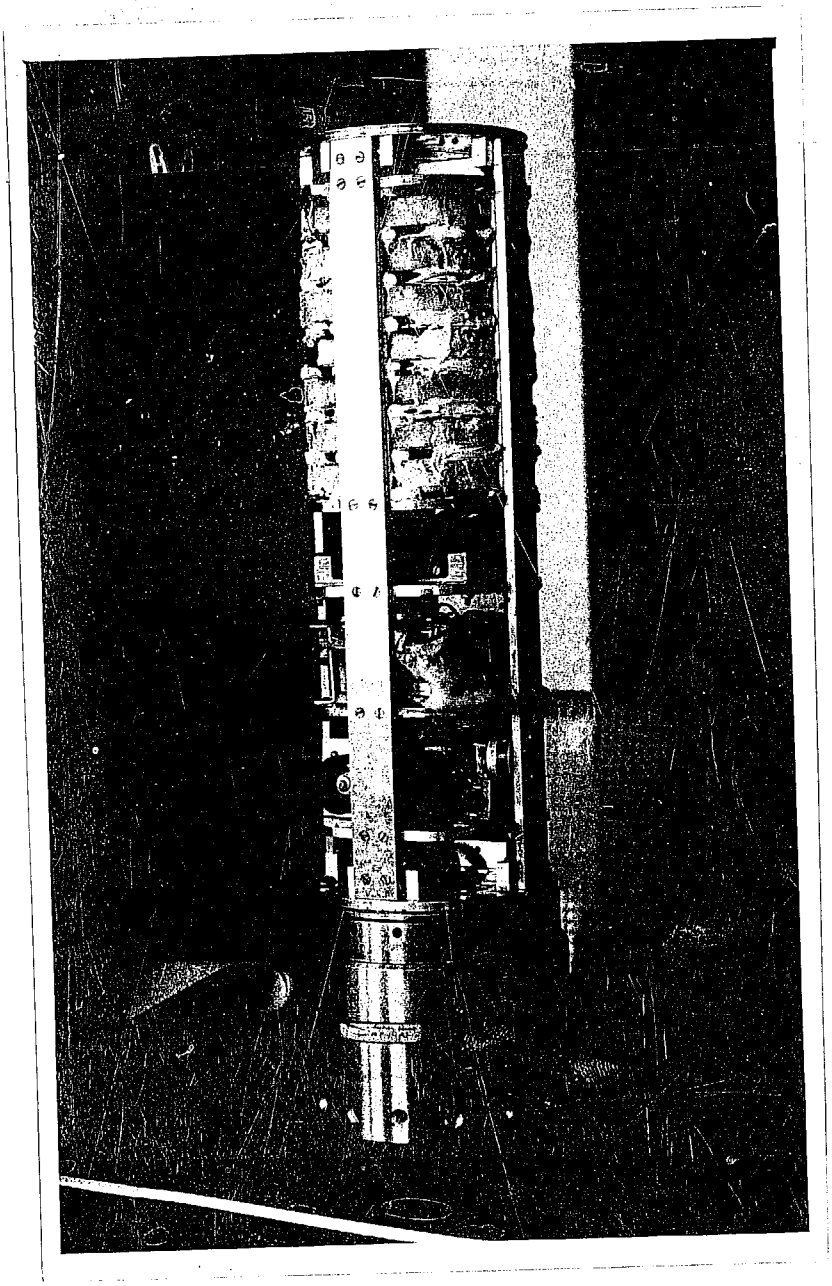

Fig.32: A Langmuir probe payload assembled in the payload housing of a Nike Apache rocket.

CHAPTER V

LANGMUIR PROBE FLIGHTS FROM THUMBA AND THE EXPERIMENTAL RESULTS

Several Langmuir probe payloads based on the design detailed in Chapter IV were constructed and flown on Nike Apache and Centaur rockets from Thumba (8°31'N, 76°52'E, dip 0°47'S). The following gives a brief summary of the flights and the rocket and payload performance.

1. Summary of Langmuir probe flights from Thumba:

Flight 1. Cenatur 15.01, 30th April 1965, 05.22 Hrs. IST. Side sensors were used. The Langmuir probe payload was accompanied by a sodium vapour payload. The Langmuir probe electronics functionad satisfactorily. But the probe function was affected by the presence of insulating paint on the nosecone. No useful data was collected because of this and/or the following reasons:

(i) use of side sensor of small probe area

(ii) small electron densities prevailing at the time of the flight.

Flight 2. Centaur 15.03, 8th January 1966, 18.41 Hrs. IST. Tip sensor was used. The Langmuir probe payload was accompained by a sodium vapour payload. The performance of the payload was satisfactory until T + 40 secs, when the ground receiving station reported loss of telemetry signals. Hence no useful data was collected. The sodium vapour timer functioned prematurely at T + 38 secs.

With the sodium ignition the transmitter cables and/or the circuitry might have been damaged resulting in loss of signals.

Flight 3. Nike Apache 20.05, 7th July 1966, 13.45 Hrs. IST. Tip sensor was used. The Langmuir probe payload was accompanied by a proton precession magnetometer payload. The performance of the probe and the electronics was satisfactory throughout the flight.

Flight 4. Nike Apache 10.11, 12th March 67, 18.57 Hrs. IST. Tip sensor was used. The Langmuir probe payload was accompanied by a sodium vapour payload. The performance of the probe and electronics was in general satisfactory. Some leakage due to absorption of moisture by the boron nitride insulator was observed in the initial stages of the flight. The leakage decreased with time and became negligible at about T + 100 secs. This leakage was corrected for and the data analysed.

Flight 5. Nike Apache 10.14, 13th March 67, 05.44 HRS. IST. Tip sensor was used. The Langmuir probe payload was accompanied by a sodium vapour payload. The performance of the probe and the payload were in general satisfactory. However the power of the telemetry transmitter decreased drastically within the first minute after launch and the signal to noise ratio gradually decreased during flight. Noise became

predominant after T + 180 secs and further data was irreducible.

Flight 6. Nike Apache 10.12, 12th March 67, 22.30 Hrs. IST. The payload was a composite payload of Langmuir probe and TMA release experiment supplied by the Geophysics Corporation of America through NASA. The payload performance was in general satisfactory even though there was a slight malfunctioning of the sweep electronics. The data could be usefully analysed upto the time of TMA release (T + 246 secs).

Flight 7. Centaur 45.01, 19th April 67, 10.30 Hrs. IST. This was a test flight, primarily meant for flight testing certain indigenously developed telemetry subsystems and mechanical devices. The opportunity was utilised to flight test a wire release mechanism for projecting a long wire out into the ambient medium. The wire was used as a cylindrical Langmuir probe. The probe and the payload performance was satisfactory upto T + 100 secs when effects were observed indicating the wire going into the wake of the vehicle. The rocket performance could not be properly assessed and therefore the probe data could not be usefully interpreted.

Data from flights 3, 4, 5 and 6 where the Langmuir probe collected useful data were analysed. The results are presented in the following paragraphs.

2. Nike Apache 20.05 - July 7, 1966, 13.45 Hrs. IST.

A Nike Apache rocket carrying a Langmuir probe and a proton precession magnetometer was launched with a wind corrected azimuth of 270° and an elevation of 82°. It reached an estimated height of 176 Km.

The Langmuir probe assembly consisted of a stainless steel sensor, ogive in shape, with a surface area of 22 sq.cms (effective surface area = 6 sq. cms, (Smith, 1966)) situated at the nose tip of the rocket. The sensor was insulated from a stainless steel guard ring by a ceramic insulator 1" in height. The nose cone of the rocket was made of fibreglass. The main body of the Apache rocket was used as the reference electrode. (The area ratio between the two electrodes was of the order of 1000). The probe voltage was programmed to vary linearly from -2.4Vto + 2.4 V in about 0.6 secs and stay at a fixed voltage of + 2.4 V for 1.5 secs. During the latter interval the probe current was used to study variations in electron density. The varying portion of the sweep was used for determining the electron temperature through the analysis of retarding potentials. The probe amplifier employed field effect transistors and was similar to that shown in Fig.20. The system could cover a range of 10^{-8} amp to 25 x 10^{-6} amp of electron current and 10^{-8} amp to 10^{-6} amp of positive ion current. The input-output characteristics of the amplifier are shown in fig.22. The amplifier output was fed to two subcarrier channels of 22 khz and 40 khz. The 22 khz channel saturated at 1.2 μa of electron current and 0.15 μa

of positive ion current. The 40 khz channel covered the full range of the amplifier. The two channels were mixed using simple resistance networks and the mixed signal frequency modulated the 235 Mhz signal from a Bendix transmitter. The power requirements of the Langmuir probe system (excluding the transmitter) were 30 ma at 33V and were provided by using five Mallory Mercury cells TR 135R (6.75V, 1000 mah each) in series, which formed a part of the Langmuir probe system. The net payload weight was 1.9 kg, including potting.

The performance of the rocket and the payloads was satisfactory. Signals were received at the ground telemetry station on all channels upto 408.5 secs. from the time of rocket take off. Magnetometer signals continued to be received up to 410.5 secs, When all signals (including the carrier) were lost. The rocket was launched towards the sea. Assuming that the signals were lost when the transmitting antennas got submerged under the sea 410.5 secs. was taken to be the total flight time of the rocket. Using this time and the launch parameters a typical Nike Apache trajectory was computed and used for interpreting the experimental data. (No direct information was available about the rocket trajectory).

During the flight, Langmuir probe current could be first detected at 58 secs. from launch. Current was measured from this instant onwards through the rocket-apogee up to 366 secs from launch when it went below the sensitiveness of the probe amplifier. The saturation electron current (more correctly the electron current at +2.4V) obtained on this flight is shown as function of time in fig.33. It shows a

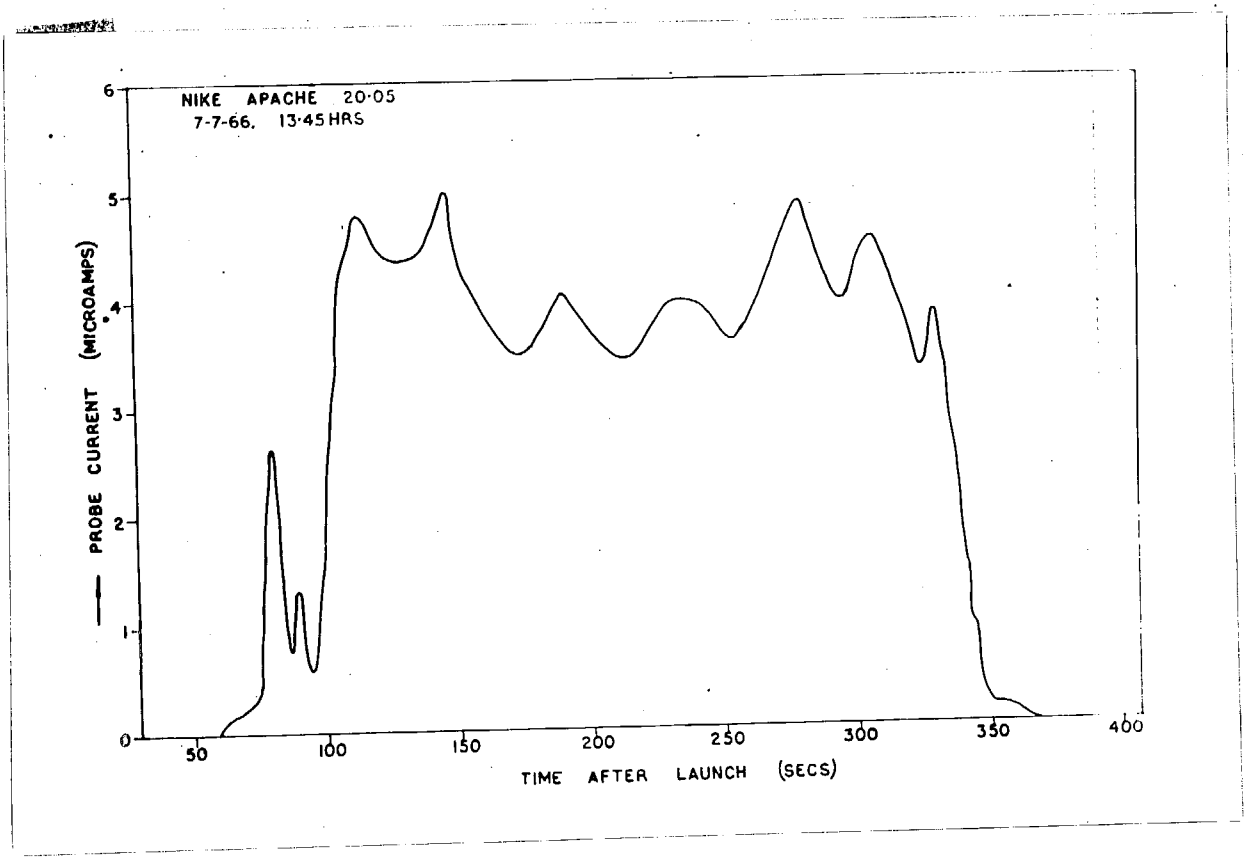

Fig.33: Electron current to the probe at +2.4 V measured on flight 20.05.

periodicity of about 40 secs. between 110 secs. and 310 secs. when the rocket was in the E region and where the ambient electron density was not varying over a wide range. This periodicity is due to rocket precession as discussed on pages 31-33. The maximum variation during a precession cycle is seen to be 8 to 10%. No significant effects were observed due to rocket spin and wake of the vehicle during descent.

A study of the volt-ampere curves obtained during the flight showed that for every sweep the net probe current

becomes zero at a voltage which is consistently positive and this value varies from + 0.7 to 1.3 V during the flight. The values were shown in fig.6 and the possible causes were discussed on pages 34-37.

The experimental values of the positive ion current when the probe was at -2.4 V were also not consistent with theory. The measured currents are everywhere more than an order of magnitude larger than those expected from theoretical considerations. The ratio of the electron current at + 2.4 V to the positive ion current at -2.4 V is about 10 for most of the sweeps. The theoretically expected value is about 170. Previous experimenters have observed ratios ranging from 20 to 50 (Serbu, 1963; Smith, 1964). The present values are even smaller than their observations. They are likely to be due to the combined effect of the enhanced positive ion currents observed and the reduced efficiency of the probe for the collection of electrons. While photoemission can give rise to enhanced positive ion currents the observed values are too large to be explained away by such a cause. Outgassing from the fibreglass nose cone may also be responsible for the large positive ion currents. The reduced efficiency for electron collection may be partly due to the smaller than optimum value of the area ratio of the electrodes. Smith (1964) has shown that under such circumstances the electron current to the probe saturates at much larger probe voltages. It may also be due partly, to the observed contact potentials, the effect

of which is to reduce the effective probe voltage, thereby reducing the electron current collected by it.

In spite of the large positive ion currents and the observed contact potentials, the shapes of the current voltage characteristics were satisfactory. The curves could be subjected to ratarding potential analysis and the electron temperature,

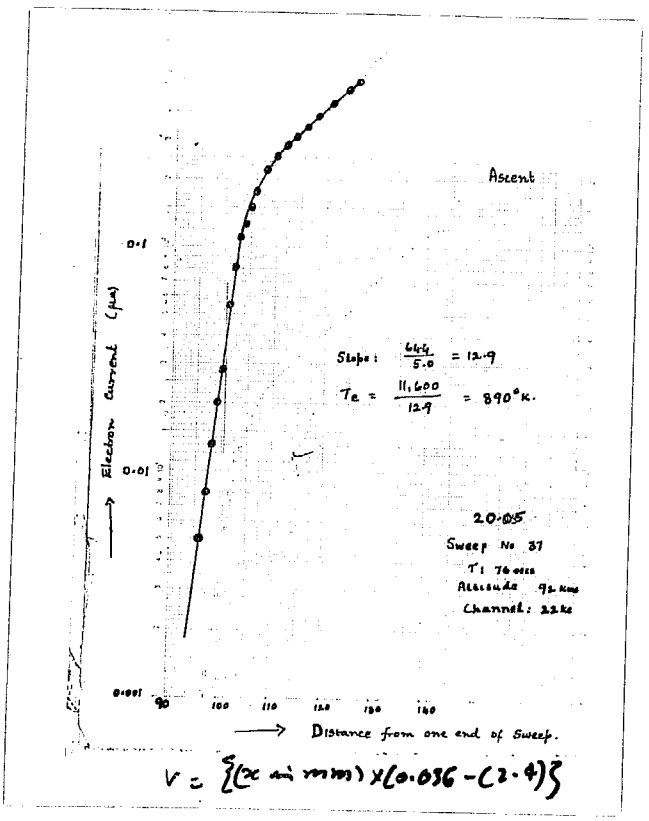

Fig. 34: A typical semi log plot of the electron current to the probe, measured on flight 20.05. The distances plotted on the X axis are measured from the negative end of the sweep and are related to the probe voltage by $V = \{(x \text{ in mm}) \times (0.036) - (2.4)\}$ Volts. The positive ion current measured at -2.4 V was 0.03 μ a.

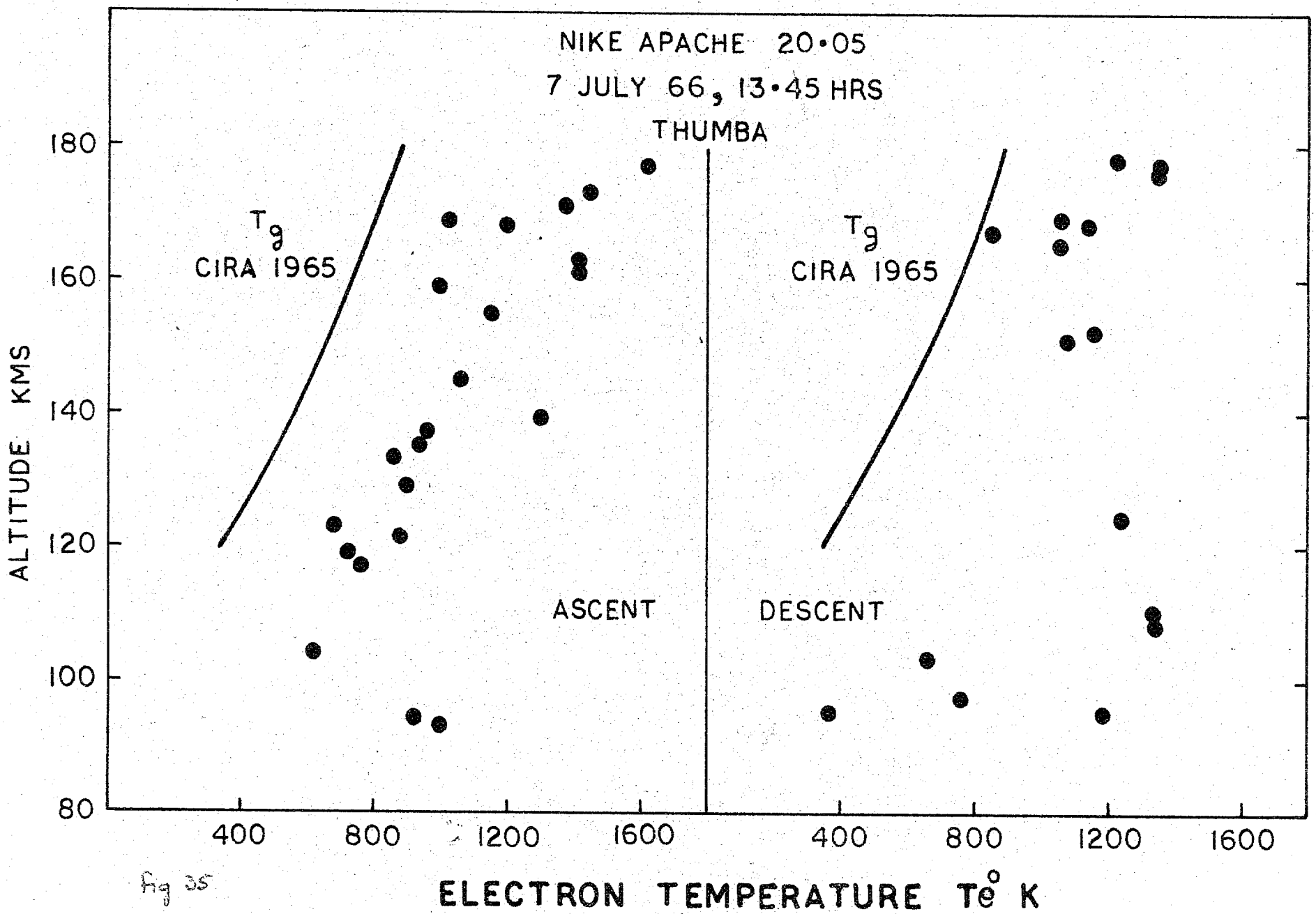
NIKE APACHE 20.05
7 JULY 66, 13.45 HRS
THUMBA
T_g
CIRA 1965
T_g
CIRA 1965
ASCENT
DESCENT
ALTITUDE KMS
180
160
140
120
100
80
400
800
1200
1600
400
800
1200
1600
ELECTRON TEMPERATURE T_e° K

Fig 35

determined. Fig.34 shows a typical semilog plot of the electron current and fig.35 the measured electron temperatures plotted against height. Neutral gas temperatures at 14.00 Hrs for the corresponding state of solar activity (S = 100) taken from the CIRA standard atmosphere 1965 are also shown in the figure.

It has been pointed out in chapter III that in practice the current voltage characteristic of a Langmuir probe can not be used to determine the electron density in the ionosphere absolutely and that the saturation electron current to a probe kept at a fixed positive potential can be used to study the electron density variations in the ionosphere, if the electron temperature variations can be neglected. The observed probe current profile can be converted into an electron density profile if the proportionality factor is known from the E region critical frequency obtained by the nearest ionosonde. The proportionality factor can change with height due to the changing sensitiveness of the sensor with changing properties of the ambient medium such as the electron density, electron temperature, collision frequency etc. The change in proportionality factor can be specially large below about 90 km where the ionospheric conditions undergo large transitions.

The CRPL 4 ionosonde at the Thumba rocket range was operating during the launch period and ionograms were taken at 13.42 Hrs (just before rocket launch), and at

13.51 Hrs. (when the rocket was still in the downward leg of its trajectory). These ionograms and the ionograms taken during the rest of the day were characteristic of a normal equatorial ionosphere. Both the ionograms at 13.42 Hrs.and 13.51 Hrs. showed a critical frequency of 3.6 Mhz for the E region. A non blanketing sporadic E reflection was seen upto 9 Mhz and this is due to reflection from the irregularities associated with the electrojet (Cohen and Bowles, 1963) and not due to a genuine layer. The probe current profile does not show any feature which can be associated with this reflection. Ionograms taken at Kodaikanal (10.2°N, 77.5°E and magnetic dip 1.7°N) at 13.45 and 14.00 Hrs. also showed similar features.

The critical frequency of 3.6 Mhz was taken to correspond to the probe current peak observed at 100 km during ascent and the observed probe currents were converted into electron densities. Since the ionograms were not clear at the low frequency end they could not be subjected to a true height analysis and therefore only one calibration point was available. This was used for the entire profile.

From the well known equation:

$$N_e = 1.24 \times 10^4 f_c^2 \qquad (19)$$

where f_c is the critical frequency, in Mhz, the electron density N_e corresponding to 3.6 MHz is 1.6×10^5 electrons/cc.

The observed probe current at 100 km being 2.65 μa, the conversion factor for the electron density is:

$$\frac{1.6 \times 10^5}{2.65} = 6 \times 10^4 \text{/cc per microamper of observed probe current.}$$

The probe sensitiveness is therefore $\frac{2.65}{1.6 \times 10^5} = 1.66$ μa per 10^5 electrons/cc.

The electron density profile obtained from this conversion factor is shown in fig.36. Although the absolute values of electron density below 90 km could be uncertain due to the variations in the conversion factor, the shape of the electron density profile in these height regions, appears to be real.

Fig.36 shows that in the D region the ascent and the descent profiles agree fairly well. The small height differences in height between similar points in the profiles cannot be taken seriously because of the approximate nature of the trajectory used. The D region profiles show a well defined layer between 80 and 90 km. Maximum electron density of about 10^4/cc is reached at 87 km during ascent and at 84 km during descent. Above 90 km, at the base of the E region the ascent and the descent profiles agree with one another above 130 km. But below 130 km there is a marked difference between the ascent and the descent prifiles. These differences are discussed in greater detail in the next chapter.

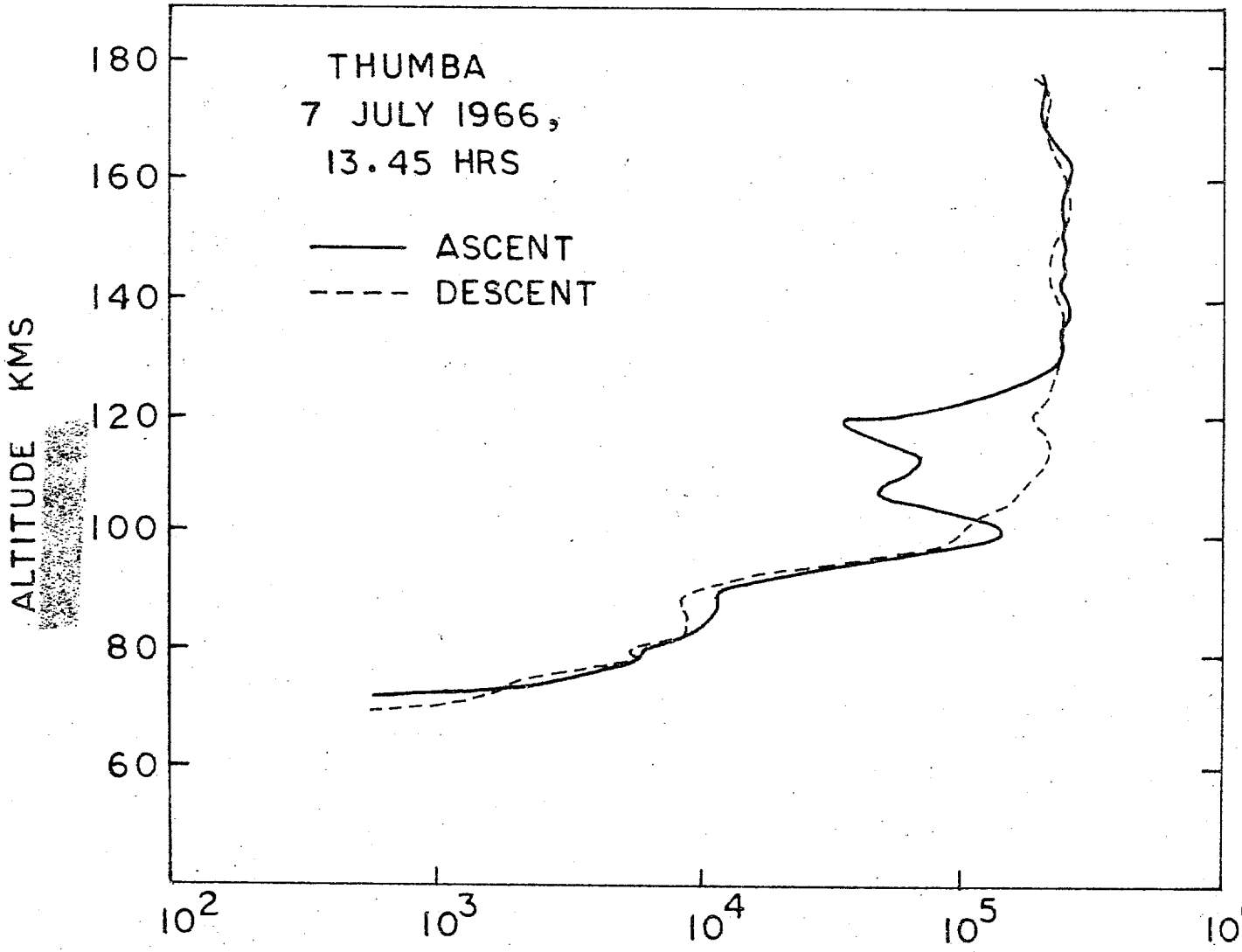

Fig 26 ELECTRON DENSITY PROFILE OBTAINED FROM FLIGHT 20.05 ON JULY 7, 1966 13.45 HRS IST

3. Nike Apache 10.11 - March 12, 1967, 18.57 Hrs. IST

The probe assembly on this flight consisted of a stainless steel ogive electrode of surface area 22 Sq. cms. (effective surface area 6 sq. cm) at the nosetip of the rocket and insulated from a stainless steel guard ring, half-an-inch in height, by means of a boron nitride ring 1/8" in height. The guard ring was insulated from the nose-cone of the rocket with the help of a ¼" teflon ring. The probe voltage was programmed to vary from -1 V to+4 V in about 0.5 secs, and stay at a fixed voltage of + 4 V for about 1 sec. The modifications in sweep levels were suggested by the experience gained from flight 20.05. It showed (i) that the net probe current becomes zero only for positive values of the probe voltage, (ii) that the electron current does not show a tendency to saturate at + 2.4 V, and (iii) that the slope of positive ion current to the probe for negative voltages is small and a good section of the negative voltage part of the sweep is not useful during data analysis. The larger repetition frequency was aimed at more frequent measurements of the electron temperature.

The probe amplifier employed the electrometer tube CK587 (Raytheon) with a rated grid current of less than 10^{-14} amp and was similar to that of fig.21. With the feedback element used, the amplifier became sensitive to currents down to 10^{-9} amp. The amplifier could cover a range of 10^{-9} amp to 10^{-5} amp of electron current and 10^{-9} amp to 0.5×10^{-6} amp of positive-ion current. The probe output was telemetered

on two subcarrier channels of 40 khz and 70 khz respectively. An inflight calibration marks was obtained for 50 millisecs. at the end of every sweep, by shorting the feedback element through a relay.

A sine wave of about 2 mv at 800 hz was superposed on the sweep and the a.c component of the output of the probe amplifier was telemetered on a third subcarrier channel at 22 khz after suitable filtering, amplication and detection. When the probe voltage was varying, this output measured the instantaneous slope of the J-V characteristic of the probe.

A calibrated baroswitch with two pairs of contacts, set at 50,000 ft and 70,000 ft respectively, was used to obtain information about the rocket trajectory. When the ambient pressure reached the reference value, the switch closed, making a contact which altered the d.c level of a point in the payload electronics. This was telemetered on a fourth subcarrier channel at 10.5 khz.

The four subcarrier outputs were mixed using linear passive network following the procedure mentioned on page 71 and the mixed signal frequency modulated the carrier frequency of 241.6 Mhz from a Bendix transmitter.

The power requirements of the Langmuir probe payload excluding the transmitter, 60 mA at 34 V were provided by five Mallory mercury cells TR 135 R (6.75 V, 1000 mah) in series. They formed part of the Langmuir probe system. The payload weighed 3 kg. after potting.

During the flight, data was received on all the four subcarrier channels upto 336 secs. from launch, when all modulation disappeared. The rf signals continued to be received upto 405 secs. which was taken to be the total flight time. The loss of modulation at 336 secs may be due to the snapping of the cables from the mixer stage to the transmitter or due to some malfunctioning in the probe electronics which might have occured at that time. The time 336 secs.corresponds roughly to that stage in the rocket trajectory when the rocket flips over during descent and starts travelling with its nose down.

Telemetry records showed the presence of leakage between the sensor and the guard electrode when the rocket was still on the launch pad. The leakage gradually decreased during rocket ascent and became negligible at about 100 secs. from launch. At 80 secs when the probe current had just begun to be collected, the leakage constituted only a small fraction of the probe current and could be corrected for. It is believed that the leakage was due to absorption of moisture by the boron nitride insulator during the pre-launch period and that it gradually decreased during rocket ascent due to frictional heating and consequent evaporation of the moisture.

The current to the probe could first be detected at 75 secs from launch. During flight, the probe current was measured from 75 secs upto 325 secs, when it went below the sensitiveness of the amplifier. Any modulation of the probe current due to rocket precession if present, could not be

separated from the genuine variations in probe current. No effect was seen due to rocket spin. Since the flight took place during twilight hours, effects due to photoemission were negligible. Analysis of the volt ampere curves showed that as in 20.05 the net probe current becomes zero only when the probe voltage is positive. The voltages were much larger on this flight. The values were shown in fig.7. Except when leakage was present the ratio of the saturation electron current to the saturation positive ion current was found to be fairly large. The ratio was about 150. Fig.9 is a typical volt - ampere curve obtained on this flight.

Operation of the baroswitch could be recorded only during ascent. This record together with the total flight time was used to check the rocket trajectory. This indicated that the rocket had reached an altitude of 163 km.

Fig.37 shows a plot of the electron current to the probe at + 4 V as a function of height. Flight time ionograms did not show any E reflection. Apparently the ambient electron densities were too low for the sensitiveness of the ionospheric recorders at Thumba and Kodaikanal. Hence direct normalisation of the probe currents into electron densities was not possible. However a normalisation was attempted by comparing the performance of this probe with the performance of the probe on flight 20.05.

On several sweeps at different sections of the rocket trajectory and under varying conditions of electron densities and electron temperatures the electron current to

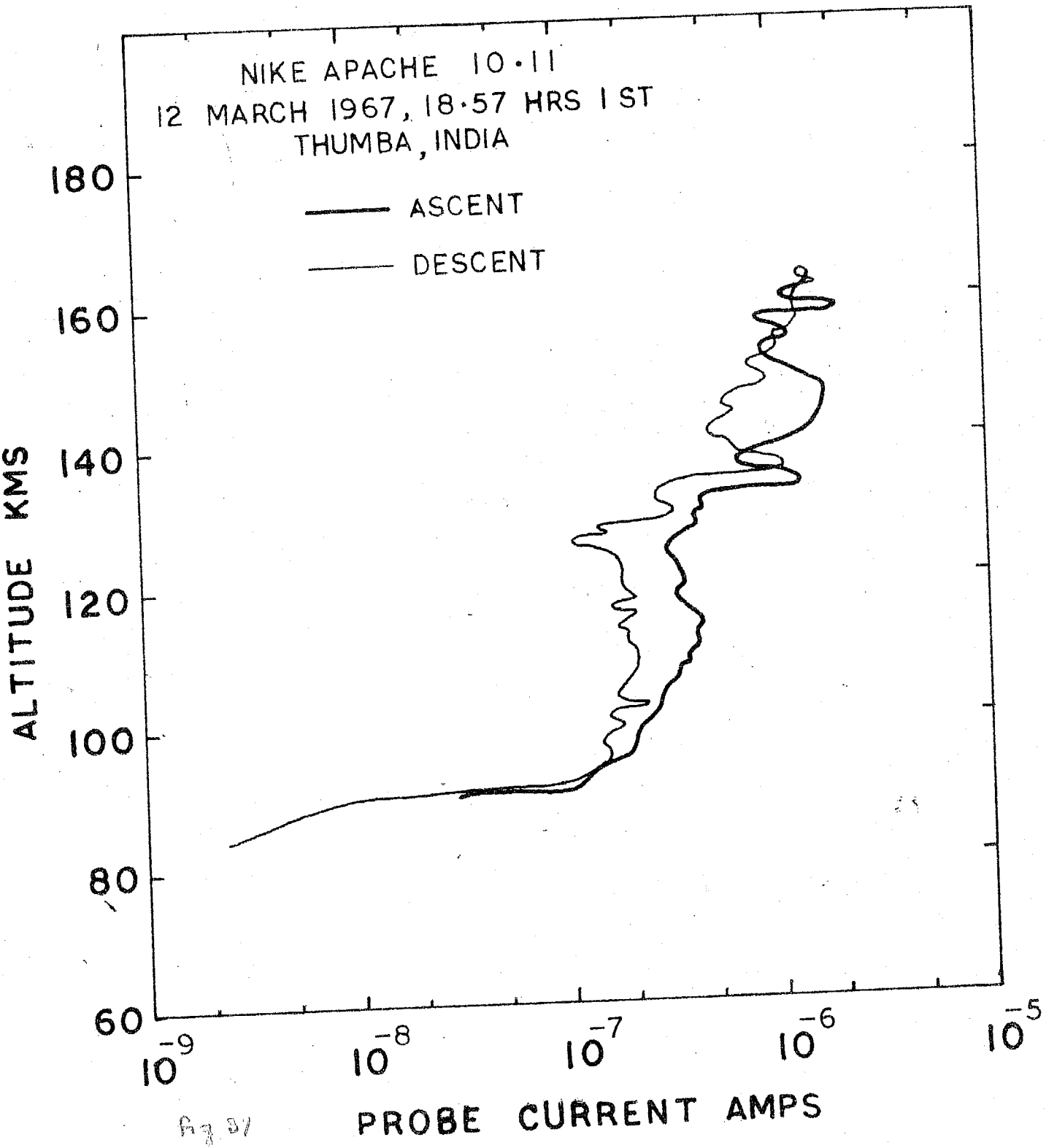
NIKE APACHE 10.11
12 MARCH 1967, 18.57 HRS I ST
THUMBA, INDIA
ASCENT
DESCENT
ALTITUDE KMS
180
160
140
120
100
80
60
10^{-9}
10^{-8}
10^{-7}
10^{-6}
10^{-5}
PROBE CURRENT AMPS

Fig 37

the probe is determined when it is at + 4 V and + 2.4 V. The ratio of the current at + 4 V and + 2.4 V was nearly constant around 2.8. So dividing the probe current by a factor of 2.8 we can obtain a profile which can be compared with that of 20.05.

Sensitivity of the probe on 20.05 at + 2.4 V is

$$1\,\mu a = 6.1 \times 10^4 \text{ electrons/cc}$$

Sensitivity of the probe 20.05 at + 4 V would be

$$1\,\mu a = \frac{6.1 \times 10^4}{2.8}$$

$$= 2.15 \times 10^4/cc$$

Therefore if the probes on 20.05 and 10.11 are identical (which they were, geometrically) the normalising factor for probe currents would be $1\,\mu a = 2.15 \times 10^4/cc$ i.e. sensitiveness of the ogive on 10.11 is $4.6\,\mu\,a/10^5$ electron per cc. This value agrees well with the value $4.5\,\mu\,a/10^5$ electron per cc obtained by Smith (1965) for a sensor of similar geometry and size during a twilight flight.

The probe current profile shows that in the D region the ionisation had already almost completely decayed. 1×10^{-9} amp, the lower limit of the sensitiveness probe amplifier would on the above normalisation considerations, be about 20 electrons/cc. So at 80 km and below the electron densities were below this limit both during ascent and descent. The probe current then increased rather sharply to the base of the E region. In the

E region there is considerable ionisation between 100 and 120 km and a distinct layering in the 130-140 km region both during ascent and descent. The profile is in general smoother during ascent than during descent. In the 120-90 km region the descent profile closely follows the ascent profile but the probe current is everywhere smaller during descent than during ascent. The difference is believed to be genuine and not due to any effect associated with the vehicle. The rocket was spin stabilised and the shape of the sensor was such that no large sensitiveness to the rocket aspect is expected. Smith et al (1966) have seen that the variations of electron current to an ogive electrode (similar to ours) kept at a fixed voltage is less than 10% for a 20° change in rocket aspect. The maximum change in rocket aspect is expected to be of this order. Further, on flight 20.05 the variation in probe current due to changing rocket aspect was seen to be less than 10%. Fig.37 shows a decrease in probe current from ascent to descent by a factor of about 2. This is too large to be due to changes in rocket aspect. Leakage effects in this region were negligible, and the correction factor an order of magnitude less, so that the observed effect cannot be due to any overcorrection of leakage. Effects due to the rocket going into the wake of the vehicle are also small because of the low launch angle (Smith et al loc cit).

The effect is apparently genuine and it may be due to the effect of recombination after sunset and/or the change in locality of about 100 kms horizontally of the ascent and

descent limbs of the sensor in this height region. If it is attributed to recombination effect alone an effective recombination coefficient of about 6×10^{-7} cm^3/sec will have to be inferred. Other considerations indicate that this value is too large to be true.

The difference in heights between ascent and descent, of similar features in the probe current profile, such as the base of the E region, the layer of large increase in probe current in the 130-140 km region etc. may not be wholly genuine. It may be partly due to the approximate nature of the rocket trajectory used.

The electron temperature values obtained by the usual retarding potential analysis are plotted against height in fig.38. Because of the leakage observed, no attempt was made to determine electron temperatures below 120 km during ascent. Fig.38 also shows neutral gas temperatures taken from CIRA 1965 for S = 65, which corresponded to the conditions on the flight day. Comparison shows that during descent the electron temperature gradually increases with increasing height and follows neutral gas temperatures up to 130 km. But the electron temperature increases sharply around 135 km during descent and around 130 km during ascent. The increase in temperatures seem to be localised since the temperatures tend to fall after 150 km. These regions of enhanced temperatures seem to be well correlated with the regions of enhanced probe current of fig.37.

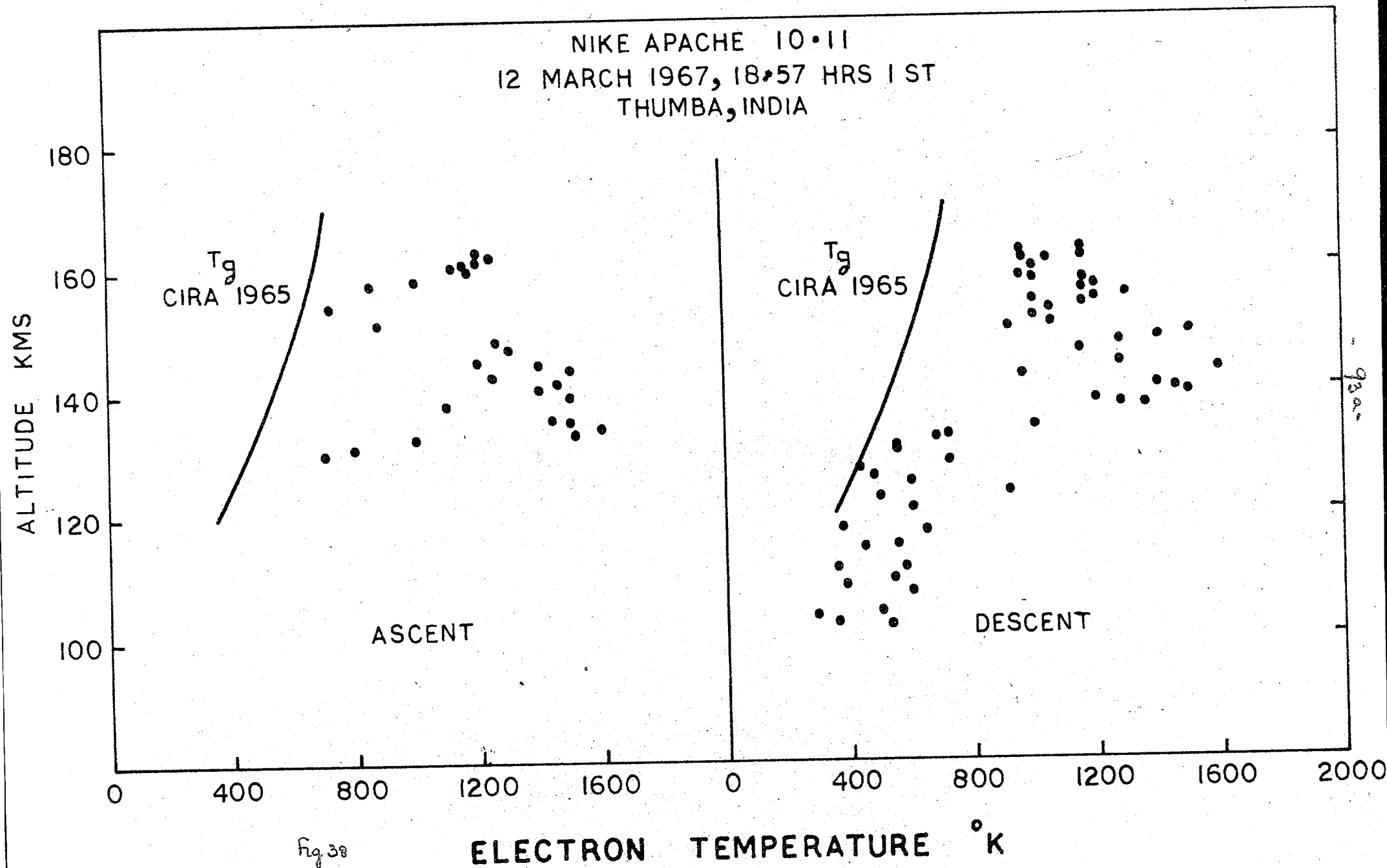
NIKE APACHE 10.11
12 MARCH 1967, 18.57 HRS I ST
THUMBA, INDIA
ALTITUDE KMS
180
160
140
120
100
T_g
CIRA 1965
ASCENT
T_g
CIRA 1965
DESCENT
0
400
800
1200
1600
0
400
800
1200
1600
2000
ELECTRON TEMPERATURE °K

Fig 38

4. Nike Apache 10.14, March 13, 1967. 05.44 Hrs. IST.

The Langmuir probe payload on this flight was similar to that of flight 10.11, except that on this flight the 22 khz channel (for information on space potential and plasma noise was absent). The 10.5 khz channel monitored the operation of the baroswitch. The transmitter used was a transistorised version manufactured by Sud Aviation and Co. of France. The general performance of the sensor and the payload electronics was satisfactory. However the rf carrier level received at the ground station became low within a minute of the rocket take off and soon touched the threshold level of 20 v. As the carrier level decreased, the signal to noise ratio deteriorated. Noise predomenated over the signal after 180 secs on all the subcarrier channels and further data was irreducible. In the time interval of 120-180 secs the record was noisy and electron temperature analysis could not be performed. Electron temperature measurements were possible only upto 120 secs. However the saturation electron current to the probe could still be measured within an accuracy of $\pm$ 10%.

Since the experimental data could be reduced only upto 180 secs from launch the baroswitch recording of the rocket crossing the reference altitude could not be monitored during descent. However during ascent the time of crossing the 70,000 ft reference altitude was same as that recorded on flight 10.11 within a few tenths of a sec. This along with the similarity of the rockets, the payload weights and the

launch parameters led to the assumption of the same rocket trajectory for flights 10.11 and 10.14.

Fig.39 shows the electron current to the probe at + 4 V plotted against height. In this flight also no direct calibration for converting probe currents to electron densities was possible since no E reflection was seen on the ionograms at Thumba and Kodaikanal. But the conversion factor of 2.15 x 10^4 electrons/cc per a of probe current which was derived for flight 10.11 can be used.

The probe current profile shows very little ionisation in the D region, a sharp rise from the D region to the base of the E region and an already well formed E region. The signal to noise ratio being poor the probe currents above 140 km can be in error by $\pm$ 10%. In this height region, the profile shown in figure represents a smoothed out picture of the actual profile. It is seen that this profile is altogether different from the one obtained during the previous evening.

Fig.40 shows the electron temperatures that could be obtained from this flight along with the corresponding neutral gas temperatures from CIRA 1965 (S = 65). In spite of the limited height range where measurements are possible the results are extremely interesting. The similarity with the results from the evening flight (fig.38) is very striking.

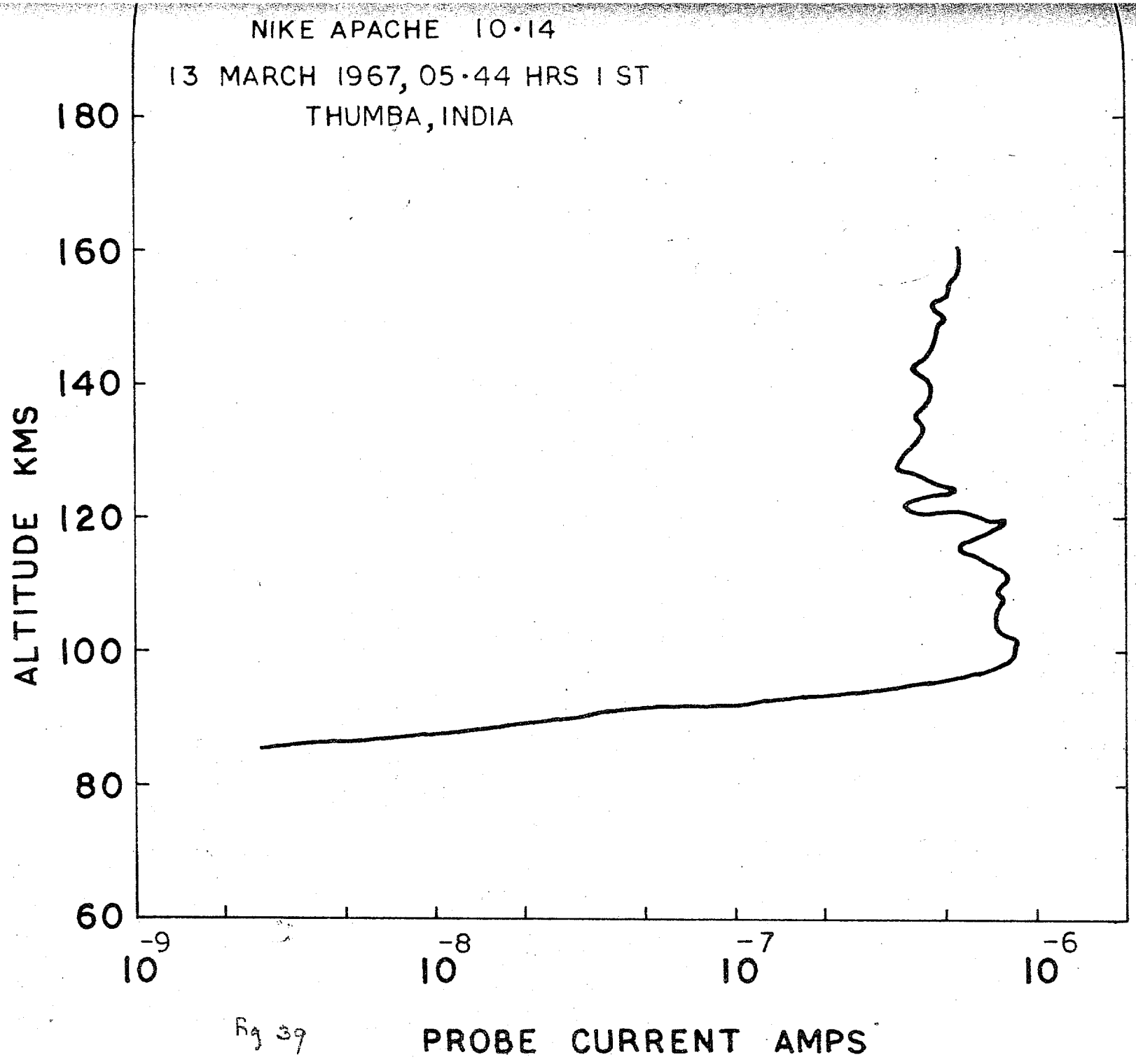
NIKE APACHE 10·14
13 MARCH 1967, 05·44 HRS I ST
THUMBA, INDIA
ALTITUDE KMS
180
160
140
120
100
80
60
10^{-9}
10^{-8}
10^{-7}
10^{-6}
PROBE CURRENT AMPS

Fig 39

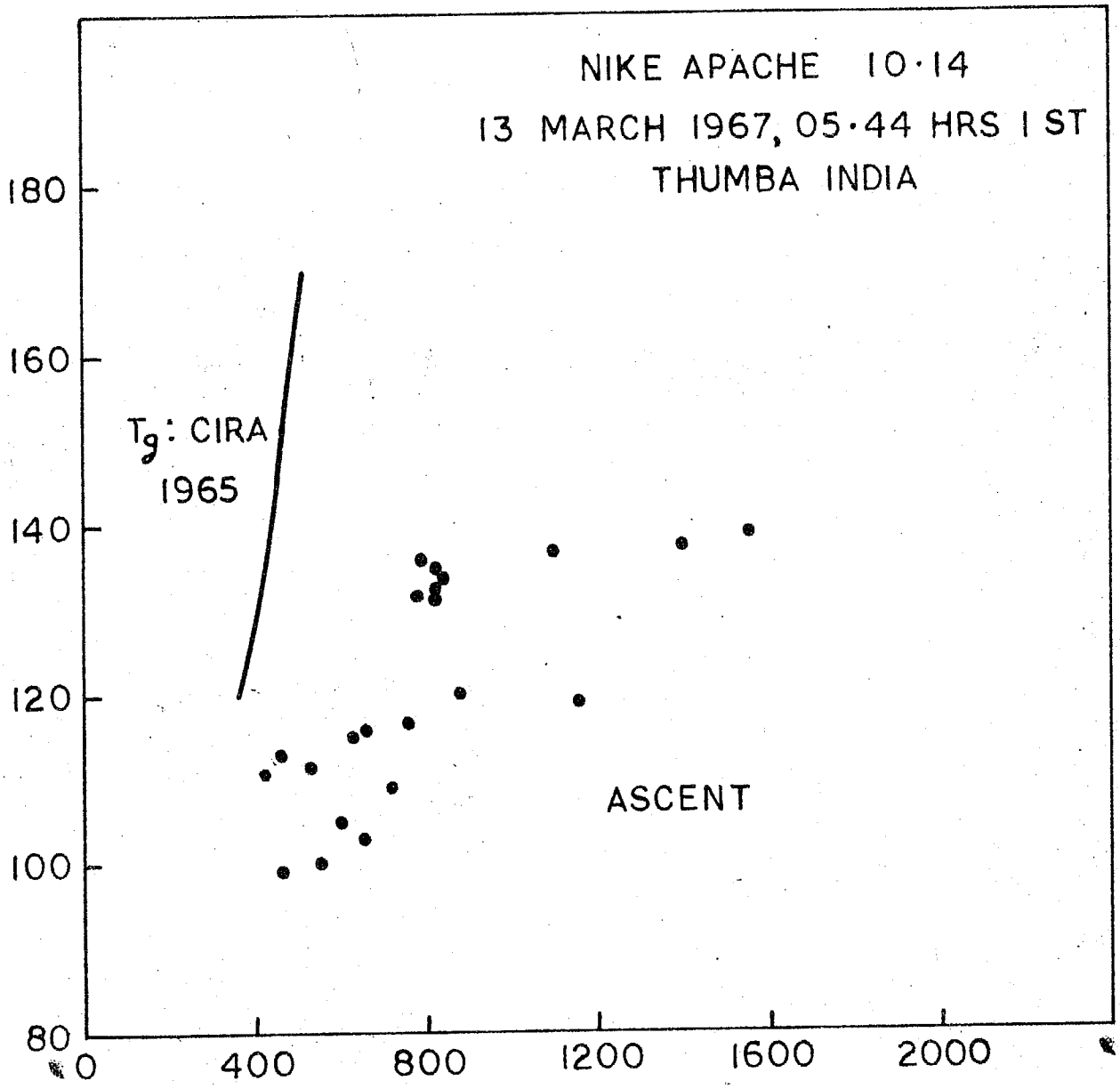
NIKE APACHE 10·14
13 MARCH 1967, 05·44 HRS I ST
THUMBA INDIA
T_g: CIRA
1965
ASCENT
180
160
140
120
100
80
0
400
800
1200
1600
2000
ELECTRON TEMPERATURE °K

Fig 40

5. Nike Apache 10.12, March 12, 1967, 22.30 Hrs. IST.

Nike Apache 10.12 carried a composite payload of Langmuir probe and TMA release experiment instrumented by the Geophysics Corporation of America. Langmuir probe measurements were made on the upward leg of the rocket trajectory. TMA was released for neutral wind measurements during descent. TMA release was actuated by a mechanical timer set for 240 secs.

The Langmuir probe consisted of an ogive electrode of dimensions similar to the ones used on flight 10.11 and 10.14, and the probe assembly was similar to the one extensively used by Smith (1964). The probe amplifier was sensitive to currents from 10^{-9} amp to about 20×10^{-6} amp of electron current and about 2×10^{-7} amp of positive ion current. There was provision for inflight calibration of the feedback element every 16 sweep cycles i.e. every 32 secs and a provision for the calibration of amplifier zero at the end of every sweep.

The payload also consisted of a magnetic aspect sensor which monitored the transverse aspect of the rocket during flight. A baroswitch set for 70,000 ft was used tp obtain a check on the rocket trajectory. From the baroswitch readings the rocket was estimated to have reached a height of 180 km.

TMA release started at 246 secs when the rocket was at 173 km in the downward trajectory. While the release of TMA affected the probe performance the general features

of the probe current profile could be made out even after release of TMA. The effect of TMA release on the probe performance is shown in Fig.3. The effects are (i) to decrease the sensitiveness of the probe by a factor of about 4 and (ii) to produce a marked aspect sensitiveness in the electron current to the probe.

An examination of the volt-ampere curves of the probe and the inflight calibrations showed that there was a minor malfunctioning of the sweep electronics. The negative battery starting the sweep from -2.7 V had either discharged or got shorted. The sweep was starting from a positive voltage and therefore no positive ion current was collected by the probe. Consequently electron temperatures could not be unambiguously determined. However with the help of the preflight characteristics of the feedback element of the electrometer amplifier and the inflight calibration it was possible to reconstruct the sweep voltage during flight. The sweep was found to vary from +1.6 to +5.4 V. This made the sensor collect more current than other GCA payloads flown by Smith, for the same ambient electron density and electron temperature. In order to be able to compare the results of this flight with those of other flights the volt ampere curves were studied carefully and currents at +5.4 V, +4.0 V, +2.7 V and +2.4 V determined for several sweeps at various positions of the rocket trajectory. The following table gives the efficiency of the probe for electron current collection at various fixed positive voltages.

Probe voltage (V)	Efficiency (relative)	Probe current at V volts / Probe current at 2.4 Volts
2.4 Volts	1	
2.7	1.7	
4.0	3	
5.4	3.95	

2.4 V is taken as the reference level so that the results may be comparable with those of flight 20.05.

The ratio of the efficiencies at 5.4V and 2.7 V is $\frac{3.95}{1.7}$ = 2.33 (Simple formula for a spherical probe would give a factor of 2). This figure enables us to compare the results of this flight with results obtained by L.G. Smith (1965) on his flights using the G.C.A. probe.

The ratio of the efficiencies at 4.0 Volts and 2.4 Volts is 3. This figure compares well with the ratio 2.8 obtained on flight 10.11 and therefore gives greater reliance to the conversion factor used to convert the probe currents of flight 10.11 to electron densities.

The ratio of the efficiences at 5.4 V and 4.0 V is $\frac{3.95}{3}$ 1.32. (The actual observed values for this ratio varies from 1.22 and 1.36). Therefore by dividing the probe currents obtained on this flight by 1.32 they can be compared with the results of flight 10.11 and 10.14.

Fig.41 shows the probe currents observed on this flight plotted against heights. The probe currents are not plotted after 246 secs (after release of TMA). For the factor

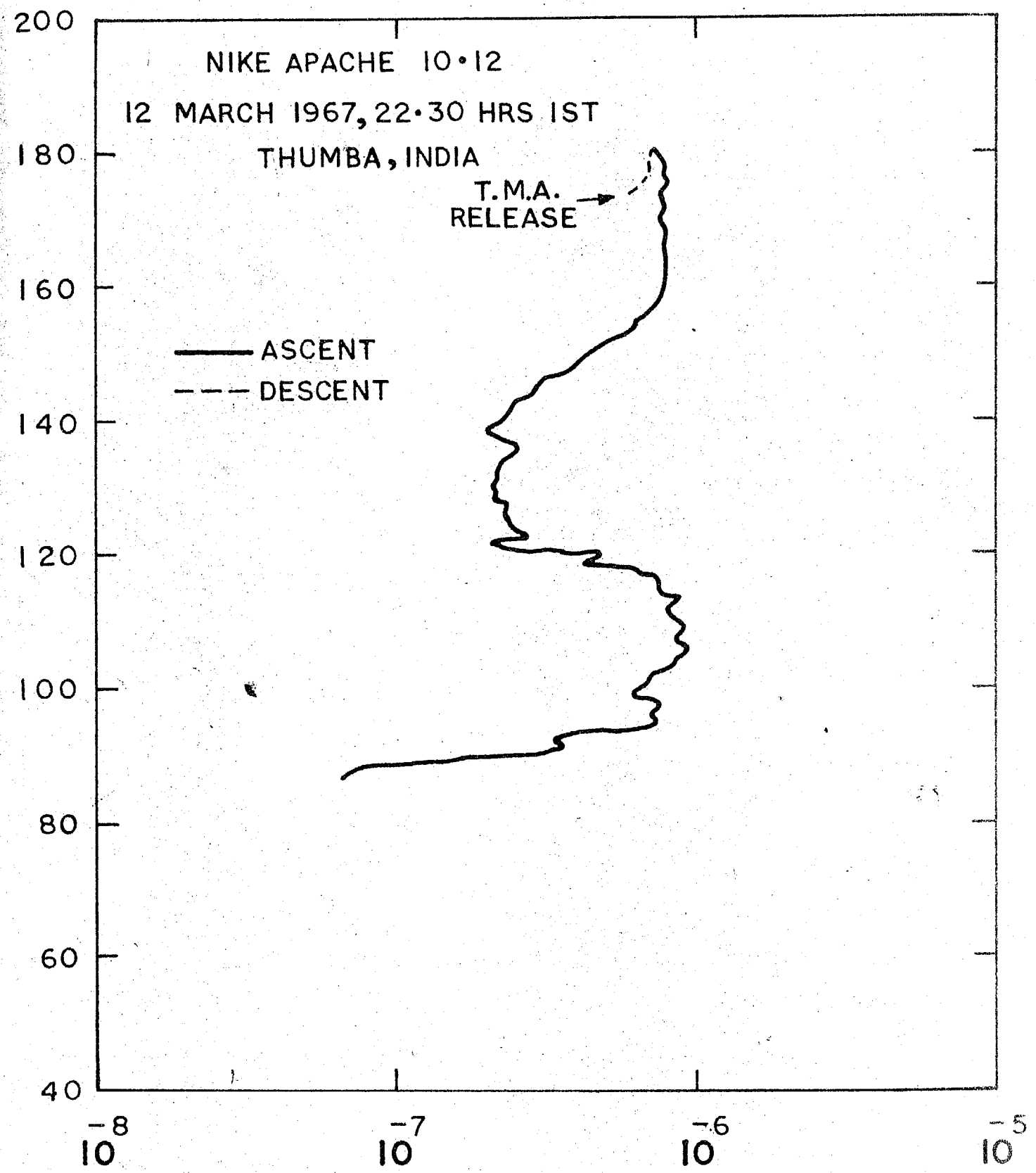
NIKE APACHE 10•12
12 MARCH 1967, 22•30 HRS IST
THUMBA, INDIA
T.M.A. RELEASE
ASCENT
DESCENT
200
180
160
140
120
100
80
60
40
10^{-8}
10^{-7}
10^{-6}
10^{-5}
PROBE CURRENT AMPS.

Fig 91

by which the probe sensitiveness decreased might have been affected by the variations in the rate of emission of TMA.

The profile of fig.41 shows two interesting features: (i) the probe current in the height range 100-120 kms are larger than the currents of fig.37 obtained during the evening of the same day even after correcting for different probe voltages; (ii) the presence of a deep valley in the 120-140 km region, where the electron density falls by a factor of 4 or 5. This valley could be made out even during descent. It is not shown in figure for reasons mentioned earlier. The larger electron densities during the night and the presence of the valley in the electron density both need explanations.

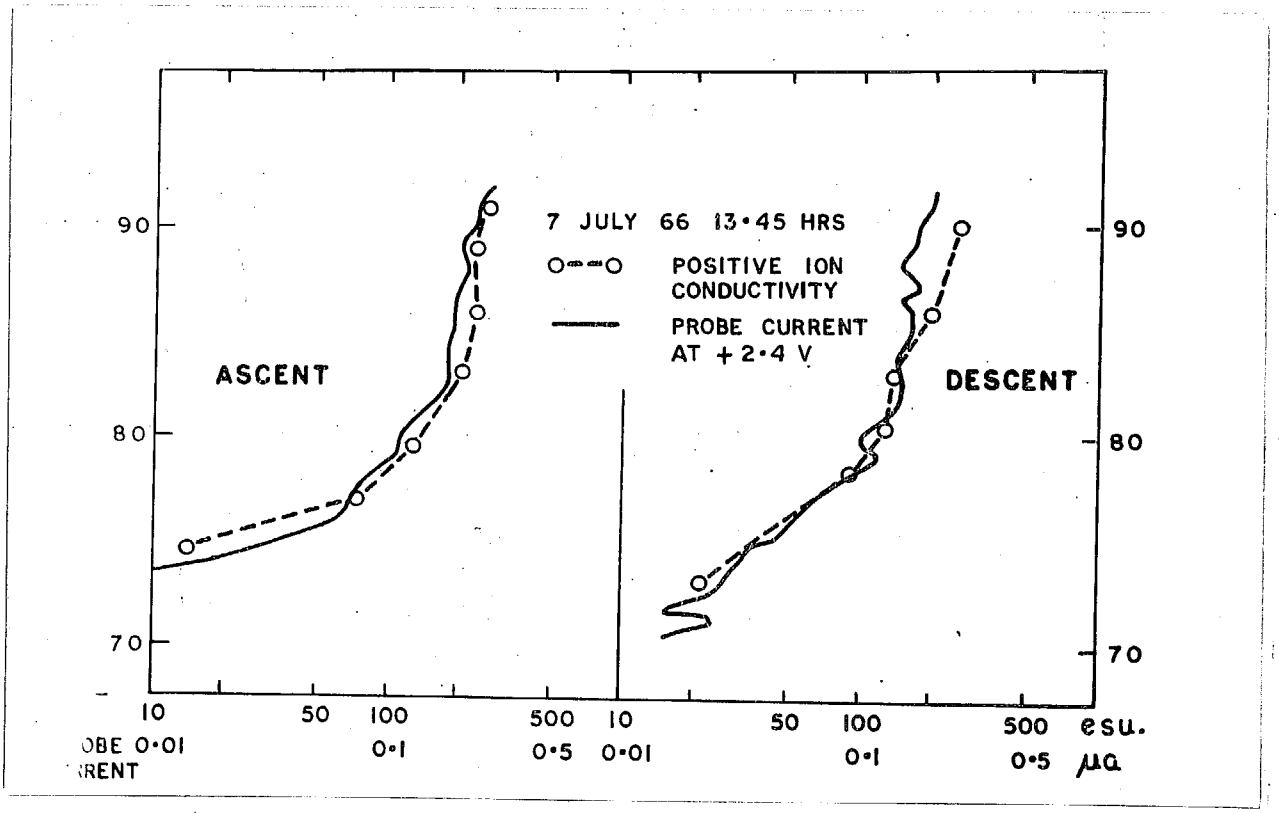

Fig.42: Positive ion conductivity and probe current at $\pm$ 2.4 V, measured on flight 20.05, in the D region, plotted against height.

In principle it is possible to determine the positive ion concentration n_+ in the medium from these values of conductivity σ_+

$$\sigma_+ = \frac{n_e e^2}{\nu_{in} m_+} \qquad (20)$$

where ν_{in} is the ion-neutral collision frequency and m_+ is the ion mass. But this requires a knowledge not only of the ion mass but also the collision frequency, both of which are not known with certainty. Here the conductivity profile is taken to represent only the electron density profile in the medium as pointed out by Smith.

The probe current at fixed positive voltage is also shown in fig.42 for comparison with the conductivity values. It is seen that the probe current profile follows closely the conductivity variations both during ascent as well as descent. This gives additional support to the practice of using the probe current profile to study variations in electron density even in the D region.

Mechtly et al (1967) have attempted a comparison of the electron current to a positive probe and the electron density in the 90-55 km region of the ionosphere. The electron densities were determined by Faraday rotation and differential absorption measurements simultaneously with probe current measurements. Even though the electron density values used in this study are not likely to be equally accurate throughout the height range considered by the authors, their results are very interesting. Fig.43 which is a reproduction from their

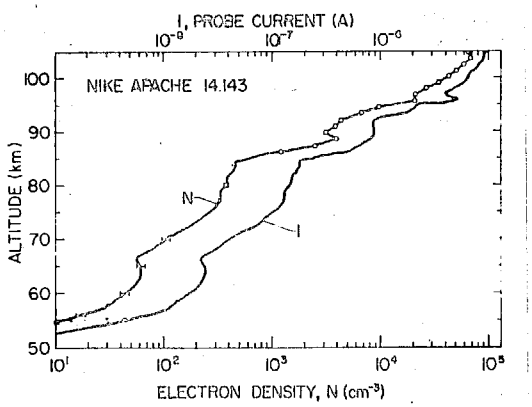

Fig.43: Electron current to a probe at fixed positive voltage, compared with the electron density in the ambient medium at heights below 100 km. Diagram after Mechrly et al, JGR 1967.

peper shows that the probe current profile closely follows the electron density profile throughout this region. However, a close study of this figure shows that the ratio between the probe current and the electron density does not remain constant throughout this height range. The ratio changes by a factor of about 4 from 100 km to 55 km as the electron density goes down by more than three orders of magnitude. The variation is the combined effect of the decreasing electron densities and the changing atmospheric conditions in this height region. The actual variation is gradual so that the electron density profile and the probe current profile agree rather closely.

In the following, the experimental probe current profile has been taken to correspond to the electron density profile. To preserve continuity the normalisation factor obtained at a about 100 km is used even in the lower height regions. Hence in the height region below 90 km the actual electron density values are likely to be uncertain by a factor which gradually increases with decreasing height. This feature prohibits any serious attempt at a quantitative study of the data in terms of photochemical processes occuring in this region.

1.2 Sources of Ionisation in the D regiong: According to Nicolet and Aikin (1960), D region ionisation in the middle and low latitudes is due to (i) Lyman α (1215.6Å) photo-ionising molecular nitric oxide which is a trace constituent in the ionosphere, (ii) X rays in the wavelength range 1 to 10 Å producing mass ionisation, and (iii) ionisation due to

galactic cosmic rays. Ultraviolet radiation in the Schumann Runge bands can ionise metallic atoms such as sodium, calcium etc but the concentrations of these atoms is so low that the contribution of this radiation to the ionisation in the D region can be neglected. Of the three sources of ionisation the galactic cosmic ray contribution exhibits a latitudinal variation due to the cut off rigidities being different at different latitudes and is a minimum at the equator. Its contribution is important only below about 50 km. It is therefore, neglected in the following analysis. The relative importance of Lyman α and X-rays in producing D region ionisation is not yet certain. Nicolet and Aikin (loc cit) had come to the conclusion that Lyman α is the major source of the entire upper D region ionisation under solar quiet conditions and the X-rays would assume importance only under disturbed conditions. Whitten et al (1964) however, based on more recent information about the X-ray emission from the sun, concluded that X-rays are more important than assumed by Nicolet and Aikin and even under conditions of solar minimum X-rays (1-10 $\mathring{A}$) form the major source of ionisation in the height range above 85 km and that Lyman α is important only between 73 and 84 km. During disturbed conditions and at solar maximum, the X-ray contribution can completely mask the Lyman α contribution to the ionisation in the D region. The height distribution of molecular nitric oxide in the ionosphere which is vital for a proper evaluation of the Lyman α contribution, is not definitely known and information on X-ray

emission from the sun has been available for only the past solar cycle or so. Hence the above conclusions cannot be final.

Contribution due to Lyman : The rate of ion production due to photoionisation of nitric oxide by Lyman α radiation is given by

$$q = \sigma_i(NO) \cdot n(NO) \cdot Q_\infty \exp(-\tau) \qquad (21)$$

where $\sigma_i(NO)$ = ionisation cross section of nitric oxide = 2×10^{-18} cm^2

$n(NO)$ = number density of molecular nitirc oxide

Q_∞ = Lyman α flux at the top of the atmosphere

τ = Optical depth, given by

$$\tau = \sigma_a(O_2) \int_x^\infty n(O_2) \sec\chi \, dz \qquad (22)$$

with

$\sigma_a(O_2)$ = absorption cross section of molecular oxygen for Lyman α radiation = 1×10^{-20} cm^2

$n(O_2)$ = number density of molecular oxygen

χ = solar zenith angle.

The molecular oxygen concentration can be taken from a suitable atmospheric model. Therefore the rate of ion production due to Lyman α can be determined if the concentration of molecular nitric oxide in the atmopshere is known.

The nitric oxide distribution in the upper atmosphere is not known for certain. According to nicloet (1965), the nitric oxide concentration is determined above about 100 km by photoionisation equilibrium considerations, while below 100 km it is determined by considerations of photochemical equilibrium. The latter consideration gives

$$n(NO) = A \cdot n(O_2) \cdot \exp\left(\frac{-3000}{T}\right) + 5\times10^{-7} n(O) \qquad (23)$$

where A is a constant $n(O_2)$ and n(O) represent the concentrations of molecular and atomic oxygen respectively and T is the neutral gas temperature. Values varying between 0.1 and 0.01 have been used for the coefficient A of the first term (Nicolet and Aikin loc cit; Mitra 1966; Sechrist 1967). Except at heights where atomic oxygen is important (above 90 km) the nitric oxide concentration as given by eq.23 is strongly temperature dependent. Therefore, unless the temperature is exactly known only rough estimates of the concentration can be made. Grenade experiments have shown that ~~atmospheric~~ at mesospheric heights the neutral gas temperature exhibits considerable variation from day to day and during the year (cf W.Smith et al 1964).

Barth (1966) has made rocket measurements of ultraviolet dayglow in the 1500-3200 Å wavelength range and from these measurements has estimated the concentration of molecular nitric oxide at different heights in the

atmosphere. Barth's values are orders of magnitude higher than the estimates made from eq. 23. It has not so far been possible to explain this discrepancy.

Ionisation due to X-rays: Photoionisation due to X-rays is given by

$$q = \sum_{\lambda=1}^{10} q_\lambda \, d\lambda \tag{24}$$

where

$$q_\lambda = \sum_{M} E_\lambda \sigma_\lambda(M) \cdot n(M) \cdot A_\infty(\lambda) \cdot \exp(-\tau_\lambda) \tag{25}$$

with

E_λ = efficiency for photoionisation = $\frac{\text{Photon energy in eV} - 500}{32}$

$\sigma_\lambda(M)$ = absorption cross section for the molecule of type M for the wavelength λ .

$n(M)$ = number density of molecule of type M

$A_\infty(\lambda)$ = Radiation flux of wavelength at the top of the atmosphere at λ

τ_λ = optical depth, given by

$$\tau_\lambda = \sum_{M} \sigma_\lambda(M) \int_z^\infty n(M) \sec\chi \, dz$$

X-ray emission from the sun strongly varies with solar activity. During disturbed periods and with increasing solar activity there is an enhancement in solar X-ray emission

and a hardening of solar X-rays. Therefore, the determination of the ionisation produced by solar- X-rays needs a knowledge of the solar X-ray spectrum.

1.3 Ion production rates for July 7, 1966: X-ray fluxes in the wavelength bands 0-3 Å, 0-8 Å, 8-20 Å and 44-60 Å were measured on the flight day by an NRL solar radiation satellite and the observations were available from the published data (CRPL Solar and Geophysical data 1966). The flux values corresponded to a disturbed sun but not to flare conditions. There was a strong flare during the early hours of the morning of 7th July 1966, but the activity had decreased by the flight time. The flight time ionograms from Thumba and Kodaikanal indicated only a normal equatorial ionosphere. Using the observed flux values, an X-ray spectrum of the sun was constructed in the wavelength band 1-10 Å. Absorption cross-sections at the various wavelengths were available from the Smithsonian Astrophysical tables and the number densities of the atmospheric constituents from the atmospheric model CIRA 1965. Hence using the above X-ray spectrum ion production rates in the D region due to X-rays were calculated.

The ultraviolet spectrum of the sun is relatively insensitive to solar activity. The Lyman α flux in the atmosphere has been measured under a variety of conditions over the past years and a value varying from 3 to 6 ergs/cm^2 sec from solar minimum to solar maximum, has been estimated

at the top of the atmosphere. Using a value of 5 ergs/cm^2 sec for the Lyman α flux at the top of the atmosphere, which was probably the best assumption for a slightly disturbed condition during 1966, production rates due to photoionisation of nitric oxide were calculated. Barth's experimental values of nitric oxide densities and a height distribution of nitric oxide density as calculated from eq. 23 using $n(O_2)$, n(O) and T from the CIRA atmospheric model 1965, were employed for the calculation.

The ion production rates due to Lyman α and X-rays (1-10 Å) are compared in fig.44. With the theoretical distribution of nitric oxide there would be a clear bifurcation of the Lyman α and the X-ray layers. With Barth's values of nitric oxide the bifurcation would not be so clear. It is also seen from this figure that under the flight conditions, even with the smaller values of nitric oxide given by eq.23 the Lyman α contribution to D region ionisation would be more important than the X-ray contribution upto about 78 km. With Barth's values of nitric oxide the Lyman α contribution would be greater than the X-ray contribution upto 86 km and would be an order of magnitude more important throughout the height range 70 - 83 km. These conclusions would not alter even if a smaller value of Lyman α flux such as 3 ergs/cm^2 sec were chosen.

Aikin et al (1964) had also concluded that Lyman was more important than X-rays in the height region below 85 km to explain the results from a mid-latitude rocket

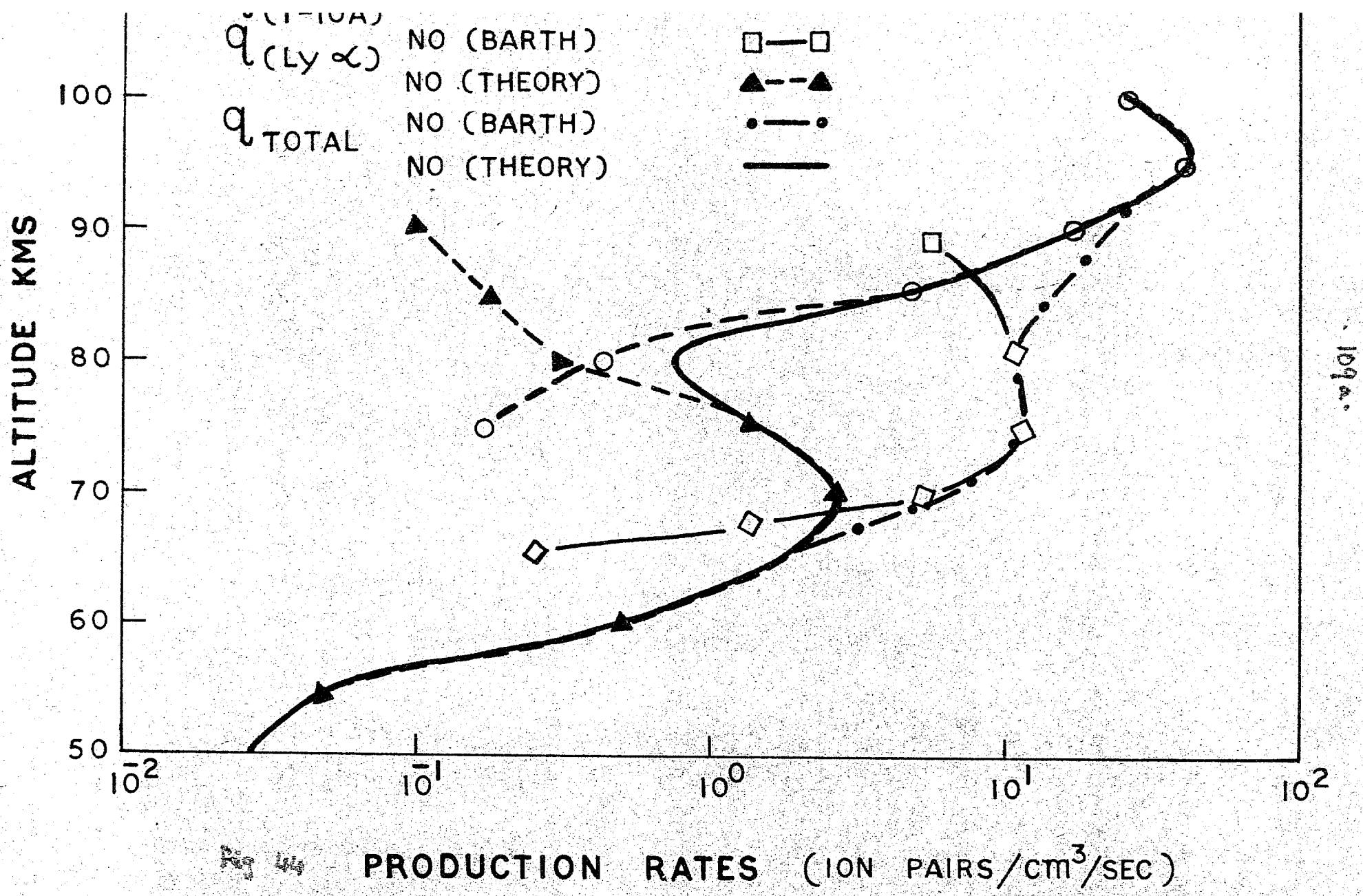
$q_{(Ly\alpha)}$
NO (BARTH)
NO (THEORY)
q_{TOTAL}
NO (BARTH)
NO (THEORY)
ALTITUDE KMS
100
90
80
70
60
50
10^{-2}
10^{-1}
10^{0}
10^{1}
10^{2}
PRODUCTION RATES (ION PAIRS/cm^3/SEC)

Fig 44

experiment conducted close to solar minimum (March 8, 1963). Bourdeau et al (1966) from the experimental results of two rocket flights conducted during the IQSY concluded that X-rays (2-8 Å) were the important ionising source in the height range 82-88 km. Results presented in their paper suggested that the height range 66-82 km was ionised by Lyman α although no definite conclusion was arrived at. The above mentioned conclusions were for periods close to the solar minimum. The calculations presented here are for slightly disturbed conditions during the year 1966, nearly midway between solar minimum and solar maximum.

1.4 Comparison of the ion production rates with the observed electron density profile: In fig.45 the experimental electron density profiles below 95 km are compared with the ion production rates calculated above. Curve 1 in figure gives the total production rates for Lyman and X-rays with the nitric oxide distribution calculated from eq.23. Curve 2 gives the total production rates for Lyman α and X-rays with Barth's values of nitric oxide. Even though experimental data on electron density is not available below 70 km, it appears that the experimental results follow more closely the production rates of curve 2 than those of curve 1, thereby showing a preference for Barth's values of nitric oxide. There is no feature in the experimental data which corresponds to the dip in curve 1 around 80 km nor the well defined peak at 70 km.

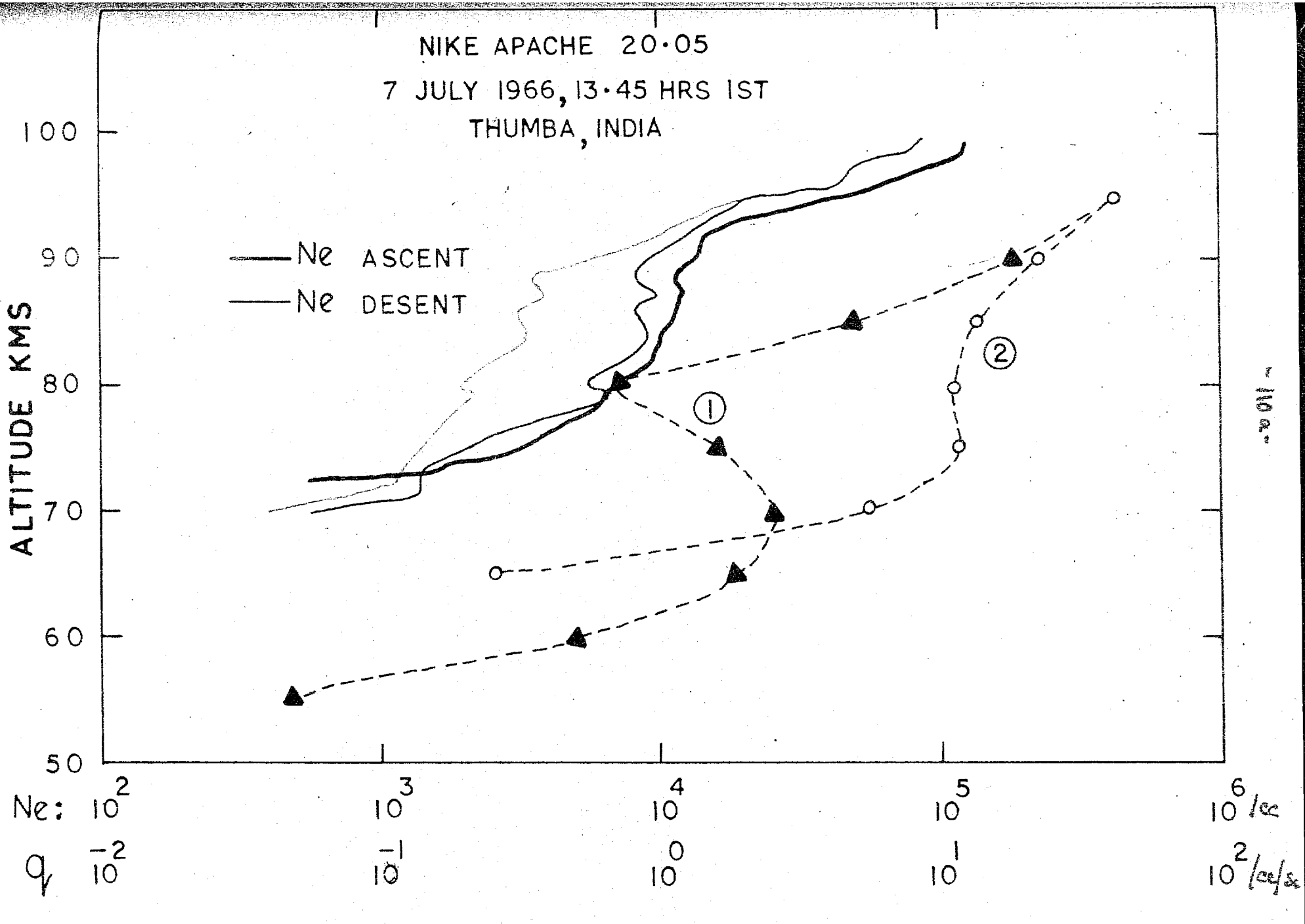
NIKE APACHE 20·05
7 JULY 1966, 13·45 HRS IST
THUMBA, INDIA
Ne ASCENT
Ne DESENT
ALTITUDE KMS
100
90
80
70
60
50
①
②
Ne: 10^2 10^3 10^4 10^5 10^6 /cc
q 10^{-2} 10^{-1} 10^0 10^1 10^2 /cc/s

Fig 45

Another feature that emerges from this comparison is the relative shift between the electron density peak and the peak in ion production. The D region peak in the electron density appears around 85 km, which is at least 10 km above the ion production peak. This height difference seems to be genuine and not due to an error in the rocket trajectory. It can be due to one or more of the following factors.

(1) A large variation in the effective recombination coefficient in the 70-85 km region due to the varying nature of the photochemical processes occuring there.

(2) The presence, in considerable mumbers of metallic ions (such as sodium ions) in the E region. This would result in additional absorption of the Lyman α radiation at E region heights, causing an upward shift in the production peak (Sagalyn and Smiddy, 1967).

(3) The actual height distribution of nitric oxide molecules in the atmosphere being different from the one assumed here. This is certainly possible in view of ill-understood distribution of nitric oxide in the atmosphere.

1.5 The D region after sunset: Results from the three flights of March 1967 show that there is little ionisation in the D region except during the sunlit hours. No probe current was detected below 80 km on any of the three flights, showing that the electron density, if any, was less than about 20 electrons per cc. After sunset the solar ultra violet and X radiations which are responsible for the bulk

of the daytime D region ionisation are absent. The ionisation that was present at sunset decays rapidly due to dissociative recombination and, at lower heights, due to attachment followed by ion-ion recombination. Even with a margin of an order of magnitude in the combined effective recombination coefficient, the ionisation would decay in less than half an hour. The only source of ionisation present at night is galactic cosmic rays. The ion production rate due to cosmic rays at the equator at a height of 70 km is about 2×10^{-3}/cc sec and this would give rise to an electron density of not more than ten electrons per cc, a quantity below the detection limit.

The results of all the three flights are similar in the height region below about 95 km. There is negligible ionisation below about 85 km and the electron density rises rather rapidly above this height to the base of the E region. The base of the E region is rather flat except probably on the morning twilight flight. These results are consistent with the above considerations.

ionosphere or not remains to be explored.

The proton precession magnetometer which accompanied the Langmuir probe on this flight detected a thick current layer with a peak intensity of 5 amp/km^2 at about 102 km during ascent and a similar current layer with peak at about 106 km during descent (Sastry, 1968). This similarity in the electrojet current profiles during ascent and descent contrasts with the marked dissimilarity in the electron density profiles during ascent and descent. This contrast shows that the electrojet is not solely determined by the local properties of the medium. It is a manifestation of a global phenomenon and is determined by the average properties of the medium over a much larger spatial extent than the spatial separation seen by the rocket between ascent and descent.

2.2 Small scale structures: Another interesting feature of the lower E region records (which is not apparent from fig.36) is that, during ascent, in the 100-120 km region the probe current shows a marked modulation at 6 cycles per second which is the expected spin frequency of the rocket. Such a modulation is not seen in any other height region. It is again seen in the same height region during descent, but over a much smaller height range and with a much reduced amplitude of modulation. The ratio of the maximum to minimum probe current during a spin cycle is about 1.8 where the effect is maximum. Fig. 46, which is a portion of the record in this height region is shown here to illustrate this feature.

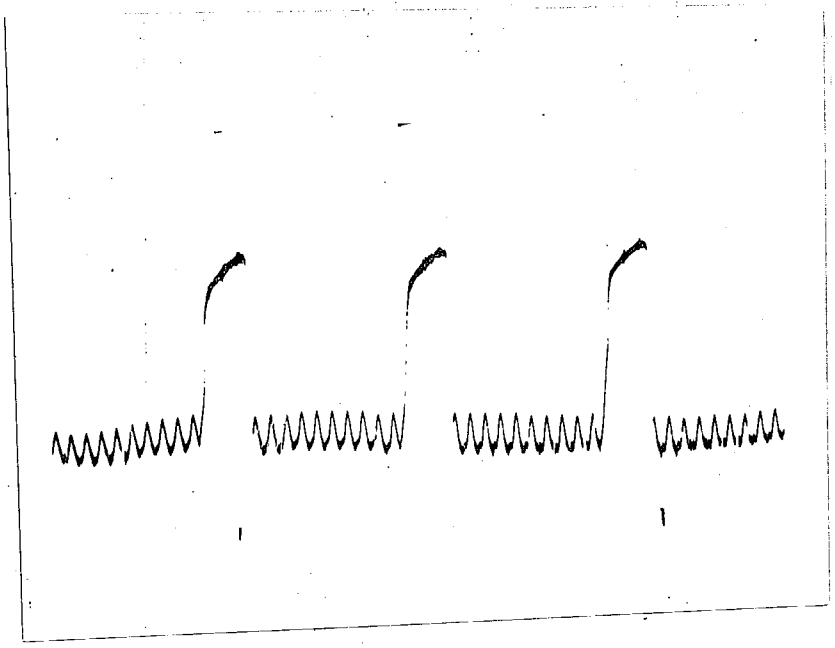

Fig. 46: A portion of the telemetry record of flight 20.05 obtained during rocket ascent, in the height region 100-120 km illustrating the spin modulation on the Langmuir probe current in that region.

While it can not be ruled out that the observed spin modulation can be created by the outgassing from the rocket (the nose cone of the rocket was made of fibreglass), the fact that the modulation is seen only over a limited height range and that the effect repeats itself during descent in the same height range, even though to a much smaller extent suggests that the observed modulation is a genuine feature of the ambient medium. Also there was no obvious large asymmetry of the rocket body around its axis, which can give rise to such large modulations.

It has been seen that even though the sensor is ogive, and symmetrical about the axis of the rocket, it is sensitive to irregularities in the medium. Therefore the observed modulation can be attributed to either horizontal gradients or irregularities present in the ambient medium. If it is attributed to horizontal gradients they should occur within distances comparable to the lateral dimensions of the rocket which is about 15 cms.

The height region where the modulation is observed suggests an association with the electrojet. The presence of small scale irregularities with scale sizes of the order of a few meters in the electrojet is well known from the backscatter work at Jicamarca (for ex Bowles and Cohen, 1963; 1967). But no definite conclusion can be arrived at regarding the present observation since the modulation is weak during descent while the electrojet profile obtained by Sastry shows similar features during both descent and ascent.

That the modulation should occur in the same height range where the large scale structure discussed above is seen, is also interesting. It is known (Gallet, 1955) that in the presence of a background gradient of ionisation turbulence can give rise to small scale irregularities in the medium with scale sizes of 100 to 200 meters. The percentage fluctuation expected from Gallet's work is only a few percent. But the observed fluctuations are very much larger.

3. Electron temperatures in the lower ionosphere:

3.1 Theoretical knowledge: The equilibrium electron temperatures in the ionosphere are determined by the heat input to the electron gas and the various loss processes. Absorption of solar radiation produces a general heating of the atmosphere. But the ionisation resulting from the absorption of certain radiations gives rise to photoelectrons with initial energies ranging from a few electron volts to a few hundreds of electron volts. These electrons loose energy to the ambient electrons, ions and neutral particles. The predominant loss process depends on the initial energy of the photoelectron and the properties of the surrounding medium. Due to collisions amongst themselves the electrons quickly establish equilibrium and attain a temperature of their own. Heat losses from the electron gas to the positive ions and neutral particles is a much slower process since energy loss per collision is small and hence $T_e > T_g$. In determining the electron temperature, heat loss by the electrons to positive ions becomes important only above about 200 km. At lower heights only the heat loss to neutrals is important. The positive ions and neutrals quickly attain equilibrium amongst one another and $T_i \simeq T_g$ in most of the regions except in the upper F region.

Hanson and Johnson (1961) first considered the theoretical problem of determining the electron temperatures in the ionosphere along these lines. Later Hanson (1963), Dalgarno et al (1963) and Willmore (1964) have extended this work,

but along similar lines. From their work it is concluded that the electron temperature increases with height in the ionosphere, is nearly equal to the neutral gas temperature below about 150 km, but above this height $T_e > T_g$ and $T_e - T_g$ increases with height, reaches a maximum around 250 km and then decreases. Geisler and Bowhill (1965) have considered the problem by taking into account thermal conduction along the magnetic field lines by the electron gas and non-local heating due to long range interactions between the escaping photoelectron flux and the ambient plasma. While their study shows up certain different features in the F region, the main conclusions about the lower E region remain unaltered.

3.2 Results, Discrepancy with theory: Thus, theoretically, the electron temperature should be nearly equal to the neutral gas temperature below about 150 km. But the experimental results of chapter V on electron temperature as shown by figs.35, 38 and 40 show a different picture. These results indicate that T_e is everywhere larger than T_g even at heights around 95 km (fig.35). Even after sunset, when the source of heat is removed, the measured electron temperatures are seen to be larger than the corresponding neutral temperatures (fig.38). These results do not represent an exceptional case. Most probe results on electron temperature in the E region during different hours of the day and the night, during different seasons of the year and during different conditions for solar

activity, from solar minimum to solar maximum have given values of electron temperature everywhere larger than the neutral gas temperatures. The results have been similar with different types of sensors. This discrepancy between theory and experiment may be due to one or more of the following causes.

(1) The presence of a non Maxwellian distribution in the medium.

(2) Presence of inherent defects in the probe technique as applied to determination of electron temperature in the ionosphere,

(3) Incompleteness of the theoretical treatments mentioned above.

Even though the photoionisation processes give rise to a hump in the high energy tail of the Maxwell's distribution and inelastic collisions only selectively remove energy, elastic collisions of the electrons amongst themselves are very efficient in randomising the electron energies quickly. Therefore the distoration in the Maxwellian distribution is small and it is generally believed that for all practical purposes a Maxwellian distribution can be assumed in the ionosphere. The second alternative, namely the possibility of some inherent difficulties in applying the probe technique for electron temperature determination in the ionosphere becomes particularly important in view of the recent report from backscatter measurements in France

that $T_e = T_i$ even at 130 km (Carru et al 1967). (However determination of T_e / T_i from backscatter measurements needs a knowledge of the ion species and hence these measurements are not without an uncertainity factor). Also Bowhill (1966) reports an evaluation of T_e / T_g in the 85-100 km range from rocket measurements of gas density, scale height and collision frequency in which the ratio was found to be nearly equal to 1 (within a few percent).

Possible sources of error in probe measurement of electron temperature such as charge build up near insulators, variable work functions of different parts of the sensor have been suggested (Wehner and Medicus, 1952). Of these the second source is very difficult to eliminate, requiring great care in the manufacture and handling of the sensor. The effect of charge build up near insulators can be reduced by the use of a guard electrode which is at the same potential as the sensor and which is physically close to it. Since a guard electrode was used close to the sensor in all the present flights the results are expected to be free from this effect, especially the electron temperatures shown in figs.38 and 40 for the flights 10.11 and 10.14 in which the size of the insulator was very small.

Regarding the third possibility, namely the incompleteness of the theoretical treatments which predict nearly equal electron and gas temperatures for the lower E region, one possibility which might explain the experimental observations is the presence of additional sources of heat, not taken into

account in the above mentioned theoretical treatments. All the above treatments assume that local heating due to solar radiation is the only source of heat in the E region. Electric fields are known to be present and most of the ionospheric currents are known to flow in these regions. That these can provide an additional heat source was first considered by Cole (1962 a, b) and by Kato (1962). It was shown by Kato (loc cit) that the electron temperature can rise upto several thousands of degrees K soon after certain ionospheric current disturbances occur, while the neutral temperature varies only slowly. Joule heating near the magnetic equator due to the electrojet current was considered by Kato (1963) who showed that Joule dissipation of the electrojet current system can give rise to electron temperatures several tens of degrees higher than neutral gas temperatures. The following table is reproduced from Kato's paper.

$T_e - T_g$ due to Joule dissipation of the electrojet:

λ	E_o millivolts per meter		
	0.5	1.0	2.0
4×10^{-5}	140°K	500°K	2200°K
2×10^{-4}	28°K	100°K	440°K
10^{-3}	5.3°K	21°K	85°K

λ = mean fractional energy loss per collision = $2\, m_e/M \simeq 2 \times 10^{-4}$

E_o = electric field

Typical values of electric field that are suggested are 0.5 to 1.0 millivolt per meter. This gives values of $T_e - T_g$ varying between 28°K and 100°K. (Incidentally, the above electric fields are weak enough so as not to disturb the thermodynamic equilibrium amongst the electrons). It is seen that even these figures are insufficient to explain the experimental observations.

3.3 Heat input needed to give rise to the observed electron temperatures: According to Dalgarno et al (loc cit) the heat input Q and the resulting equilibrium electron temperature T_e in the ionosphere are related by

$$Q = \frac{-3kn_e}{2}\left\{\left(\frac{dT_e}{dt}\right)_O + \left(\frac{dT_e}{dt}\right)_{N_2} + \left(\frac{dT_e}{dt}\right)_{O_2} + \left(\frac{dT_e}{dt}\right)_+\right\} \quad (26)$$

where the terms in the brackets represent loss terms, the suffixes indicating the particular constituent to which the heat is lost. These terms are given by

$$\left(\frac{dT_e}{dt}\right)_O = -10^{-14}\, n(O)\, T_e^{1/2}\,(T_e - T_g) \quad (27)$$

$$\left(\frac{dT_e}{dt}\right)_{N_2} = -\left\{7.6\times10^{-16}\, T_e + \left(\frac{G\bar{\nu}}{n(N_2)}\right)_{rot}\right\} n(N_2)\,(T_e - T_g) \quad (28)$$

$\frac{G\bar{\nu}}{n(N_2)}$ is the rotational loss parameter and is a function of T_g. At 300°K it is nearly equal to 1.

$$\left(\frac{dT_e}{dt}\right)_{O_2} = -4.7\times10^{-16}\, n(O_2)\, T_e\,(T_e - T_g) \quad (29)$$

$$\left(\frac{dTe}{dt}\right)_+ = -\frac{ne(Te-Tg)}{268\,Te^{3/2}} \qquad (30)$$

The last term in brackets of eq.26 which represents heat lost due to the positive ions is important only at heights above 200 km and therefore can be neglected in the present calculations. Hence, substituting for the remaining loss terms eq.6 becomes

$$Q = \frac{3kne}{2}\left\{10^{-14}n(O)Te^{1/2} + 4.7\times10^{-16}n(O_2)Te + 7.6\times10^{-16}n(N_2)Te + 10^{-11}n(N_2)\right\}(Te-Tg) \qquad (31)$$

Substituting for the atmospheric parameters T_g, $n(O)$, $n(O_2)$ and $n(N_2)$ from a suitable atmospheric model a direct relationship between Q and T_e can be obtained for a given n_e at any height in the ionosphere. This relation can be used to calculate the heat input needed for a given $(T_e - T_g)$ and hence a given T_e.

Representative calculations were made for two heights in the ionosphere, which would be relevant to the present experimental results. Electron densities of 2×10^5/cc, which would correspond to noon conditions, and 2×10^4/cc which would correspond to sunset and sunrise conditions (and perhaps also to night time conditions at these heights), were used in the calculations. The results are tabulated below:-

	n_e/cc	$T_e - T_g$ °K	Value of Q required	
			ergs/cm^2 sec	KeV
	2×10^5	100	4×10^{-9}	2.5
		700	6.8×10^{-8}	40
		1500	1.8×10^{-7}	110
100 km				
T_g=300°K	2×10^4	100	4×10^{-10}	0.25
		700	6.8×10^{-9}	4.0
		1500	1.8×10^{-3}	11.0
	2×10^5	100	2.6×10^{-9}	1.6
		700	2.0×10^{-8}	17.5
		1500	4.8×10^{-8}	30
140 km				
T_g = 480°K	2×10^4	100	2.6×10^{-10}	0.16
		700	2.0×10^{-9}	1.75
		1500	4.8×10^{-9}	3.0

3.4 Heat flux from the dissipation of currents: Heat flux due to solar radiation at 100 km around noon is of the order of 1 to 2 KeV and is therefore insufficient to give rise to the electron temperatures observed on flight 20.05 (fig. 35) which require a $T_e - T_g$ of about 700°K throughout the lower E region, since this would require a heat flux of about 40 KeV from the above table. If the difference between

the heat input required and the heat input due to solar radiation is assumed to be due to the electrojet current we can write

$$Q = \frac{J^2}{\sigma_3} \tag{32}$$

where J is the current density and σ_3 the cowling conductivity, given by

$$\sigma_3 = \sigma_1 + \frac{\sigma_2^2}{\sigma_1} \tag{33}$$

where

$$\sigma_1 = n_e e^2 \left\{ \frac{1}{m_e \nu_e} \frac{\nu_e^2}{\nu_e^2 + \omega_e^2} + \frac{1}{m_i \nu_i} \frac{\nu_i^2}{\nu_i^2 + \omega_i^2} \right\} \tag{34}$$

is the Pederson conductivity and

$$\sigma_2 = n_e e^2 \left\{ \frac{1}{m_e \nu_e} \frac{\nu_e \omega_e}{\nu_e^2 + \omega_e^2} + \frac{1}{m_i \nu_i} \frac{\nu_i \omega_i}{\nu_i^2 + \omega_i^2} \right\} \tag{35}$$

is the Hall conductivity, with

m_e and m_i are the electron and ion masses,

ν_e and ν_i are the electron and ion collision frequencies

ω_e and ω_i are the electron and ion gyrofrequencies respectively.

Substituting for these and for n_e, σ_3 can be determined.

For flight 20.05 conditions at 100 km with $n_e = 2 \times 10^5$/cc $\sigma_3 = 1.1 \times 16^{-13}$ emu. Since a $T_e - T_g$ of 700°K would require about 40 KeV, substituting Q = 40 KeV and this value of in eq.32 one gets J = 8 amp/km^2.

The proton precession magnetometer which accompanied the Langmuir probe on this flight detected a current layer with a peak current density of 5 amp/km^2 during ascent and a similar current sheet during descent.

The electron temperatures of figs.38 and 40 obtained on flights 10.11 and 10.14 are particularly interesting. Both measurements were made during twilight conditions, one during evening twilight and the other during morning twilight, and both were on extremely quiet days. The temperature values agree closely below about 120 km. The large rise seen in the 130 to 140 km region both during ascent and descent of flight 10.11 is also seen on flight 10.14. Unfortunately measurements of flight 10.14 do not extend beyond 140 km. But the available data strongly suggests a large rise in electron temperature beyond 136 km. The presence of a strong localised source of heat in the 130-140 km region is suggested by these values. The source is thought to be localised because the electron temperatures tend to decrease beyond 150 km during the flight 10.11. Such a localised source can be, the existence of current sheets at twilight. If so the strength of the current sheet can be estimated on similar lines.

At 140 km with $N_e = 2 \times 10^4$/cc which would correspond to conditions of flight 10.11 eq.33 gives $\sigma_3 \doteq 2.7 \times 10^{-13}$emu. For $T_e - T_g = 1500^\circ$K as required by the experimental observations Q needed is 3 KeV from the table. Substituting in eq.32 one gets J = 1 amp/km^2.

Maynard and Cahill (1965) in a rocket flight from Thumba on 29th January 1964 at 15.30 Hrs.IST have detected a current sheet in the 130-140 km region with a peak value of 1 amp/km^2 during ascent and 0.5 amp/km^2 during descent. No other measurements are available over the equator for similar hours of the day or for twilight hours. But Maynard and Cahill's flight was on a quiet day and their measurements are more likely to represent typical conditions rather than a special condition in the ionosphere. If so it is seen that the observed electron temperatures can easily be attributed to the flow of currents.

3.5 Conclusion: The above results show that in the lower E region the electron temperature can exceed the neutral gas temperature considerably, especially in the equatorial regions, due to Joule dissipation of electrojet currents. At the equator in the 100 km region the heat input to the electron gas due to the Joule dissipation of the electrojet currents far exceeds that due to absorption of solar radiation. Electron temperatures in these regions are therefore likely to depend on the intensity of the electrojet current. In the 130-140 km region where there are probably subsidiary currents flowing, at least during the early morning, late afternoon and the twilight hours these currents provide a substantial heat input to the electron gas and determine the electron temperature in these regions. Also the electron temperature profile in the lower ionosphere can exhibit pronounced maxima due to flow of localised current sheets.

4. The E_2 layer.

4.1 The observations: Fig.37 which represents the probe current profile obtained during the evening twilight of March 12, 1967 shows layers of enhanced current in the 130-140 km region both during ascent as well as descent. The height difference between the ascent and descent layers may be due to an error in the rocket trajectory and cannot be taken seriously. These layers of enhanced current coincide with the regions of large increase in electron temperatures observed on the same flight, as seen from fig.38. The observed increase in probe current is by a factor of about 4 and cannot be just due to the observed increase in electron temperatures. The increases represent genuine layers of enhanced electron density in the medium. These layers of enhanced electron density may be what is usually referred to as the E_2 layer in literature.

4.2 Discussion: Studies with the low frequency ionosonde at Boulder have shown that such layers are frequently shown up on ionograms during the evening and sometimes in the night time, when the frequency of the normal E layer becomes small. (Watts and Brown, 1954). From the Kodaikanal ionograms it is seen that such layers appear almost regularly in the early morning and the late afternoon hours, when the quality of the record is good. On this particular day the Kodaikanal ionosonde recorded an E_2 layer during the late afternoon hours. At 16.15 hours the layer was seen with a critical frequency of 3.4 Mhz. At 17.45 hours when the layer

was last seen for the day the critical frequency of the layer was 2.7 Mhz. It is believed that after sunset, with the rapidly decaying ionisation the critical frequency went below the sensitiveness of the recorder. If the value of the probe sensitiveness for this flight as determined on page 91 are used the critical frequency of the layer observed during flight would be 1.2 Mhz for the ascent layer and 1.0 Mhz for the descent layer.

Using the ionosonde observations at 16.15 Hrs. and 17.45 Hrs it is possible to obtain an estimate of the effective recombination coefficient and use this value to study the further decay of the layer and compare the results with the observations. The decay of ionisation is given by

$$\frac{dn_e}{dt} = q - \alpha n_e^2 + \text{div}(n_e v) \qquad (36)$$

The third term on the right hand side, which represents variations due to movement of ionisation is generally neglected for first order studies. The equation then simplifies to

$$\frac{dn_e}{dt} = q - \alpha n_e^2 \qquad (37)$$

The production rates '**q**' around sunset have been estimated by Sagalyn and Smiddy (1967). Using these values and assuming, as first approximation, that the decay rate is constant between 16.15 Hrs and 17.45 Hrs, an approximate value of α was deduced. The resulting value, $\alpha = 2.5 \times 10^{-8}$ cm^3/sec is in agreement with other estimates. Using this values of α, decay of the E_2

layer after 17.45 Hrs. is studied, once again from the eq.37. If it is assumed that there is no ion production after sunset eq.37 gives that at the flight time, 18.57 Hrs. the electron density in the layer would be about 6000/cc, which corresponds to a critical frequency of 0.7 Mhz.

In earlier investigations of the E_2 layer it has been suggested that the layer may be due to absorption of solar ultraviolet radiation in some particular wavelength regions and or neutral particles from the sun (Becker and Deimenger, 1950 a, b). On some occassions the appearance of the layer suggested that it was formed due to the separation of ionisation from the bottom of the F layer and subsequent descent to lower heights (McNicol and Gipps, 1951; Saha and Ray, 1955). Skinner et al (1954) and Shankaran (1964) have found that certain types of ledges in the F_1 trace cannot be easily distinguished from an E_2 layer on the ionograms.

The present results show a new feature of the E_2 layer which is likely to be important in explaining its production and maintenance. It is the association of enhanced electron temperatures with enhanced electron densities. From fig.38 it is seen that the electron temperatures within the E_2 layer are larger than the temperatures above and below the layer by a factor of about 2. Also the flight during the morning twilight of 13th March 1967 once again showed electron temperatures at 130 km (fig.40). While the corresponding probe current profile (fig.39) does not show an E_2 layer it is interesting to note that the ionogram taken at 06.45 Hrs

at Kodaikanal showed an E_2 layer with a critical frequency of 2.2 Mhz at a virtual height of 160 km. It is possible that at the time of the rocket flight the layer was not yet formed. There is a distinct possibility of a further instance of an E_2 layer with enhanced electron temperatures in it. It is therefore possible that there is a class of E_2 layers, seen during the early morning and the late afternoon or evening hours, at least over the equatorial regions, which are associated with enhanced electron temperatures.

4.3 A possible explanation: Most experimental evidence to date suggests that the coefficient of dissociative recombination, which is the most important loss process in the height regions under consideration, follows a power law of the type

$$\alpha_{diss} = A T_e^{n} \qquad -3/2 < n < -\frac{1}{2} \qquad (38)$$

A is a constant

(Biondi, 1964; Whitten and Popoff, 1965). With such a temperature dependence an increase in electron temperature decreases the coefficient of recombination. Since the equilibrium electron densities are given by eq.37 a decrease in recombination coefficient would give rise to larger electron densities. An increase in T_e by a factor of 2 can give rise to a lyer with a 50% increase in electron density. Thus layers of enhanced electron density can form due to the decreased loss rates resulting from an enhanced electron temperature. An E_2 layer once formed in such a manner can

also be maintained even after sunset, by the enhanced electron temperatures. The cause of the enhanced temperatures can be flow of subsidiary currents at those heights as discussed in the previous section.

E_2 layers with enhanced electron temperatures in them cannot be explained on the basis of the earlier suggestion of absorption of solar radiation in specified bands. In the 140 km region the daytime ionisation is largely due to solar ultraviolet radiation in the C III line (977 Å) and the Lyman continuum and to a small extent solar X-rays in the wave length range 40-70 Å. These radiations would not be able to reach the heights where the layers are seen, under the experimental conditions. Also the maximum energy input due to photoionisation by the C III line which is the most important of the above radiations around 140 km, is of the order of 600 eV and is insufficient to give rise to the electron temperatures observed within the E_2 layer. During twilight conditions an alternate heat source is necessary to give rise to the observed temperatures. Subsidiary current sheets flowing in these regions have been suggested in the previous section as the cause of the observed electron temperatures.

Such an association of enhanced ionisation with current sheets is intriguing. There has been no direct evidence for such a phenomenon so far. As pointed earlier Maynard and Gehill have detected such a subsidiary current sheet at 130 km over Thumba during a flight on a similar day

at 15.30 Hrs. This observation together with the results of flights 10.11 and 10.14 suggest the possibility of occurrence of such a phenomenon in the equatorial regions on quiet days. This possibility needs further verification. Rockets carrying magnetometers (preferably of the rubidium vapour type, since proton precession magnetometers may be unable to detect the small currents involved) and Langmuir probes may be sent up when the ground ionosonde is showing an E_2 reflection. The resulting measurements of electric currents, electron densities and electron temperatures will enable a more quantitative estimate of the effect than has been possible here and establish the feasibility of the above process.

5. Night-time E region:

5.1 The observation: The results of 10.12 have shown the existence of considerable amount of ionisation in the E region at night. Even with a wide margin for the proportionality factor which is used to convert probe currents to electron densities, from fig.41 it is seen that the electron density in the 100-120km region is between 5000 and 8000/cc. With the known values of effective recombination coefficient the evening ionisation is expected to die out within a few hours. The observed values are comparable to, if not larger than, the densities present during evening twilight. These measurements seem to be typical of night-time conditions in the E region. Direct probing as well as ground based experiments (ex. Ratcliffe and Weeks 1960, Blumle 1965; Smith 1966) have consistently shown up the presence of such ionisation in the night time E region.

5.2 Discussion: Night time ionisation in the E region can be explained by taking recourse to one or more of the following alternatives.

(1) Presence of sources of ionisation in the night.

(2) Variation of recombination coefficient during the night.

(3) Movement of ionisation from the F region.

Of these causes (1) and (2) have been considered before. The third possibility by itself appears to be inadequate to explain the observations. In order to off set

the effects of rapid recombination after sunset, ionisation from the F region will have to move down with large velocities. Otherwise the ionisation at 100 km would first disappear within a few hours after sunset and then reappear or build up again. The second alternative can give rise to the observed ionisation as follows. After sunset the ionisation will first decay with a recombination coefficient which is characterisitc of the normal E region (10^{-8} cm^3/sec). After sometime the faster recombining ions disappear leaving behind the more slowly recombining species (α eff = 10^{-9} cm^3/sec or less) such as the metallic ions. These constitute the bulk of the night-time ionisation in the region. While such a process seems possible certain experimental observations show contrary features. Holmes et al (1965) have measured the ion composition of the night-time E region and find that even at 01.00 Hrs in the night the E region ions are mostly O_2^+ and NO^+ (These have dissociative recombination coefficients of the order of 10^{-8} cm^3/sec only).

5.3 Night-time source of ionisation: The existence of sources of ionisation in the night-time E region has been considered in literature for quite sometime now (Ratcliffe and Weeks, loc cit). Nicolet (1955) has shown that the ionisation seen on some occasions in the night E region can be attributed to meteors. Swider (1965) has discussed the problem in some detail and shown that the Lyman α and β radiations in the geocorona and meteoric ionisation are likely to play an important role in the maintenance of the night-time E region. The existence of these radiations in

the night sky was first discovered by Kupperian et al (1959). More recently deMendonca (1967) has measured these radiations and their attenuation in the upper atmosphere in the night using rocket borne ultra violet detectors.

An attempt was made to study the possible role played by the Ly α and the Ly β radiations in the night time E region. Scattered fluxes of 0.01 erg/cm^2/sec at Ly α (0.3% of the day time flux) and 5 x 10^{-5} erg/cm^{2}sec at Ly (0.1% of the day time flux) were assumed to be present at the top of the atmosphere during the night. Attenuation of these radiations is calculated using the atmospheric composition as given by CIRA 1965. Using a nitirc oxide distribution given by Nicolet (1965) based on photo ionisation equilibrium considerations above 100 kms and Barth's values below 100 kms production rates for Ly α were calculated at various heights. Production rates of O_2^+ for Ly β were calculated by taking the oxygen concentration from CIRA 1965. The results are shown in Fig.47. It is seen that Lyα is important only at the base of the E region; above 100 km, O_2^+ production by Ly β becomes predominant. However, it is seen that these production rates can, with a reasonable recombination coefficient (say 10^{-8}cm^3/sec) give rise to the observed electron densities.

Holmes et al (1965) have made measurements of the night time ion composition. Comparing these measurements with day time measurements they conclude that their experimental results are not in keeping with the assumption of

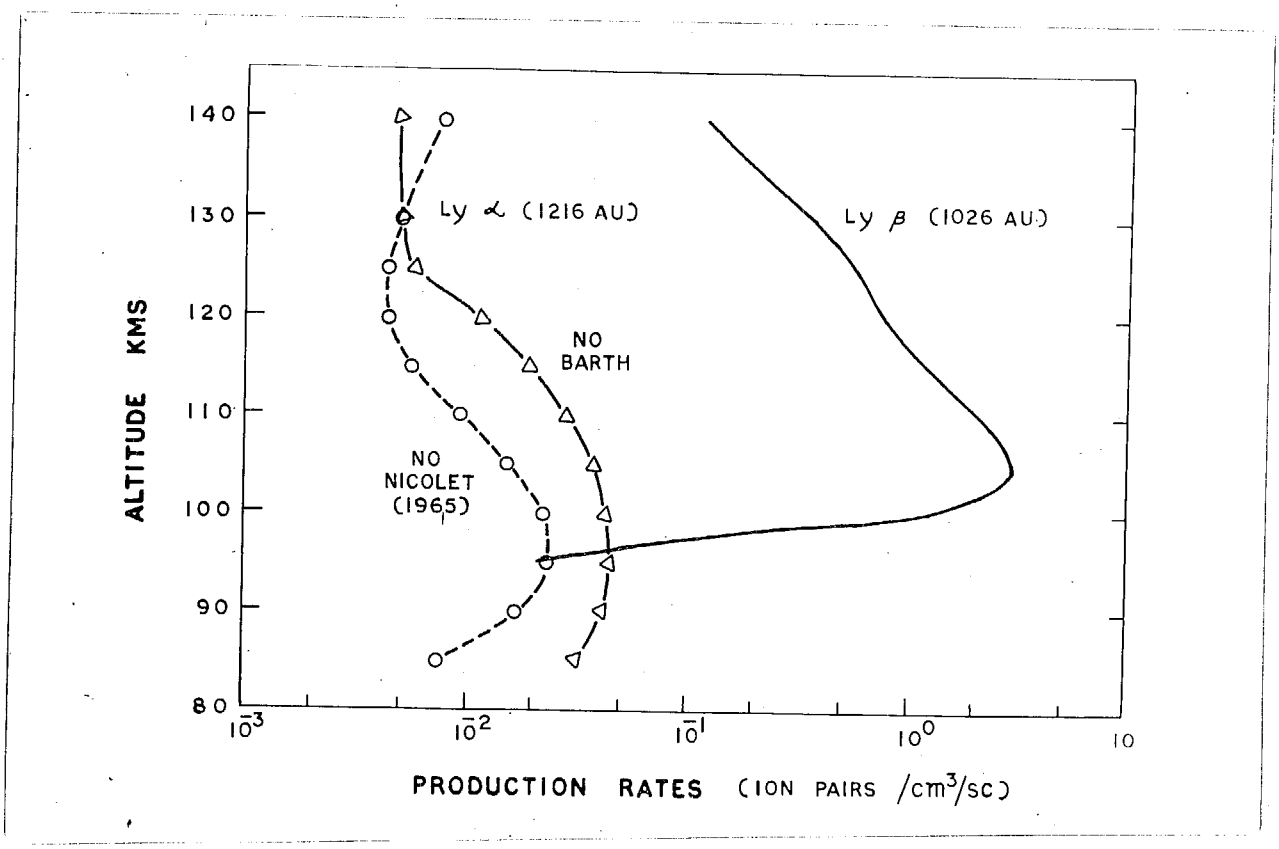

Fig.47: Ion production rates due to the scattered Lyman radiations in the night sky.

the presence of a mechanism for active production of ions during the night. They propose a simple decay via a recombination coefficient which decreases with decreasing temperature to explain their results. Values of diss obtained from certain theoretical considerations and which agree with their experimental results are given in their paper.

The dissociative recombination coefficient is actually a complicated function of temperature. According to Bates and Dalgarno (1962).

$$\alpha_{diss} = C T^{-3/2} \frac{\omega_{AB}}{\omega_{AB^+}} \cdot \frac{g_0(T)}{\tau_a + g_0(T)\tau_p} \qquad (39)$$

where C is a const, ω_{AB} and ω_{AB^+} are the statistical weights of the electronic states in the neutral and the molecular ions respectively τ_a and τ_p are the lifetimes for autoionisation and stablisation processes. $g_0(T)$ is given by

$$g_0(T) = \int_0^\infty f_0(\epsilon) \cdot \exp\left(-\frac{\epsilon}{KT}\right) d\epsilon$$

ϵ is the energy of transition.

Therefore it is not easy to predict from theory the nature of variation of α_{diss} with temperature. But all laboratory measurements of the dissociative recombination coefficient of O_2^+ and NO^+ (which are the ions of interest here) have shown it to decrease with increasing temperature, at least in the range 200°K to 1500°K. Whitten and Popoff (1965)

have summarised these results. Biondi (loc cit) and Whitten and Popoff have found a relation of the form

$$\alpha_{diss} = A T_e^{-1\,1\,0.5} \qquad (40)$$

where A is a constant, to be the best fit for all observations.

The conclusions of Holmes et al (loc cit) cannot be taken as final not only because of these reasons, but also because their arguments are not quite conclusive. The arguments are not without alternatives and their results can be explained without taking recourse to a dissociative recombination coefficient which increases with increasing temperature. Their study deals only with the height region above 120 km in the ionosphere. The 90-120 km region, which would be the most important region where Lyman radiation and meteors have significant effects, is excluded from their study.

5.4 <u>The valley in the 120-140 km region:</u> Another interesting feature of the night time E region profile is the deep valley in the 120-140 km region. The electron density falls by a factor of 4 to 5 in the valley. It may be observed that during the evening twilight of the same day there was no indication of the development of the valley. Such a valley, sometimes even deeper, has been observed previously by several workers during the late evening and night hours. L.G. Smith (1966) and Blumle et al (1965) observe similar valleys though not so deep. From their profiles it appears that the valley

deepens through the night. Lalonde (1966), using the back-scatter technique observed the variations in the electron density profile after sunset and through the night hours. His results show a very deep valley developing early in the evening. Right through the night no ionisation was seen between 120 and 200 km (The lower limit of the sensitiveness of the Arecibo system is 100 electrons/cc) Lalonde's results probably represent an exceptional case. Wakai's analysis (1967) of the low frequency (50 khz to 2 Mhz) night time ionograms of Boulder has also shown up the existence of a valley above 110 km. The valley is wide and deep during quiet nights with the electron density in the valley falling to as low as one tenth that at 100 kms and tends to get filled up during disturbed nights. An intermediate layer develops during strong disturbances around 140 kms and this layer shows a latitudinal variation with a maximum around latitude 70° and a minimum at the equator.

From these results the presence of such a valley in the E region at night can be taken as a common feature. The time at which the valley develops, the depth of the valley and its variation through the night probably vary from day to day. While the existence of such a valley is accepted there is no explanation for the same. Obviously a simple decay via dissociative recombination of the ionisation present at sunset cannot explain the presence of such a valley. Widely varing values of recombination coefficient, increasing by more than an order of magnitude and recovering

to its original value will have to be taken recourse to in the height region 100-150 km. With the known composition of the night time ionosphere and the temperatures existing therein it is not possible to reconcile oneself with such variations. Incidentally the presence of such a velly alone is sufficient evidence against Holmes et al's suggestions of a dissociative recombination coefficient which increases with increasing temperature in the E region.

Another explanation of the valley would be the night time presence of a source of ionisation which has a production profile exhibiting a fairly sharp minimum around 120 km. Referring to fig. 47 it is seen that the production profile of scattered Lyman α at night has such features. It shows a maximum production rate at about 100 km, a minimum in the 100-120 km region where the production rates fall by a factor of 3 to 4, with an increase in the rates aloft. With such a production profile and an allowable margin for the variation in the recombination coefficients, it is possible to reproduce an electron density profile similar to what is observed in fig.41. There is no reason to expect Lyman α to be the only hydrogen radiation present during night time; so other hydrogen radiations such as Lyman β can be present in similar proportions (no observations on Lyman β in night are available because of the difficulties in measurements) . As Lyman β ionises atomic and molecular oxygen, and since oxygen is relatively abundant, production of O_2^+ by Lyman β can be far more important than Lyman α production of NO^+ in the height

regions above 100 km. Even if the Lyman β flux present during night (relative to its day time flux) is less than the Lyman α flux (relative to its day time value) by an order of magnitude, production of O_2^+ by Lyman β would be more important than the production of NO^+ by Lyman α. However, production profile due to Lyman β does not show the features required for a velly in the 120-140 km region.

Probably the presence of a night time source of ionisation together with the movement of ionisation from above can give rise to the observed profile. Presence of sources would give rise to the electron densities observed in the 100 km region, while movement of ionisation from above would give rise to the electron densities observed in the region above 150 km. If the vertical motions are small (not more than a few meters/sec) there can be a valley in between. The day to day variations in the profile could then be explained in terms of variations in these motions.

CHAPTER - VII

SUMMARY AND CONCLUSIONS

A rocket launching station capable of launching two stage rockets carrying aeronomy payloads of 20 to 30 kg to altitudes of 150 km or more, close to the geomagnetic equator was established at Thumba (magnetic dip $6^{\circ}47'S$) in 1963. A programme involving measurements of the neutral as well as the charged components of the atmosphere through payloads carried by the rockets launched from Thumba was undertaken by various workers interested in problems of equatorial aeronomy. The author developed a Langmuir probe system and used it to make measurements of electron density and electron temperature in the lower ionosphere over Thumba. This thesis describes and discusses the results of these measurements.

The electron density and electron temperatures measured by the Langmuir probe are only two of the many parameters needed for a proper study of any process or phenomenon in the ionosphere. Such studies can at best show up interesting features of the ionosphere and point out possibilities of certain phenomena and process. Some of the observations presented here are single observations and in many cases need confirmation through further measurements. The discussions given in chapeter VI lead us to the following conclusions, some of which are necessarily tentative.

1. Adopting the experimental values of nitric oxide concentrations determined by Barth for the D region, photo-

ionisation of nitric oxide by Lyman α radiation from the sun appears to be a more important source of ionisation in the height range 70-84 km, than solar X-rays, even on a moderately disturbed day in the year 1966. On the other hand, if the nitric oxide concentrations in the atmosphere determined by the photochemical considerations of Nicolet are adopted Lyman α contribution would be important only below 78 km.

2. The equatorial electrojet currents apparently do not depend on the local electron density of the medium, suggesting that these currents are significantly influenced by fields which prevail over distances much larger than 100 kms.

3. The experimental observations suggest the possibility of the existence of small scale irregularities in the height region 100-130 km. These irregularities are not likely to be those produced by the rocket and are likely to be characteristic of the ambient medium. While the cause of these irregularities is not known, an association with the electrojet is not ruled out.

4. Even though the Langmuir probe measurements of electron temperatures are possibly larger than the actual ambient values it is likely that the electron temperature in the lower equatorial ionosphere (below 150 kms) are everywhere larger than the neutral gas temperatures. Joule dissipation of electric currents such as in the equatorial electrojet can be more important than solar radiation in heating the lower ionosphere. Dissipation of the average daytime electrojet is

seen to be sufficient to give rise to electron temperatures of about 1000°K at 100 km. Dissipation of current can also give rise to pronounced maxima in the electron temperature profile at altitudes of 130-140 km shown by the rocket launching during the evening twilight on March 12, 1967.

5. The E_2 layer apparently occurs fairly frequently in the equatorial regions during morning, late afternoon and twilight hours. There is evidence for enhanced electron temperatures within the layer. A decrease in the effective recombination coefficient due to increased electron temperatures can be partly responsible for the maintenance of such E_2 layers even after sunset.

6. In the night-time E region, electron densities are large (several thousands per cc) in the 100-120 km region, while there is a valley in the electron density profile between 120 and 140 kms. The electron densities in the 100-120 km region are likely to be due to the Lyman radiations scattered by the hydrogen in the geocorona, whereas the shape of the observed profile above about 120 km is apparently due to the combined effect of (i) the above sources of ionisation and (ii) the movement of ionised particles from above.

Conclusion 1 is supported by some observations of other workers. Conclusions 2 and 3 are in accordance with the present understanding of the properties of the lower equatorial ionosphere. A detailed study of the small scale irregularities utilising a rocket borne plasma noise probe

is planned. This would throw more light on the irregularities considered in 3. Rocket flights with composite payloads of Langmuir probe and magnetometers are needed before conclusions 4 and 5 can be established. Such flights are planned in the near future. A rocket flight with a composite payload of Langmuir probe and ultraviolet detectors would establish the validity of conclusion 6. Such flights are also planned in the near future.

REFERENCES

Aikin, A.C. — Report on Equatorial Aeronomy Edited by F. de Mendonca, p 1, CNAE-LAFE 32, SAO Jose' dos Campos. (1965).

Aikin, A.C. — Conference digest programme Conference on ground base radio wave propagation studies of the lower ionosphere, held at Ottawa, Canada, in April 1966 (1966).

Aikin, A.C., J.A.Kane., and J. Troim., — Journal of Geophysical Research, 69, 4621, (1964).

Allen, J.E., R.L.F. Boyd, and P. Reynolds. — Proceedings of Physical Society, 70, 297, (1957)

Alpert, J.L., A.V.Gurevich, and L.P. Pitaevsky. — Space Science Reviews, 2, 680, (1963).

Alpert, J.L., — Space Science Reviews, 4, 373, (1965).

Aono, Y., K.Hirao, and S. Miyazaki. — Journal of Radio Research Laboratories, 8, 453, (1961).

Appleton, E.V. — Nature, 157, 691 (1946).

Baker, W.G., and D.F.Martyn, — Philosophical transactions of the Royal Society, 246, 281 (1953).

Balsley, B.B. — Space Research VII, Edited by R.L.Smith Rose. p 508, North Holland Publishing Company, (1967).

Bandyopadhyay, P. and H.Montes. — Journal of Geophysical Research, 68, 2453, (1963).

Barth, C.A. — Planetary and Space Sciences, 14, 623, (1966).

Bates, D.R., and A. Dalgarno — In 'Atomic and Molecular Processes' Edited by D.R.Bates, Academic Press, (1962).

Bauer, S.J., and Jackson, J.E.	Journal of Geophysical Research, 67, 1675, (1962)
Baxter, R.G.	Journal of Atmospheric and Terrestrial Physics 26, 711, (1964).
Becker, W., and Diemenger, W.	Naturwissenchaflen 27, 90, (1950a).
Becker, W.,and Diemenger, W.	U.R.S.I., Proc. Commission on Ionosphere, second meeting held at Brussels p.126, (1950b).
Bramley, E.N. and M. Peart.	Journal of Atmospheric and Terrestrial Physics, 27, 1201, (1965).
Bernstein, I.B., and I.N.Robinowitch.	Physics of fluids, 2, 112, (1959).
Biondi, M.A.	Annales de Geophysique, 20, 34, (1964).
Blumle, L.J., A.C. Aikin, and J.E. Jackson.	Report on Equatorial Aeronomy, Edited by F. de Mendonca, p 86, CNAE-LAFE 32, SAO Jose' dos Campos (1965).
Bohm, D.	Ch III of 'Characteristics of electrical discharges in magnetic fields', Edited by A.Guthrie and R.K.Wakerling, McGrawHill Book Company, (1955).
Bohm, D., E.H.S. Burhap, and H.S.W. Massey.	Ch II of 'Characteristics of electrical discharges in magnetic fields; Edited by A. Guthrie and R.K. Wakerling, McGrawHill Book Company, (1955).
Bourdeau, R.E., and J.L. Donley.	Proceedings of Royals Society, 281, 487 (1964).
Bourdeau, R.E., A.C. Aikin, and J.L. Donely.	Journal of Geophysical Research 71, 727, (1966).
Bourdeau, R.E., E.C.Whipple, Jr., and J.F.Clark.	Journal of Geophysical Research, 64, 1363, (1959).
Bourdeau, R.E., J.L. Donley, G.P. Serbu, and E.C. Whipple, Jr.	Journal of Astronautical Sciences, 8, 65, (1961)

Bowhill, S.A.	Progress in Radio Science, Proceedings of the XVth U.R.S.I. Assembly p. 856, published by U.R.S.I. (1966).
Boyd, R.L.F.,	Proceedings of Royal Society. 201A, 329, (1950).
Boyd, R.L.F.,	Aeronomy report No.10, An informal Conference record, Edited by C.F. Sechrist and J.S. Shirke, University of Illinois, (1965).
Boyd, R.L.F., and A.P. Willmore	Space Research III, Edited by W. Priester, p 1168, North Holland Publishing Company (1963).
Bowles, K.L., B.B.Balsley, and R. Cohen	Journal of Geophysical Research, 68, 2485, (1963).
Brace, L.H., and N.W. Spencer	Journal of Geophysical Research 69, 4686, (1964).
Bramley, E.N. and M. Peart	Journal of Atmospheric and Terrestrial Physics 27, 1201, (1965).
Cahill, L.J., Jr.	Journal of Geophysical Research 64, 489, (1959).
Calvert, W.,	Journal of Geophysical Research, 68, 2591, (1963).
Calvert, W., and R. Cohen.	Journal of Geophysical Research, 66, 3125 (1961).
Calvert, W., J. Hugill, and M. Field.	'The Multiple Ionospheric probe' Edited by W.J. Heikkila, DASS-65-2, South West Centre of Advanced Studies, Dallas, (1965).
Carru, H., M. Petit and P. Waldteufel.	Journal of Atmospheric and Terrestrial Physics, 29, 351, (1967).
Cicerone, R.J. and S.A. Bowhill	Aeronomy Laboratory report No.21, University of Illinois, (1967).
Cohen, I.M.	Physics of fluids, 6, 1492, (1963).

Cohen, R., and K.L. Bowles.	Journal of Geophysical Research, 66, 1081, (1961).
Cohen, R., and K.L.Bowles.	Journal of Geophysical Research, 68, 2503, (1963).
Cohen, R. and K.L. Bowles.	Journal of Geophysical Research, 72, 885, (1967).
Cohen, R., K.L. Bowles, and W. Calvert.	Journal of Geophysical Research, 67, 965, (1962).
Cole, K.D.	Nature, 194, 75, (1962)
Cole, K.D.	Australian Journal of Physics, 15, 223, (1962).
Croom, S., A. Robins, and J.O. Thomas.	Nature, 184, 2003, (1959).
Dalgarno, A., McElroy, M.B., and R.J. Moffet.	Planetary and Space Sciences, 11, 463, (1963).
Deshpande, M.R.	Ph.D. Thesis, submitted to Gujarat University (1966).
Deshpande, M.R., and R.G. Rastogi.	Annales de Geophysique, 22, 418, (1966).
Dote, T., K. Takayama, and T. Ichimnya.	Journal of the Physical Society of Japan, 17, 174, (1962).
Dote, T., K. Takayama, and T. Ichimnya.	Journal of the Physical Society of Japan, 18, 260, (1963).
Dougherty, J.P.	Journal of Geophysical Research, 64, 2215, (1959).
Duncan, R.A.	Journal of Atmospheric and Terrestrial Physics, 18, 89, (1960).
Duncan, R.A.	Journal of Geophysical Research, 69, 3741, (1964).

Farley, D.T., Jr.	Journal of Geophysical Research, 68, 6083 (1963).
Gallet, R.M.	Proceedings of IRE, 43, 1240, (1955).
Geisler, J.R., and S.A. Bowhill.	Journal of Atmospheric and Terrestrial Physics, 27, 457, (1965).
Gnanlingam, S., and A.J. Ratnasiri.	Annales de Geophysique, 22, 361 (1966).
Goldberg, R.A. and E.R.Schmerling.	Journal of Geophysical Research, 67, 3813, (1962).
Goldberg, R.A., and E.R. Schmerling.	Journal of Geophysical Research, 68, 1927, (1963).
Hale, L.C.	Space Research VII, Edited by R.L.Smith Rose, p 140 North Holland Publishing Company, (1967).
Hanson, W.B.	Space Research III,Edited by Prester, p 282, North Holland Publishing Company (1963).
Hanson, W.B., and F.S. Johnson.	Memories Soc.R.Liegi Series 5, 4, 390, (1961).
Hanson, W.B., and R.J. Moffet.	Journal of Geophysical Research 71, 5559, (1966).
Heikkila, W.J.	Aeronomy Report No.10, An informal conference record edited by C.F.Sechrist and J.S. Shirke, University of Illionis, (1965).
Heikkila, W.J., J.A. Fejer, J. Hugill, and W. Calvert.	Space Research VII Edited by R.L. Smith Rose p 395, North Holland Publishing Company, (1967).
Hinteregger, H.E., K.R. Damon, and L.A. Hall.	Journal of Geophysical Research 64, 961, (1959).
Hok, G., N.W. Spencer, and W.G. Dow.	Journal of Geophysical Research, 58, 235, (1953).

Holmes, J.C., C.Y. Johnson and J.M. Young	Space Research V, Edited by King Hele p 756, North Holland Publishing Company (1965).
Ichimiya, T. K. Takayama, and Y. Aono.	Space Research I, Edited by Kallmann Bijl,H. P 397, North Holland Publishing Company (1960).
INCOSPAR	TERLS Handbook (1967).
Jackson, J.E., and J.A. Kane	Journal of Geophysical Research 64, 1074, (1959).
Jackson, J.E. and J.C. Seddon.	Journal of Geophysical Research 63, (1958).
Johnson, E.O., and L. Malter.	Physical Review 80, 58, (1950).
Kato, S.	Planetary and Space Science 9, 939, (1962).
Kato, S.	Planetary and Space Science II, 1297, (1963).
Knoebel, H.W., and D.O. Skaperdas.	Review of Scientific Instruments 37, 1395, (1966).
Knox, F.B.	Journal of Atmospheric and Terrestrial Physics, 26, 239, (1964).
Krassovsky, V.I.	Proceedings, of IRE, 41, 289, 1959.
Kupperian, J.E., Jr. E.T. Byram, J.A. Chubb, and H. Friedman.	Planetary and Space Science 1, 3, (1959).
Lalonde, L.M.	In 'Electron density profiles in the ionosphere and exosphere', Edited by J. Frihagen, p 515, North Holland Publishing Company, (1966).
Langmuir, I.M., and H.M. Mott Smith	Physical Review, 28, 727, (1926).
Lyon, A.J.	Nature 193, 55, (1962).

Lyon, A.J.	Journal of Geophysical Research, 68, 2531, (1963).
Lyon, A.J., N.J. Skinner, and R.W. Wright.	Nature, 181, 1724, (1958)
Martyn, D.F.	Proceedings of IRE, 47, 147, (1959).
Matsushita, S.	In 'Ionospheric Sporadic E', Edited by E.K. Smith and S. Matsushita p 344, Pergamon Press, (1962).
Maynard, N.C., and L.J. Cahill.	Journal of Geophysical Research, 70, 5923, (1965).
Maynard, N.C., L.J. Cahill, and T.S.G. Sastry.	Journal of Geophysical Research, 1241, (1965).
McNicol, R.W.E., and Gipps, G. De.	Journal of Geophysical Research, 56, 24, 1951.
Mechtly, E.A., S.A. Bowhill, L.G. Smith, and H.W. Knoebel.	Journal of Geophysical Research, 72, 5239, (1967).
Mendonca, de F. and L.G. Meira, Jr.,	Space Research VII, Edited by R.L. Smith Rose, p 426, North Holland Publishing Company, (1967).
Mitra, A.P.	Journal of Atmospheric and Terrestrial Physics 28, 945, 1966.
Miyazaki, S., K. Hirao, and Y. Aono	Report on Ionosphere and Space Research, Japan, 14, 148, (1960).
Nicolet, M.	In 'Meteors' Supplement to the Journal of Atmospheric and Terrestrial Physics, p 99, (1955).
Nicolet, M.	Journal of Geophysical Research 70, 691, 1965.
Nicolet, M., and A.C. Aikin.	Journal of Geophysical Research, 65, 1469 (1960).

Norton, R.B., and T.E. Van Zandt.	Journal of Atmospheric and Terrestrial Physics, 26, 1047, (1964).
Ogbuehi, P.O., A. Onwumechilli, and Ifedilli, S.O.	Journal of Atmospheric and Terrestrial Physics, 29, 149, (1967).
Osborne, D.C.	Journal of Geophysical Research, 68, 2435, (1963).
Pederson.,	Tellus, 17, 2, (1965).
Pfister, W., J.C. Vlwick,, and R.P. Vancour.	Journal of Geophysical Research 66, 1293, (1961).
Poppoff, I.G., R.C. Whitten, and R.S. Edmonds.	Journal of Geophysical Research, 69 4081, (1964).
Praglin, J., and W.A. Nicholas.	Proceedings of IRE, 48, 771, 1960.
Rastogi R.G.	Canadian Journal of Physics 37, 874, (1959).
Rosemary Hutton.	Journal of Atmospheric and Terrestrial Physics, 29, 1411, (1967).
Ratcliffe, J.A., and K. Weekes.	In Physics of the Ionosphere Edited by J.A. Ratcliffe, Academic Press,(1960).
Saha, A.K., and S. Ray.	Journal of Atmospheric and Terrestrial Physics, 7, 107, (1953).
Sagalyn, R.C., and M. Smiddy.	Space Research IV, Edited by King Hele, p 371, North Holland Publishing Company (1964).
Sastry T.S.G.	Journal of Geophysical Research, 73, 1789, (1968)
Satya Prakash,and B.H. Subbaraya.	Review of Scientific Instruments, 38, 1132, (1967).
Satya Prakash,. B.H. Subbaraya, and S.P. Gupta.	Journal of Atmospheric and Terrestrial Physics 1968 (in press).

Sayers, J.	Aeronomy report No.1, University of Illinois (1963).
Schulz, G.J. and S.C. Brown	Physical Review, 98, 1642, (1955).
Sechrist, C.F. Jr.	Journal of Atmospheric and Terrestrial Physics, 29, 113,(1967).
Seddon, J.C.	Journal of Geophysical Research, 52, 323, (1953).
Seddon, J.C.	Journal of Geophysical Research, 63, 209, (1958).
Serbu, G.P.	IGY Rocket Report No.7, p 162, (1963).
Shankaran, K.S.	Indian Journal of Meteorology and Geophysics, 15, 75, (1964).
Skinner, N.J., and R.W. Wright.	Journal of Atmospheric and Terrestrial Physics, 9, 103, (1956).
Skinner, N.J., and R.W. Wright.	Journal of Atmospheric and Terrestrial Physics, 26, 1221, (1964).
Skinner, N.J., R.A. Brown, and R.W. Wright	Journal of Atmospheric and Terrestrial Physics, 5, 95, (1954).
Skinner, N.J. J. Hope,and R.W. Wright.	Nature, 182, 1363, (1958).
Spencer, N.W., L.H. Brace, and G.R. Carignan,	Journal of Geophysical Research, 67, 157 , (1962).
Smiddy, M., and R.C. Sagalyn.	Space Research VII, Edited by Smith Rose, p 428, North Holland Publishing Company, (1967).
Smith, L.G.	In 'Technique Manual on electron density and temperature measurement in the ionosphere' Edited by K. Maeda for COSPAR panel on Synoptic rocket soundings, (1964).

Smith, L.G.	Radio Science, 1, 178, (1966).
Smith, L.G. L.H. Weeks, and P.J. McKinnon.	NASA CR391, March, 1966.
Smith, W., L. Katchen, P. Sacher, P. Swartz, and J. Theon.	NASA Technical Report R-211, (1964).
Su, C.H., and S.H. Lam.	Physics of Fluids, 6, 1479, (1963).
Swider, W.	Journal of Geophysical Research, 70, 4859, (1955).
Thomas, J.O., M.J. Rycroft, L. Colin, and K.L. Chan.	In 'Electron density profiles in the ionosphere and exosphere' Edited by J. Frihaghan, p 322, North Holland Publishing Company, (1966).
Wakai, N.	Journal of Geophysical Research, 72, 4507, (1967).
Wasserstram, E., C.H. Su, and R.F. Probstein.	Physics of Fluids, 8, 56, (1965).
Watts, J.M., and Brown, J.N.	Journal of Geophysical Research, 59, 71, (1954).
Wehner, G., and G. Medicus.	Journal of Applied Physics, 23, 1035, (1952).
Whipple, E.C. Jr.	NASA Bulletin X-615-65, 296 (1965).
Whittan, R.C., and I.G. Poppoff.	Physics of the lower ionosphere Prentice Hall, Inc. (1965).
Willmore, A.P.	Proceedings of Royal Society, 281, 140, (1964).

....